

UNIVERSITA' VITA-SALUTE SAN RAFFAELE

**CORSO DI DOTTORATO DI RICERCA INTERNAZIONALE IN
MEDICINA MOLECOLARE**

Curriculum in Basic and Applied Immunology and Oncology

**N-glycosylation inhibition hinders
immunosuppressive tumor microenvironment cells
improving CAR T cell efficacy**

DoS: Dott.ssa Monica Casucci

Second Supervisor: Dr. Emmanuel Donnadieu

Tesi di DOTTORATO DI RICERCA di Camilla Sirini

Matr. 015648

Ciclo di Dottorato XXXV

SSD MED/15

Anno Accademico 2021/2022

UNIVERSITA' VITA-SALUTE SAN RAFFAELE


CORSO DI DOTTORATO DI RICERCA

INTERNAZIONALE IN MEDICINA MOLECOLARE

Curriculum in Basic and Applied Immunology and Oncology

**N-glycosylation inhibition hinders
immunosuppressive tumor
microenvironment cells improving CAR T
cell efficacy**

DoS: Dott.ssa Monica Casucci



Second Supervisor: Dr. Emmanuel Donnadieu

Tesi di DOTTORATO DI RICERCA di Camilla Sirini

Matr. 015648

Ciclo di Dottorato XXXV

SSD MED/15

Anno Accademico 2021/2022

CONSULTAZIONE TESI DI DOTTORATO DI RICERCA

Il/la sottoscritto/I Camilla Sirini

Matricola / *registration number* 015648

Nata a/ *born at* Magenta

il/on 18-10-1994

autore della tesi di Dottorato di ricerca dal titolo / *author of the PhD Thesis titled*

N-glycosylation inhibition hinders immunosuppressive tumor microenvironment cells improving CAR T cell efficacy

AUTORIZZA la Consultazione della tesi / *AUTHORIZES the public release of the thesis*

NON AUTORIZZA la Consultazione della tesi per 12 mesi /*DOES NOT AUTHORIZE the public release of the thesis for ..12.. months*

a partire dalla data di conseguimento del titolo e precisamente / *from the PhD thesis date, specifically*

Dal / *from*/...../..... Al / *to*/...../.....

Poiché /*because*:

l'intera ricerca o parti di essa sono potenzialmente soggette a brevettabilità/ *The whole project or part of it might be subject to patentability;*

ci sono parti di tesi che sono già state sottoposte a un editore o sono in attesa di pubblicazione/ *Parts of the thesis have been or are being submitted to a publisher or are in press;*

la tesi è finanziata da enti esterni che vantano dei diritti su di esse e sulla loro pubblicazione/ *the thesis project is financed by external bodies that have rights over it and on its publication.*

E' fatto divieto di riprodurre, in tutto o in parte, quanto in essa contenuto / *Copyright the contents of the thesis in whole or in part is forbidden*

Data /Date03/11/2022..... Firma /Signature.....

DECLARATION

This thesis has been:

- composed by myself and has not been used in any previous application for a degree. Throughout the text I use both 'I' and 'We' interchangeably.
- has been written according to the editing guidelines approved by the University.

Permission to use images and other material covered by copyright has been sought and obtained. For the following image/s (table 1.1, 1.2, 1.3), it was not possible to obtain permission and is/are therefore included in thesis under the "fair use" exception (Italian legislative Decree no. 68/2003).

All the results presented here were obtained by myself, except for:

1) ***RNAseq bioinformatics analysis.*** In detail, primary M1 and M2 macrophages RNAseq bioinformatics analysis (Results chapter, paragraph 3.2, subparagraphs 3.2.4 and 3.2.5, figures 3.7 and 3.8), were performed in collaboration with Dott.ssa Chiara Balestrieri from Prof.ssa Chiara Bonini's Unit, San Raffaele Scientific Institute, Milan.

2) ***Patient derived organoids (PDOs) generation and culture.*** In detail, PDOs generation and culture for *in vitro* and *in vivo* experiments (Results chapter, paragraphs 3.2 and 3.3, subparagraphs 3.2.8 and 3.3.5, figures 3.11 and 3.17, tables 3.1 and 3.2), were performed in collaboration with Dott.ssa Oronzina Botrugno from Dott. Giovanni Tonon's Unit, San Raffaele Scientific Institute, Milan.

3) ***Histopathological analysis.*** Livers from mice were processed and hematoxylin-and eosin-stained by the GLP SR-TIGET Pathology Unit at San Raffaele Hospital (HSR). In detail, histological analysis (Results chapter, paragraph 3.3, subparagraph 3.3.5, figure 3.17c), was performed by Dott.ssa Francesca Sanvito and Dott.ssa Federica Pedica from HSR Pathology Unit.

4) ***MRI images acquisition and analysis.*** *In vivo* MRI experiments were performed by Tamara Canu, from Preclinical Imaging Facility headed by Antonio Esposito, at San Raffaele Scientific Institute, Milan. MRI images were then analyzed by the radiologist, Dott.ssa Chiara Gnasso (Results chapter, paragraph 3.3, subparagraphs 3.3.4 and 3.3.5, figures 3.16b and 3.17b,e).

5) ***NanoString.*** hCD45+ cells sorted from subcutaneous tumor mass of *huSGM3* mice, were processed for NanoString analysis by Dott.ssa Miriam Redegalli from HSR Pathology Unit. Nanostring analysis with Rosalind software was performed by myself.

All sources of information are acknowledged by means of reference.

ABSTRACT

Adoptive transfer of CAR T cells demonstrated impressive results against B-cell malignancies, but still limited efficacy against solid tumors. In this context, multiple challenges need to be overcome, including poor tumor recognition and strong immunosuppression within the tumor microenvironment (TME).

Our Unit has recently reported that pharmacological inhibition of N-glycan synthesis in cancer cells increases CAR T cell efficacy by improving tumor recognition and preventing T cell exhaustion. In this project, we investigated the role of N-glycosylation blockade on TME cells in the context of colorectal cancer (CRC) and pancreatic adenocarcinoma (PDAC)-derived liver metastases and CEA-specific CAR T cell therapy.

To this aim, we performed tripartite co-cultures and suppressive assays including M2 macrophages (M2-M) and hepatic stellate cells (HepSCs) treated with de-glycosylating agents. These studies revealed that N-glycosylation inhibition abolishes the ability of both TME cells to restrain T cell proliferation and increases the elimination of cancer cell lines (BxPC3 and LoVo) and patient-derived tumor organoids (PDOs from CRC-liver metastases). Interestingly, these effects were associated with profound phenotypic and transcriptional changes in M2-M and HepSCs. In particular, the treatment was able to inhibit M2-polarization in terms of surface markers expression, IL-10 secretion and gene expression profile, and was shown to hinder the activation of HepSCs and inhibit the PD-1/PDL-1 axis.

To evaluate the effect of N-glycosylation blockade on TME cells *in vivo*, we exploited immunodeficient mice reconstituted with a human immune system (*huSGM3*), engrafted intra-hepatically with tumor cells (either BxPC3, LoVo or PDOs) and treated with CEA CAR T cells. In this model, the presence of human immune cells supports CAR T cell responses and helps recreate an immune TME more representative of the human disease. Importantly, using these mice we observed that N-glycosylation inhibition increases CEA CAR T cell antitumor activity and this is associated with the downregulation of immunosuppressive genes in tumor-infiltrating human immune cells.

Overall, these data suggest that blocking N-glycosylation can help overcome multiple barriers that currently limit CAR T cell efficacy in solid tumors, acting not only on tumor cells, but also on immunosuppressive tumor microenvironment cells.

TABLE OF CONTENT

TABLE OF CONTENT.....	1
ACRONYMS AND ABBREVIATIONS.....	4
LIST OF FIGURES AND TABLES.....	7
1. INTRODUCTION.....	9
1.1 CAR T cell therapy of cancer: clinical point of view.....	9
1.1.1 Adoptive T cell therapy and CAR T cells for cancer.....	9
1.1.2 CAR T cell therapy for hematological tumors.....	15
1.1.3 CAR T cell therapy for solid tumors.....	18
1.2 CAR T cell therapy of cancer: efficacy and related toxicities.....	23
1.2.1 Clinical and biological determinants of CAR-related toxicities.....	23
1.2.2 Clinical and biological determinants of CAR-T efficacy in solid tumors.....	27
1.2.3 Approaches to enhance CAR T cells therapeutic index against solid tumors.....	31
1.2.4 Preclinical models to test CAR T cells products for solid tumors: limits and solutions.....	35
1.3 Glycosylation in health, tumor and tumor microenvironment.....	40
1.3.1 N-glycosylation in health and tumor.....	40
1.3.2 The role of N-linked glycosylation in the tumor microenvironment.....	44
2. AIM OF THE WORK.....	49
3. RESULTS.....	50
3.1 2DG increases CEA CAR T cells killing of CRC and PDAC cell lines.....	50
3.1.1 CEA is expressed by CRC and PDAC cell lines and CRC patient-derived liver metastases.....	50
3.1.2 N-glycosylation blockade unmask the CEA antigen to antibody recognition and increases susceptibility to CEA CAR T cells.....	52
3.2 Glycosylation blockade reduces immunosuppressive activity of cells within the tumor microenvironment and increases CEA CAR T cells function <i>in vitro</i>.....	54
3.2.1 De-glycosylated tumors dampen M2 macrophages polarization.....	54

3.2.2 THP-1 derived M2 macrophages lose their immunosuppressive activity upon N-glycosylation blockade.....	56
3.2.3 Primary M2 macrophages are less immunosuppressive upon N-glycosylation inhibition.....	59
3.2.4 N-glycosylation blockade downregulates immunosuppressive genes in M2 macrophages.....	62
3.2.5 De-glycosylated M2 macrophages acquire M1-like features.....	66
3.2.6 N-glycosylation inhibition reduces hepatic stellate cells activation.....	69
3.2.7 N-glycosylation blockade increases CEA CAR T cells functions despite the presence of TME cells.....	72
3.2.8 2DG increases CEA CAR T cells killing capacity against PDOs from CRC-liver metastases.....	75
3.3 Human TME <i>in vivo</i> modeling in the context of liver metastases.....	77
3.3.1 Intra-liver injection of CEA CAR T cells outperforms the intravenous one.....	77
3.3.2 Humanized mice recreate a human immune tumor microenvironment.....	79
3.3.3 Intra-liver administration of CEA CAR T cells better controls tumor growth in BxPC3-bearing <i>huSGM3</i> mice.....	83
3.3.4 TCR knock-out CEA CAR T cells control tumor growth in LoVo-bearing <i>huSGM3</i> mice, without the occurrence of xeno-GvHD.....	85
3.3.5 Patient derived organoids from CRC-liver metastases develop metastatic lesions in the liver of <i>huSGM3</i> mice.....	88
3.4 N-glycosylation blockade inhibits immunosuppressive TME myeloid cells and increases CEA CAR T cells efficacy <i>in vivo</i>.....	91
3.4.1 N-glycosylation blockade increases CEA CAR T cells efficacy in LoVo-bearing <i>huSGM3</i> mice.....	91
3.4.2 N-glycosylation blockade downregulates myeloid immunosuppressive gene expression in <i>huSGM3</i> mice.....	94
4. DISCUSSION.....	98
5. MATERIALS AND METHODS.....	107
5.1 Cells and Media.....	107
5.1.1 Primary cells.....	107

5.1.2 Generation of patient derived organoids (PDOs) from CRC-liver metastases samples.....	107
5.1.3 Cell lines.....	108
5.2 Viral vectors.....	109
5.2.1 CAR construct.....	109
5.2.2 LV vector production and titration.....	109
5.3 Cell-manipulation conditions.....	110
5.3.1 T-cell activation and expansion.....	110
5.3.2 Generation of TCR knocked-out T cells.....	110
5.3.3 T-cell transduction with LV vector.....	110
5.3.4 Generation of MGAT5 knocked-out THP-1, BxPC3 and LoVo cell lines.....	111
5.4 Flow cytometry.....	111
5.4.1 Antibodies and procedures.....	111
5.4.2 Analysis of branched N-glycan surface expression.....	111
5.5 In vitro functional assay.....	111
5.5.1 RNA extraction and qPCR analysis.....	111
5.5.2 Lactate production assay.....	112
5.5.3 Macrophages phagocytosis assay.....	112
5.5.4 PDL-1/PD-1 binding assay.....	112
5.5.5 T cells proliferation assay.....	112
5.5.6 M2 macrophages and tumor cell lines co-culture.....	113
5.5.7 CAR T cells killing assay.....	113
5.5.8 Cytokine-release assay.....	114
5.5.9 RNAseq analysis.....	114
5.5.10 Hepatic stellate cells immunofluorescence.....	115
5.6 In vivo experiments.....	116
5.6.1 <i>In vivo</i> functional assays.....	116
5.6.2 MRI images.....	117
5.6.3 Histopathological analysis.....	118
5.6.4 NanoString analysis.....	118
5.7 Statistical analysis.....	119
6. REFERENCES.....	120

ACRONYMS AND ABBREVIATIONS

ACT: Adoptive Cellular Therapy
ALI: Air-Liquid Interface Culture
ALL: Acute Lymphoblastic Leukemia
AST: Aspartate aminotransferase
 α -SMA: α -Smooth Muscle Actin
BCMA: B-Cell Maturing Antigen
CAF: Cancer Associated Fibroblast
CAIX: Carbonic Anhydrase IX
CAR: Chimeric Antigen Receptor
CCR: Chimeric Co-stimulatory Receptor
CD: Cluster differentiation
CDX: Cell line Derived Xenograft
CEA: Carcinoembryonic antigen
CLL: Chronic Lymphoblastic Leukemia
CNS: Central Nervous System
CR: Complete Response
CRC: Colorectal Cancer
CRS: Cytokine released syndrome
CTLA-4: Cytotoxic T-Lymphocyte protein 4
CXCL: Chemokine (C-X-C motif) ligand
DC: Dendritic cell
ECM: Extracellular matrix
EGFR ν III: Epidermal growth factor receptor variant III
EPCAM: Epithelial cellular adhesion molecule
ER: Endoplasmic Reticulum
FAO: Fatty Acid Oxidation
FAP: Fibroblast Activation Protein
FDA: Food and drug administration
FR- β : Folate Receptor β
GBM: Glioblastoma Multiforme
GM-CSF: Granulocyte-macrophage colony-stimulating factor

Gal: Galectin
GVHD: Graft-Versus-Host Disease
GVL: Graft-Versus-Leukemia
HSC: Hematopoietic Stem Cell
HPSE: Heparanase
HAI: Hepatic Artery Infusion
HepSC: Hepatic Stellate Cell
HSV-TK: Herpes Simplex Virus Thymidine Kinase
HBP: Hexosamine Biosynthetic Pathway
IL: Interleukin
ICANS: Immune effector Cell-Associated Neurotoxicity Syndrome
iCas9: Inducible Caspase 9
IDO: Indoleamine 2,3 dioxygenase
Ig: Immunoglobulin
IFN- γ : Interferon γ
Ko: Knock-out
LAG-3: Lymphocyte-activating 3
LV: Lentiviral Vector
LPS: Lipopolysaccharide
MM: Multiple Myeloma
MGL: Macrophage Galactose-specific Lectin
M1/M1-M: M1 Macrophage
M2/M2-M: M2 Macrophage
MHC: Major Histocompatibility Complex
mAb: Monoclonal antibody
NSG: immune-deficient NOD/SCID/IL2R γ ^{-/-}
NGFR: Nerve Growth Factor Receptor
NHL: Non-Hodgkin Lymphoma
NIH: National Institute of Health
NK: Natural Killer
OXPHOS: Oxidative Phosphorylation
OS: Overall Survival

PMN-MDSC: Polymorphonuclear Myeloid-Derived Suppressor Cells
PDL-1: Programmed Death Ligand-1
PD-1: Programmed cell Death Protein-1
PDGFR- β Platelet-derived Growth Factor Receptor β
PHA-L: Phytohemagglutinin-L
PPP: Pentose Phosphate Pathway
PBMC: Peripheral Blood Mononuclear Cell
PAMP: Pathogen Associated Molecular Pattern
PDAC: Pancreatic Ductal Adenocarcinoma
PDO: Patient Derived Organoid
SIGLEC: Sialic acid-binding Immunoglobulin-like Lectin
ScFv: Single-chain variable fragment
TIL: Tumor Infiltrating Lymphocytes
Th1: T helper 1 cell
TRUCK: T cells redirected for universal cytokine-mediated killing
TME: Tumor Microenvironment
TNF- α : Tumor Necrosis Factor α
TAA: Tumor Associated Antigen
TIM-3 T-cell immunoglobulin and mucin-domain containing-3
Treg: Regulatory T cell
TANs: Tumor Associated Neutrophils
TAMs: Tumor Associated Macrophages
TGF- β : Transforming growth factor β
TLR: Toll-like receptor
TCR: T cell receptor
TLS: Tumor lysis syndrome
TCA: Tricarboxylic acid cycle
UPR: Unfolded protein response
VH: Variable region of the heavy chain
VL: Variable region of the light chain
2DG: 2-deoxy-D-glucose

LIST OF FIGURES AND TABLES

Figure 1.1: Adoptive T-cell therapy process

Figure 1.2: Solid tumors obstacles for T cells fitness and functions

Figure 1.3: Models and tools to test efficacy and toxicity of CAR T cells

Figure 1.4: The hexosamine biosynthetic pathway (HBP)

Figure 3.1: CEA is expressed by CRC and PDAC cell lines and CRC patient-derived liver metastases

Figure 3.2: N-glycosylation blockade unmask the CEA antigen to antibody recognition and increases susceptibility to CEA CAR T cells

Figure 3.3: De-glycosylated tumors dampen M2 macrophages polarization

Figure 3.4: THP-1 derived M2 macrophages lose their immunosuppressive activity upon N-glycosylation blockade

Figure 3.5: N-glycosylation blockade inhibits M2 macrophages polarization

Figure 3.6: Primary M2 macrophages are less immunosuppressive upon N-glycosylation inhibition

Figure 3.7: N-glycosylation blockade downregulates immunosuppressive genes in M2 macrophages

Figure 3.8: De-glycosylated M2 macrophages acquire M1-like features

Figure 3.9: N-glycosylation inhibition reduces HepSCs activation

Figure 3.10: N-glycosylation blockade increases CEA CAR T cells functions despite the presence of TME cells

Figure 3.11: 2DG increases CEA CAR T cells killing capacity against PDOs from CRC-liver metastases

Figure 3.12: Intra-liver injection of CEA CAR T cells outperforms the intravenous one

Figure 3.13: Tumor engraftment does not impair human immune reconstitution in humanized mice

Figure 3.14: 2DG reduces the frequency of liver M2 macrophages in tumor-bearing *huSGM3* mice

Figure 3.15: Intra-liver administration of CEA CAR T cells better controls tumor growth in BxCP3-bearing *huSGM3* mice

Figure 3.16: TCR^{ko} CEA CAR T cells control tumor growth in LoVo-bearing *huSGM3* mice, without the occurrence of xeno-GvHD

Figure 3.17: Patient derived organoids from CRC-liver metastases develop metastatic lesions in the liver of *huSGM3* mice

Figure 3.18: N-glycosylation blockade increases CEA CAR T cells efficacy in LoVo-bearing *huSGM3* mice

Figure 3.19: N-glycosylation blockade downregulates myeloid immunosuppressive gene expression in *huSGM3* mice

Table 1.1: Commercially available CAR T cells products

Table 1.2: Advanced outcomes of commercial CAR T cells products

Table 1.3: Ongoing clinical trials of CAR T cells against solid tumors

Table 3.1: PDOs engraftment in *huSGM3* mice

Table 3.2: PDOs engraftment in *huSGM3* mice infused with different cord blood (CB) donors

1. INTRODUCTION

1.1 CAR T cell therapy of cancer: clinical point of view

In recent years, the use of cell-based therapies has animated the field of cancer immunotherapy. Starting with tumor-infiltrating lymphocytes and moving to engineered T cells with antigen specific T cell receptors (TCRs) or chimeric antigen receptors (CARs), each of these technological strategies displayed a gradual improvement for the treatment of neoplastic diseases (Leon et al., 2020).

1.1.1 Adoptive T cell therapy and CAR T cells for cancer

The concept of the immune system as a tool for treatment of neoplastic diseases was conceived in the twentieth century with Paul Erlich, who hypothesized that tumors in human body are eradicated by immune cells. This idea was confirmed when, in 1956, a leukemic patient received for the first-time hematopoietic stem cell (HSC) transplantation from the monozygotic twin as treatment, resulting in a complete tumor remission through graft-versus-leukemia (GVL) effect. However, allogenic HSCs transplantation presented the toxic effect of graft-versus-host disease (GVHD), limited by the delayed transfusion of donor lymphocytes, after T cell-depleted stem cell transplantation (Thomas et al., 1957). In the late 1900s, the discovery of monoclonal antibodies (mAbs) allowed new therapeutic products to be available for the cancer field (Maloney et al., 1997; Barrett et al., 2014). Indeed, starting with the Food and Drug Administration (FDA) approval of Rituximab, many other mAbs have been approved, including bi-specific antibodies such as the anti-CD19/anti-CD3 Blinatumomab, to tackle both T cells and B-cell leukemia blasts (Barret et al., 2014; Zugmaier et al., 2013). Impressive clinical results were reported, but unfortunately mAbs showed a poorly predictable pharmacokinetics and pharmacodynamics.

A crucial contribution in the field of cellular immune-gene therapy was given in the 1980s by Steven Rosenberg from the US National Institute of Health (NIH), who pioneered the concept of adoptive T cell therapy. He based his work using tumor-infiltrating lymphocytes (TILs) to treat metastatic melanoma. Lymphocytes isolated from tumor biopsies were expanded *ex vivo* with interleukin (IL)-2 and then reinfused

intravenously in the same patient, where they induced complete tumor regression in combination with IL-2 (Rosenberg et al., 1988; Rosenberg et al., 2011).

TILs strategy, however, presents intrinsic limitations, including the extensive manipulation and expansion for a feasible therapeutic product and the paucity of functional anti-tumor lymphocytes in most patients affected by other malignancies rather than melanoma (Dudley et al., 2013; Hinrichs & Rosenberg, 2014).

To overcome these limitation, cellular immune-gene therapy rapidly evolved, leading to the generation of T cells simply retrieved from peripheral blood and genetically modified *ex vivo* to express TCRs or CARs. With both approaches it is possible to generate large numbers of engineered T cells within few weeks, consistent with clinical application and T-cell fitness preservation. Even if these technologies share many advantages, CAR and TCR-based strategies are different. TCR-based T cells have shown successful results in melanoma, myeloma and HPV-associated cancers (Morgan et al., 2006; Robbins et al., 2011; Doran et al., 2019), but have also demonstrated some limitations. First, despite the potential of targeting any peptide, the strategy is MHC-restricted. Second, MHC downregulation or antigen processing machinery impairment, as determinants for tumor escape mechanism, are concrete possibilities (Seliger et al., 2002).

Synthetic CARs can overcome MHC restriction and direct T cell-mediated cytotoxicity to any surface target molecule. CAR T cells were described in the late 1900s as artificial molecules composed by a single chain variable fragment (scFv) derived from monoclonal antibodies fused to the signaling domain of TCR ζ -chain. Compared to mAbs, CAR T cells show a wider bio distribution, proliferative capacity, migration and multiple effector functions. Moreover, their tumor recognition is MHC-independent, making them extensively applicable to multiple individuals. Contrary to TCRs, CARs can bind also surface carbohydrate and glycolipid structures, but lack the ability to target intracellular molecules (Leon et al., 2020).

CARs are synthetic molecules and their design has been modified over time, to improve CAR T cell efficacy against different malignancies. The ligand-binding domain is commonly composed by single chain fragment variants, where variable heavy (VH) and light (VL) chains are separated by a flexible linker. The affinity and avidity of this domain affect CAR T cell functionality and represent a key parameter that can be modified to

increase CAR specificity and reduce “on-target, off-tumor” toxicity, a CAR-T related side effect relevant when the target antigen is also expressed on healthy tissues (Park et al., 2017). Indeed, anti-ErbB2 CAR with a micromolar affinity showed selective cytotoxicity and increased efficacy mice, compared to high-affinity scFv CAR T cells (Chmielewski et al., 2004; Liu et al., 2015). However, reducing affinity to improve CAR specificity may also reduce CAR potency. Indeed, anti-ROR1 CARs with a higher-affinity scFv demonstrated higher therapeutic index compared to scFv with lower affinity (Hudecek et al., 2013). Avidity is another important parameter regarding multiple receptor-ligand interactions and it is modulated by ligand densities, CAR expression levels and affinity of ligand-binding domains (Jayaraman et al., 2020).

Another crucial element of CAR structure is the spacer domain, which connects the ligand-binding domain to the transmembrane domain, conferring flexibility to the scFv, improving the binding with the specific target epitope. Spacer domain modulation is a relevant point to regulate the distance between CAR T cells and target cells, which is crucial to obtain a functional immunological synapse formation. To preserve optimal synapse distance, shorter spacers are preferred for membrane-distal epitopes, while longer spacers are required for membrane-proximal epitopes (Hudecek et al., 2013). Apart from limiting exclusion of inhibitory phosphates, such as CD45, the distance between epitope and paratope can also impair delivery of granzymes and perforins, altering the cytolytic effect of CAR T cells (Woodsworth et al., 2015). The most commonly used long spacer is the one that includes CH₂CH₃ portion of immunoglobulins G1 (IgG1) or G4 (IgG4) (Hudecek et al., 2015; Haso et al., 2013), whereas the short ones derive from the extracellular portions of CD28 (Haso et al., 2013; Lynn et al., 2015), CD3 (Weijtens et al., 1996), CD4 (Willemsen et al., 2005) or CD8 (Carpenito et al., 2009; Hasom et al., 2013). Several groups reported that CAR T cells endowed with IgG spacers display reduced anti-tumor activity due to their premature clearance by Fc-receptor-expressing myeloid cells (Jonnalagadda et al., 2015). To avoid this phenomenon several approaches have been pursued, including mutation or deletion in the CH₂CH₃ spacer sequences (Smith et al., 2019). In addition to these strategies, another possibility is NGFR-derived spacers, previously reported by our group; this technology presents the additional advantage of enabling CAR-T cell enrichment through

clinical-grade magnetic beads purification and the *in vivo* monitoring during time (Casucci et al., 2018).

Transmembrane domains in CAR structures work in the signal transduction from ligand recognition to the intracellular domain, which is a key part for the correct functionality of CAR T cells. In classical T cells, the intracellular signaling domain of the TCR-CD3 complex transduces the necessary “signal 1” after the engagement with the target antigen and co-stimulatory receptors, such as CD28, are required for “signal 2”, important to sustain signaling and T cells proliferation, avoiding anergy. (Jayaraman et al., 2020).

First-generation CARs were characterized by the absence of co-stimulatory domains, lacking the “second signal” that is crucial for correct CAR functionality. These suboptimal products were first evaluated in pioneering clinical trials targeting the tumor antigen Carbonic anhydrase IX (CAIX) in patients with renal cancer (Lamers et al., 2006) and CD171/LI-CAM against pediatric neuroblastoma (Park et al., 2007). Even if these trials did not demonstrate significant anti-tumor activity, they were instrumental to the implementation aimed at improving CAR T cells persistence and function. Indeed, these first-generation CARs failed to elicit a robust cytokine response, necessary to support T cell expansion and to guarantee T cell persistence *in vivo*.

For these reasons the following improvement of CAR design was the inclusion of additional co-stimulatory signals, such as CD28 (Kowolik et al., 2006; Savoldo et al., 2011), 4-1BB (Milone et al., 2009; Lee et al., 2002), OX40 (Pulè et al., 2005) or ICOS (Guedan et al., 2014), that sustain T cell proliferation, persistence and potency. These implemented constructs were named “second” or “third”-generation CARs (Carpenito et al., 2009; Finney et al., 2004), according to the presence of one or more co-stimulatory signals, respectively. Most commonly second generation CARs present CD28 or 4-1BB which differ in metabolism (Kawalekar et al., 2016), T-cell memory development (Kalos et al., 2012; Kawalekar et al., 2016), and antigen-independent tonic signaling (Long et al., 2015). The first strong clinical evidence of the superior activity of endo-costimulated CARs compared to first generation ones derived from the work of Barbara Savoldo and Gianpietro Dotti. Their group measured the activity of two autologous CAR-T cells products, both targeting CD19 in patients with non-Hodgkin lymphomas (NHLs). Patients were simultaneously infused with a first and a second-generation CAR T cells

and CD28-endo-costimulated CAR displayed enhanced expansion and persistence with increased efficacy in patients (Savoldo et al., 2011).

Although a variety of configurations of the co-stimulatory domain has been proposed over time, several groups have developed a variety of combination of the co-stimulatory domain and exhaustive comparisons have just more recently emerged. CD28 based CAR T cells proliferate and expand more rapidly and release large amounts of Th1 cytokines like IL-2 and interferon- γ (IFN- γ); 4-1BB endo-costimulated CAR T cells, conversely, show a more gradual response, but with a less exhausted phenotype and increased *in vivo* persistence (Frigault et al., 2015; Van Der Stegen, Hamieh et al., 2015). These distinctions also reflect typical metabolic pathways. CD28-CAR T cells rely on aerobic glycolysis, resulting in effector memory phenotype with a reduced persistence capacity. In contrast, 4-1BB CAR T cells rely on oxidative phosphorylation, leading to an early memory phenotype and a prolonged *in vivo* persistence (Van Der Stegen et al., 2015; Kawalekar et al., 2016). Recently, Majzner et al. demonstrated that CD19 CAR endo-costimulated with CD28 outperforms CD19 CAR with 4-1BB to tackle tumor cells with low antigen density. They have shown that the replacement of CD8 hinge-transmembrane (H/T) with a CD28-H/T reduces the threshold for antigen recognition also in CD19-4-1BB CARs, due to improved immunological synapse formation (Majzner et al., 2020). Moreover, the group of Michel Sadelain implemented the design of CD28-CD3 ζ endo-costimulated constructs, since the simultaneous signaling through CD28 and CD3 ζ could lead to excess T cell differentiation and exhaustion. For these reasons, they generated several CAR constructs with calibrated ITAM activities by mutating selected tyrosine residues. It was observed *in vivo* that one particular mutant outperforms the others, and also classical 28 ζ CAR as well, in terms of improved therapeutic index and increased long-lived memory T cells (Feucht et al., 2019).

Third-generation CARs, with both CD28 and 4-1BB domains, have been exploited against different antigens such as CD19, GD2, PSMA and mesothelin. These studies showed that third-generation CAR T cells present stronger activation with a superior tumor eradication capacity (Ramos et al., 2018; Zhong et al., 2010; Quintarelli et al., 2018; Carpenito et al., 2009). Anti-mesothelin CAR T cells endowed with ICOS and 4-1BB costimulatory domains demonstrated increased anti-tumor potency and prolonged *in vivo* persistence (Guedan et al., 2018). However, the superiority of third-generation

CAR T cells over second-generation is still under discussion. Indeed, a study showed that anti-PSCA CARs with CD28-4-1BB domains confer increased *in vivo* persistence, but a reduced anti-tumor potency, in comparison to second-generation CAR (Abate-Daga et al., 2014).

More recently, fourth-generation CARs (or “armored” CARs) that introduce additional stimulatory domains have been studied. Armored CAR T cells named “T cells redirected for universal cytokine-mediated killing” (TRUCK) were engineered to secrete inflammatory cytokine IL-2 to activate innate immune response against tumor cells (Chmielewski et al., 2017). Other soluble secreted factors have been investigated, including IL-15 or IL-18 to increase T cell expansion, but also CCL19 and IL-7 to stimulate immune cells and favor a persistent memory response against tumors (Adachi et al., 2018; Hoyos et al., 2010).

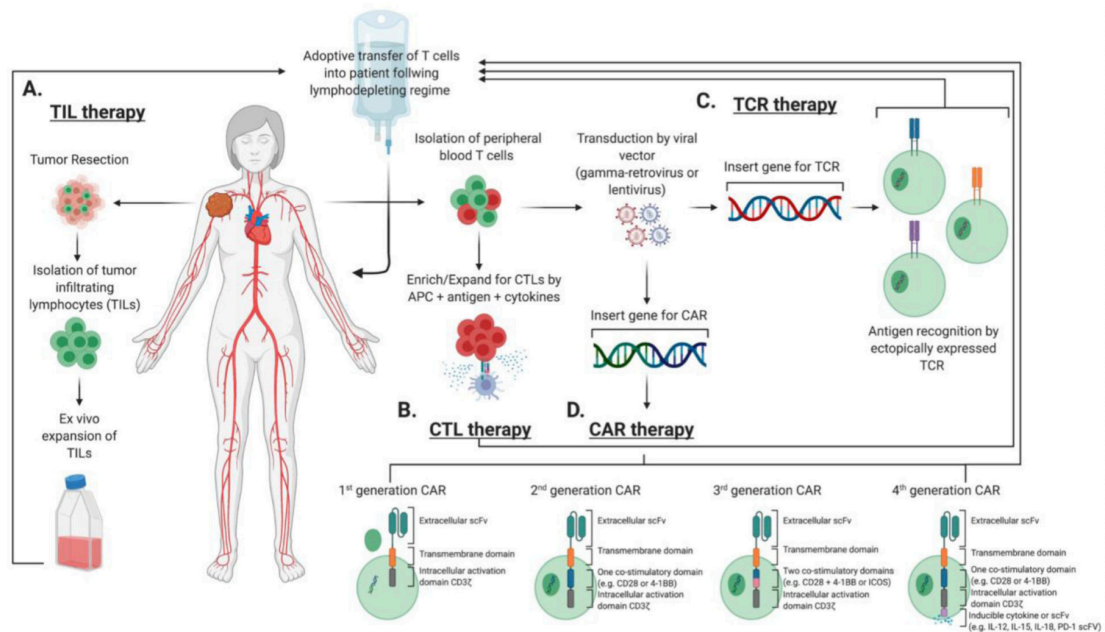


Figure 1.1 | Adoptive T-cell therapy process. (A) TILs are isolated directly from tumor resections, *ex vivo* expanded and infused back into the patient. (B) CTLs derived from peripheral blood T cells reactive to specific TAA. (C & D) CAR and TCR engineered T cells are generated from PBMCs in a manufacture process including the activation of T cells and the subsequent modification by viral vectors to express a specific antitumor TCR or CAR. In all these ACT approaches, patients are pretreated with a lymphodepletion regime. TILs, tumor-infiltrating lymphocytes; CTLs, cytolytic T cells; TAA, tumor-associated antigen; CAR, chimeric antigen receptor; TCR, T cell receptor; PBMCs, peripheral blood mononuclear cells; ACT, adoptive T-cell therapy.

From Leon E., Ranganathan R., Savoldo B., *Semin. Immunol.* 2020

1.1.2 CAR T cell therapy for hematological tumors

The first application of CAR T cell therapy has been for hematological B-cell malignancies, like acute lymphoblastic leukemia (ALL), chronic lymphoblastic leukemia (CLL) and multiple myeloma (MM), easier to target than solid cancers. So far, six CAR T cell products have been approved by the FDA, four targeting CD19 antigen and two targeting BCMA (Haslauer et al., 2021).

The first CAR T cell product that receive U.S. FDA approval was Tisagenlecleucel (KYMRIAH, Novartis) in August 2017 to treat patients aged 25 or younger with relapsed or refractory B-cell acute lymphoblastic leukemia (B-ALL). The approval came after the publication of the results from the phase II multicenter ELIANA trial, which demonstrated complete response (CR) rate around 81% at 3 months and overall survival (OS) at 12 months around 76% (Maude et al., 2018). In the real world, in 255 patients treated so far, CR rate was assessed to be around 86%, and the estimated 12-month event-free survival rates were 52% (Pasquini et al., 2021). One year later this promising CAR T cell product was approved also for the treatment of adult relapsed or refractory diffuse large B cell lymphoma, after the JULIET trial. The CR rate was around 40% in the pivotal JULIET trial and in the real world (155 treated patients) (Schuster et al., 2019). Tisagenlecleucel is an anti-CD19 CAR endowed with 4-1BB costimulatory domain, but in 2017 an anti-CD19 CAR endo-costimulated with CD28 domain, named Axicabtagene ciloleucel (YESCARTA, Kite Pharma) was also approved by FDA. In large B-cell lymphoma patients treated with Axicabtagene, the CR and 12-months progression-free survival were 58% and 44%, respectively, in the ZUMA-1 trial, compared with 64% and 45% among 275 patients treated in the real world (Neelapu et al., 2017; Nastoupil et al., 2020). Last year, in 2021, the FDA approval of Axicabtagene ciloleucel was extended to treat follicular lymphoma (from ZUMA-5 trial), where it led to a complete response of around 80% and a progression-free survival around 74% (Jacobson et al., 2020). In the last two years, other three CAR T cell products have been approved and commercialized. In July 2020, Brexucabtagene autoleucel (TECARTUS, Kite Pharma) has been approved by FDA for the treatment of mantle cell lymphoma, after the results obtained from ZUMA-2 trial. In this clinical trial 68 patients were treated with CR around 67% and with progression free survival and overall survival at 12 months around 61% and 83%, respectively (Wang et al., 2020). In 2021, Lisocabtagene maraleucel (BREYANZI, Juno

Therapeutics) has been approved for relapsed and refractory B-cell lymphoma, thanks to the results obtained from TRANSCEND trial, showing CR around 53% and progression-free survival around 44% (Abramson et al., 2020). The most recent FDA approved CAR T cell product was Idecabtagene vicleucel (ABECMA, BMS and Bluebird Bio) to treat patients with relapsed or refractory multiple myeloma, targeting the B-cell maturing antigen (BCMA). The KarMMa trial has shown a complete response around 33% in 128 treated patients and an overall survival of 78% at 12 month (Munshi et al., 2021). Finally, in the beginning of 2022 FDA approved the application of Ciltacabtagene autoleucel (CARVYKTY, Janssen Biotech) targeting BCMA for the treatment of adult patients with relapsed or refractory multiple myeloma. The safety and efficacy profile was evaluated in the CARTITUDE-1 clinical trial and in 97 patients enrolled the overall response rate was 97.9% and the duration of response was around 22 months (fda.gov).

Beside these six commercialized CAR T cell products, multiple CAR T cells have been evaluated in ongoing clinical trials, in particular for AML (Frey et al., 2020; Ghorashian et al., 2019) and large B lymphoma (Cappell et al., 2020), but also for the treatment of CLL (Frey et al., 2020), MM (Zhao et al., 2018), myeloid malignancies (Baumeister et al., 2019) and Hodgkin lymphoma (Ramos et al., 2020).

All the numerous ongoing clinical trials suggest that the therapeutic arsenal of CAR T cells for hematological malignancies is growing rapidly, and represent a promising therapeutic strategy.

Name	Indication	Date of FDA Approval	Manufacturer	Trial Data Reported
Tisagenlecleucel	Pediatric and young adult (age ≤ 25) R/R acute lymphoblastic leukemia	August 30, 2017	Novartis	Pivotal ELIANA ¹ and real world ²
Axicabtagene ciloleucel	R/R large B-cell lymphoma (DLBCL, PMBCL, high-grade B-cell lymphoma, transformed FL)	October 18, 2017	Kite Pharma	Pivotal ZUMA-1 ³ and real world ⁴
Tisagenlecleucel	Adult R/R DLBCL	May 1, 2018	Novartis	Pivotal JULIET ⁵ and real world ²
Brexucabtagene autoleucel	Mantle cell lymphoma	July 24, 2020	Kite Pharma	Pivotal ZUMA-2 ⁷⁹
Lisocabtagene maraleucel	R/R large B-cell lymphoma	February 5, 2021	Juno Therapeutics	Pivotal TRANSCEND NHL001 ⁵¹
Axicabtagene ciloleucel	R/R FL	March 5, 2021	Kite Pharma	Pivotal ZUMA-5 ²⁰
Idecabtagene vicleucel	Multiple myeloma	March 26, 2021	BMS and Bluebird Bio	Pivotal KarMMa (not published)

Abbreviations: DLBCL, diffuse large B-cell lymphoma; FDA, U.S. Food and Drug Administration; FL, follicular lymphoma; PMBCL, primary mediastinal B-cell lymphoma; R/R, relapsed/refractory.

Table 1.1 | Commercially available CAR T cell products.
From Gill S. and Brudno J.N., 2021 ASCO educational book

Name	Reference	Patients	Responses	Survival
Pediatric and Young Adult (≤ 25 years) Patients With R/R Acute Lymphoblastic Leukemia				
Tisagenlecleucel	Pivotal ELIANA ¹	92 enrolled, 75 treated	Per protocol: CR/CRi, 81% at 3 months	Per protocol: EFS, 50%; OS, 76% (12 months)
Tisagenlecleucel	Real world ²	255 treated	CR, 86%	EFS, 52%; OS, 77% (12 months)
R/R Large B-Cell Lymphoma				
Axicabtagene ciloleucel	Pivotal ZUMA-1 ³	111 enrolled, 101 treated	ORR, 82%; CR, 58%	PFS, 44% (12 months); OS, 52% (18 months)
Axicabtagene ciloleucel	Real world ⁴	275 treated	ORR, 82%; CR, 64%	PFS, 45%; OS, 64% (12 months)
Axicabtagene ciloleucel	Real world ⁵⁰	122	ORR, 70%; CR 50%	OS, 57% (12 months)
Tisagenlecleucel	Pivotal JULIET ⁵	165 enrolled, 93 treated	ORR, 52%; CR, 40%	RFS, 65%; OS, 49% (12 months)
Tisagenlecleucel	Real world ²	155 treated	ORR, 62%; CR, 40%	PFS, 39%; OS, 71% (6 months)
Lisocabtagene maraleucel	Pivotal TRANSCEND NHL001 ⁵¹	344 apheresed, 269 treated, 256 evaluable for efficacy	ORR, 73%; CR, 53%	PFS, 44%; OS, 58% (12 months)
Mantle Cell Lymphoma				
Brexucabtagene autoleucel	Pivotal ZUMA-2 ⁷⁹	74 enrolled, 68 treated	ORR, 93%; CR, 67%	PFS, 61%; OS, 83% (12 months)
R/R Follicular Lymphoma				
Axicabtagene ciloleucel	Pivotal ZUMA-5 ²⁰	123 treated (follicular lymphoma only)	ORR, 94%; CR, 80%	PFS, 74%; OS, 93% (12 months)
Multiple Myeloma (BCMA)				
Idecabtagene vicleucel	Pivotal KarMMa ¹¹⁵	140 enrolled, 128 treated (dose escalation)	ORR, 73%; CR, 33%; MRD-ve, 26%	Median PFS, 8.8 months; OS 78% (12 months)

Abbreviations: CR, complete response; CRi, CR with incomplete hematologic recovery; EFS, event-free survival; MRD-ve, minimal residual disease negative; ORR, overall response rate; OS, overall survival; PFS, progression-free survival; RFS, relapse-free survival; R/R, relapsed/refractory.

Table 1.2 | Advanced outcomes of commercial CAR T cell products.
From Gill S. and Brudno J.N., 2021 ASCO educational book

1.1.3 CAR T cell therapy for solid tumors

Focusing on the outstanding clinical results achieved with CD19 CAR T cell therapy to treat B cell malignancies, several clinical trials have been initiated all over the world targeting solid tumors. However, compared to hematologic malignancies, solid tumors share unique challenges to CAR T cell therapy. First, solid tumors display high antigen heterogeneity, which contribute to an escape mechanism from CAR T cells that commonly recognize a single target antigen. Second, solid tumors are often surrounded by physical barriers, such as the stroma, which prevent T cell infiltration. Moreover, solid malignancies are characterized by a highly immunosuppressive tumor microenvironment (TME), which inhibits T cell function and leads to T cell exhaustion (Hou, et al., 2021).

GD2 is one of the most-studied tumor associated antigen for brain tumors, specifically for neuroblastoma and glioblastoma. Immunotherapy with anti-GD2 CAR T cells has demonstrated to be safe and shown some objective clinical responses. However, it has also provided insights into reasons for limited success, including low T cell persistence and a suppressive TME. Tumino et al. reported that polymorphonuclear myeloid-derived suppressor cells (PMN-MDSCs) confer a resistance mechanism to anti-GD2 CAR T cells, since this myeloid population increases in patients with relapse. In this interesting study, they have demonstrated that isolated PMN-MDSCs inhibit *in vitro* the anti-tumor cytotoxicity of different generations of GD2 CAR-T, downregulating genes involved in cell activation, signal transduction, inflammation and cytokine/chemokine secretion. (Tumino et al., 2021). Targeting central nervous system (CNS) tumors requires specific and careful considerations of the optimal delivery of CAR T cells. An ongoing phase I trial exploits the feasibility, safety and efficacy of treatment with anti-IL13R α 2 CAR T cells in patients with recurrent and refractory malignant glioblastoma. Results from a patient case study related to this clinical trial have shown a transient complete response when CAR T cell are administrated intraventricular. Moreover, an immediate increase in endogenous immune cells and inflammatory cytokines was detected after each intraventricular CAR T cells infusion, suggesting a recruitment and stimulation of the host immune system, able to eradicate also the antigen negative tumor cells. The clinical response in this patient was sustained for 7.5 months after therapy initiation and improvements in quality of life were reported (Brown et al., 2016). In the context of glioblastoma, another CAR T target is the human epidermal growth factor receptor 2

(HER2), a tyrosine kinase receptor overexpressed in glioblastoma, but also in other human cancers, including pancreatic cancer. In patients with progressive glioblastoma, a phase I dose-escalation clinical trial showed promising results (Ahmed et al., 2018), while in a phase I study for advanced pancreatic cancers of 11 patients enrolled, one patient reported a partial response after 4.5 months and 5 patients achieved stable disease (Feng et al., 2018). Similarly, anti-EGFRvIII CAR T cells also proved to be safe in 10 glioblastoma patients, even though antigen loss and tumor heterogeneity were the major source of adaptive resistance to therapy (O'Rourke et al., 2017).

Besides CNS antigens, other typically targeted antigens in on-going clinical trials for solid tumors are PSCA, PSMA and CEA. PSCA is the prostate stem cell antigen, overexpressed in pancreatic and prostate cancers. Regarding PSCA for prostate cancer, one phase I trial is investigating anti PSCA-CAR T cell therapy for the treatment of metastatic castration-resistant prostate cancer, studying safety, tolerability and recommended phase II dose (Patel et al., 2022).

CEA, the carcinoembryonic antigen, is a classical tumor marker overexpressed in more than 80% of colorectal cancer patients, but also in other tumor types such as pancreatic cancer and CEA positive liver metastases. Interestingly, even before clinical testing of CAR T cells, CEA has been exploited as target antigen for TCR-based immunotherapy in a clinical trial of patients with metastatic colorectal cancer (Parkhurst et al., 2011). In this clinical experience, all patients have shown strong reductions in serum CEA levels, and one patient showed regression of cancer metastases to the lung and liver. However, all three patients developed severe inflammatory colitis due to the recognition by adoptively transferred T cells of cytoplasmic CEA expressed by healthy epithelial cells throughout the gastrointestinal tract. As consequence, the clinical trial was halted from the FDA.

Despite this first disappointing result, CEA has been extensively investigated in clinical trials as a suitable target for CAR products. Indeed, this antigen is exceptionally promising due to its peculiar distribution pattern on normal adult pulmonary and gastrointestinal epithelial cells. In fact, its expression is restricted to the apical surface of cell membranes, thus becoming invisible to immune cells (Nap et al., 1988). However, during malignant transformation the apical-basal polarity is lost and CEA acquires a homogeneous pattern of expression on the cell surface, hence becoming visible to the

circulating immune cells as well (Saeland et al., 2012). Nowadays, clinicaltrials.gov lists 12 trials that target CEA with CAR T cells, three of which actively recruiting.

Altogether, the clinical experience of CEA CAR T cells proved hint of efficacy in the absence of significant toxicities in patients with liver metastasis of pancreatic cancer or colorectal carcinoma. An exception must be made for one phase I clinical trial, testing the infusion of high doses of first generation anti-CEA CAR T cells in patients with relapsed-refractory gastrointestinal tumor, in which one cohort of patients experienced an acute respiratory toxicity. This adverse event was the result of CEA expression on normal lung epithelium, which hints to a possible on-target off-tumor reaction as the primary trigger of toxicity. Interestingly, however, clinical manifestations also included raised levels of inflammatory cytokines, including IL-6, which might implicate another CAR T related toxicity, cytokine released syndrome (CRS) (Thistlethwaite et al., 2017). Another step forward, trying to improve the therapeutic index of CEA CAR T cells for the treatment of liver metastases, was exploited in two different phase I/Ib clinical trials. In these studies, the regional delivery of anti-CEA CAR T cells through hepatic artery infusion (HAI) was evaluated. These trials confirmed the safety of this delivery route with promising signs of clinical activity (Katz et al., 2015; Katz et al., 2020). More recently, the same group reported a case study where they tested the safety and feasibility of local CEA CAR T injection with Pressure-Enabled Drug Delivery (PEDD), a device designed to overcome high intra-tumoral pressure, for treatment of liver metastases. They reported that this combinatory strategy with three doses of CEA CAR T cells and IL-2 delivery demonstrated a complete metabolic response within the liver, durable and sustained for 13 months, without any serious adverse events (Katz et al., 2020).

So far, CEA CAR T cell therapy for liver metastases represent an interesting strategy, but with still limited application due to the efficacy to be improved and the toxicities effects to be managed.

Antigen target	Number of unique CARs in active clinical trials	CAR generation	Number of CARs	Clinical trial phase	Number of trials	Clinical trial identifiers
AXL	2	Third	1	I	1	NCT03198052, NCT03393936
		Unspecified	1	I/II	1	
B7-H3	7	Second	3	I	5	NCT03198052, NCT04385173, NCT04185038, NCT04077866, NCT04483778, NCT04483778, NCT04432649
		Third	1			
		Fourth	1	I/II	2	
		Unspecified	2			
CD147	2	Unspecified	2	I	2	NCT03993743, NCT04045847
CD171	3	Second	2	I	3	NCT02311621, NCT02311621, NCT02311621
		Third	1			
CD20	1	Unspecified	1	I	1	NCT03893019
CD44v6	2	Fourth	2	I/II	2	NCT04430595, NCT04427449
CD70	2	Unspecified	2	I	1	NCT02830724, NCT04438083
				I/II	1	
CEA	6	Unspecified	6	I	4	NCT03818165, NCT04348643, NCT03682744, NCT02850536, NCT04513431, NCT04037241
				I/II	1	
				II/III	1	
CLDN18.2	3	Unspecified	3	I	3	NCT04404595, NCT04467853, NCT03874897
CLDN6	1	Unspecified	1	I/II	1	NCT04503278
DLL3	1	Unspecified	1	I	1	NCT03392064
DR5	2	Unspecified	2	I/II	2	NCT03638206, NCT03941626
EGFR	6	Second	3	I	6	NCT03198052, NCT03638167, NCT03542799, NCT03618381, NCT03618381, NCT04153799
		Third	1			
		Fourth	2			
EGFRvIII	2	Unspecified	2	I/II	2	NCT03638206, NCT03941626
EpCAM	4	Second	1	I	2	NCT03563326, NCT03013712, NCT02915445, NCT04151186
		Third	1			
		Unspecified	2	N/A	1	
ErbB	1	Second	1	I/II	1	NCT01818323
FR α	2	Second	1	I	1	NCT03585764, NCT03185468
		Fourth	1			
GD2	13	Second	2	I	9	NCT03356795, NCT04196413, NCT04539366, NCT02761915, NCT03373097, NCT02765243, NCT04099797, NCT03635632, NCT04430595, NCT03721068, NCT02992210, NCT01953900, NCT01822652
		Third	2			
		Fourth	6	I/II	4	
		Unspecified	3			
gp100 (MHC-I)	1	Second	1	I	1	NCT03649529
GPC3	10	Second	1	I	10	NCT03198052, NCT04506983, NCT03198546, NCT03198546, NCT04121273, NCT04377932, NCT02905188, NCT02932956, NCT03980288, NCT03884751
		Third	2			
		Fourth	3			
		Unspecified	4			
HER2	7	Second	3	I	6	NCT03198052, NCT03500991, NCT03696030, NCT04430595, NCT02442297, NCT04511871, NCT00902044
		Third	1			
		Fourth	1	I/II	1	
		Unspecified	2			

Antigen target	Number of unique CARs in active clinical trials	CAR generation	Number of CARs	Clinical trial phase	Number of trials	Clinical trial identifiers
IL-13Ra2	2	Second	2	I	2	NCT04510051, NCT02208362
LeY	2	Second	1	I	2	NCT03851146, NCT03198052
		Third	1			
LFA1	1	Third	1	I	1	NCT04420754
MMP2	1	Second	1	I	1	NCT04214392
MSLN	18	Second	3	I	11	NCT03198052, NCT03638206, NCT03356795, NCT03941626, NCT04503980, NCT04489862, NCT03747965, NCT03814447, NCT03916679, NCT03638193, NCT03799913, NCT03545815, NCT03497819, NCT03323944, NCT03615313, NCT03054298, NCT02414269, NCT02792114
		Third	1	I/II	6	
		Fourth	4	N/A	1	
		Unspecified	10			
MUC1	5	Third	1	I	1	NCT03198052, NCT03356795, NCT03633773, NCT03706326, NCT03525782
		Unspecified	4	I/II	4	
MUC1*	1	Second	1	I	1	NCT04020575
MUC16	1	Fourth	1	I	1	NCT03907527
MUC16ecto	1	Fourth	1	I	1	NCT02498912
NECTIN4	1	Fourth	1	I	1	NCT03932565
NKG2D	1	Second	1	I	1	NCT03692429
NKG2DL	2	Second	1	I	2	NCT04270461, NCT04107142
		Unspecified	1			
PSCA	3	First	1	I	2	NCT03198052, NCT03873805, NCT02744287
		Second	1	I/II	1	
		Third	1			
PSMA	6	Fourth	4	I	3	NCT03356795, NCT04053062, NCT04227275, NCT03089203, NCT03185468, NCT04429451
		Unspecified	2	I/II	3	
ROR1	1	Unspecified	1	I	1	NCT02706392
ROR2	2	Unspecified	2	I	1	NCT03960060, NCT03393936
				I/II	1	
TM4SF1	1	Unspecified	1	N/A	1	NCT04151186
TnMUC1	1	Unspecified	1	I	1	NCT04025216
Unspecified	6	Fourth	2	I	1	NCT03356782, NCT04085159, NCT04433221, NCT03184753, NCT03170141, NCT03356808
		Unspecified	4	I/II	5	

AXL, AXL receptor tyrosine kinase; CAR, chimeric antigen receptor; CEA, carcinoembryonic antigen; CLDN18.2, claudin 18 isoform 2; CLDN6, claudin 6; DLL3, delta-like canonical notch ligand 3; DR5, death receptor 5; EGFR, epidermal growth factor receptor; EGFRvIII, EGFR variant III; EpCAM, epithelial cell adhesion molecule; FR α , folate receptor- α ; GD2, disialoganglioside; gp100, glycoprotein 100; GPC3, glypican 3; HER2, human epidermal growth factor receptor 2; IL-13Ra2, interleukin 13 receptor α 2; LeY, Lewis Y; LFA1, lymphocyte function-associated antigen 1; MHC-I, major histocompatibility complex class I; MMP2, matrix metalloproteinase 2; MSLN, mesothelin; MUC1, mucin 1; MUC1*, extracellular domain of cleaved mucin 1; MUC16ecto, mucin 16 ectodomain; NECTIN4, nectin cell adhesion molecule 4; NKG2D, natural killer group 2D; NKG2DL, natural killer group 2D ligand; PSCA, prostate stem cell antigen; PSMA, prostate-specific membrane antigen; ROR1, inactive tyrosine kinase transmembrane receptor 1; TM4SF1, transmembrane 4L six family member 1; TnMUC1, Tn glycoform of mucin 1.

Table 1.3 | Ongoing clinical trials of CAR T cells against solid tumors.
From Hou A.J., Chen L.C., Chen Y.Y., 2021 *Nat. Rev./Drug Discovery*

1.2 CAR T cell therapy of cancer: efficacy and related toxicities

As reported in the previous paragraph, clinical trials of CAR T cells targeting CD19 and BCMA have shown clear efficacy in B-cell malignancies and multiple myeloma. Despite the interesting results obtained from clinical trials, the percentage of complete response could be increased, since around 30-50% of patient will have disease relapse. The efficacy of CAR T cells, however, is not only threatened by disease relapse due to resistance mechanism, but also hindered by severe or even fatal toxicities.

1.2.1 Clinical and biological determinants of CAR-related toxicities

One of the most common CAR related toxicity, emerging from clinical experience with CD19 CAR T cells and now also from BCMA CAR T cell trials, is the cytokine release syndrome (CRS). CRS is an acute and systemic inflammatory syndrome, which presents with systemic symptoms, such as fever, hypotension, malaise, coagulopathy and capillary leak, but can also affect any organ system of the body. The syndrome is initiated by activation and proliferation of CAR T cells soon after recognition of the cognate antigen on target cells and is characterized by peak serum concentration of IL-6, besides a broad spectrum of inflammatory mediators including IFN- γ , tumor necrosis factor- α (TNF- α), GM-CSF and IL-8 (Lee et al., 2014). CRS is treated with anti-IL-6 receptor- α (IL-6R α) antibody, such as Tocilizumab, TNF inhibitors or corticosteroids. Other important CRS drivers are GM-CSF and IL-1; indeed, in a xenograft model of ALL, antibody inhibition or genetic knockout of the gene encoding GM-CSF (CSF2) in CAR T cells demonstrated the ability to prevent CRS reaction in the presence of human peripheral blood mononuclear cells (PBMCs) (Sternier et al., 2019). Moreover, blockade of IL-1 through the treatment with IL-1 receptor agonist Anakinra was successful to protect mice from CRS mortality (Giavridis et al., 2018; Norelli et al., 2018). Correlated to CRS, other CAR-related toxicities include severe cytopenia, observed in the majority of patients with relapsed and refractory acute lymphoblastic leukemia. They developed neutropenia, anemia and thrombocytopenia and patients with higher grades of CRS have shown higher incidence of severe cytopenia during time (Wang et al., 2021).

CRS-like symptoms were also observed in a case study of a patient who received intracranial anti-IL-13R α 2 CAR T cells infusion for the treatment of glioblastoma; however, these symptoms were mild and the localized infusion of the cells didn't increase

unwanted toxicity (Brown et al., 2016). Also in a phase I trial with anti-EGFRvIII CAR T cells administered intravenously to patients with glioblastoma, typical CRS symptoms such as high IL-6 levels, fever and hypotension were recorded, but were associated with intracranial rather than systemic CRS (O'Rourke et al., 2017). Very recently, in an ongoing phase I clinical trial of Claudin18.2-specific CAR T cells for gastrointestinal tumors, all the patients treated (37) experienced severe CRS with leukopenia, neutropenia, anemia and thrombocytopenia (Qi et al., 2022). Other than these episodes, CRS has not been reported in other CAR T cell therapy for solid tumors. Indeed, in these malignancies CAR T cells are more localized and less stimulated in comparison to hematological tumors.

Along with CRS, neurotoxicity (also named immune effector cell-associated neurotoxicity syndrome, ICANS) is another potentially serious side effect related to CAR T cell therapy in clinic, occurring in up to 67% of patients with leukemia and 62% of patients with lymphoma (Santomasso et al., 2018). ICANS early manifestations include tremor, aphasia and lethargy that can progress until coma and also to fatal intracerebral hemorrhages. The mechanism of neurotoxicity has yet to be elucidated, but there is increasing evidence that myeloid cells have a role in triggering ICANS after CAR T cell administration. Myeloid cell-derived pro-inflammatory cytokines have been shown to induce systemic inflammation which correlates with severe ICANS development. Myeloid derived inflammation may lead to endothelial activation, increasing the permeability and reducing the function of the blood-brain barrier with the accumulation of inflammatory T cells in the cerebrospinal fluid (Gust et al., 2017).

As with CRS, most of the clinical experience with neurotoxicity comes from treatment of hematological tumors. No neurotoxicity was observed in a clinical trial of IL-13R α 2 CAR T cells against glioblastoma, despite repeated intracranial T cells infusion (Brown et al., 2016). However, this year, two cases of death from neurotoxicity have been reported in a clinical trial testing PSMA-targeting CAR T cells. The adverse events were associated with a specific cytokines profile and a robust macrophages activation, which did not respond to tocilizumab (Narayan et al., 2022).

The main CAR T cell-related toxicity in solid tumors is on-target off-tumor recognition of healthy tissues expressing the target antigen. Regarding this aspect, target antigen choice is a crucial determinant of efficacy and safety for CAR T cell therapy. Indeed, the

ideal targeted antigen should be expressed selectively or at elevated levels by tumor cells, while healthy cells that share CAR T targeted antigen remain at high risk of on-target off-tumor toxicity. During years, clinical experience has reported several on-target off-tumor effects, which could also be fatal in some cases. CAR T cell therapies targeting CD19 antigen reported B cell aplasia, which is an expected consequence clinically managed by immunoglobulin transfusion (Sadelain et al., 2015). In the field of solid tumors, the majority of target antigens are shared with healthy and indispensable tissues. In a clinical trial with anti-CAIX CAR T cells for metastatic renal carcinoma, a patient showed a dose-limiting toxicity to the liver and bile duct epithelial cells (Lamers et al., 2006). The most severe case was the fatal event of a patients receiving anti-HER2 CAR T cells for the treatment of lung carcinoma. In this particular case, the HER2 expression on pulmonary epithelia triggered CAR T cells activation and led to edema with cytokine release syndrome and multi-organ failure (Morgan et al., 2010).

Activation of CAR T cells upon antigen recognition, however, not only might result in killing of healthy cells, but also in the development of tumor lysis syndrome (TLS), which mirrors the rapid tumor elimination by CAR T cells. Rapid tumor death leads to metabolic abnormalities such as hyperuricemia and hyperkalemia, resulting ultimately in tissues and organs damage. This toxicity is not so rare, and to mitigate this reaction reducing tumor size before CAR T cells infusion and splitting doses of CAR-T are both approaches that have been pursued (Hartmann et al., 2017).

To reduce the risk of targeting tumor associated antigens that are not unique to malignant cells, several engineering strategies have been developed. One strategy includes the affinity reduction of the single-chain variable fragment of CARs, in order to kill only tumor cells overexpressing the target antigen, sparing healthy cells expressing lower level of the same antigen (Liu et al., 2016; Caruso et al., 2015). More recently strategies to avoid on-target off-tumor toxicities include multi-input receptors that activate T cells only in the presence of a specific combination of target antigens. These types of CAR structures are based on the Boolean AND-gate logic, where second-generation CARs are split into a first-generation CAR paired with a second chimeric co-stimulatory receptor (CCR) that includes a scFv fused to one or more co-stimulatory domain without CD3 ζ chain. In this strategy both the targeted antigens must be present to activate CAR T cell signal (Kloss et al., 2013). Another strategy includes the synNotch

system, in which, upon binding to antigen “A”, the synNotch receptor undergoes a conformational change that causes the release of a transcription factor, which drives the expression of a CAR specific for antigen “B” (Roybal et al., 2016). In addition to AND-gate approaches, it is possible to increase CARs specificity by triggering T cells activation only in the presence of a specific tumor associated antigen (TAA) and not in the presence of antigen expressed by healthy cells; this strategy follows the Boolean AND-NOT logic. (Fedorov et al., 2013). Even if AND or AND-NOT strategies can increase CARs specificity, reducing on-target off-tumor toxicity, they present several limitations. These limits include an increased risk of antigen escape by tumor cells, losing one of the input required for the CAR T activation and also the necessity of multi-component expression in T cells with a reduced transduction efficiency and genetic stability.

Since CAR T cell therapy currently show intrinsic toxicity potential, inducible safety controls are desirable. Suicide genes could be included in CARs structure, leading to CAR T cell death upon small-molecules administration. A typical example is the use of Herpes simplex virus thymidine kinase (HSV-TK), which in the presence of Ganciclovir leads to the depletion of HSV-TK expressing cells (Bonini et al., 1997). The clinical feasibility of this approach is limited due to its immunogenicity (Berger et al., 2006). Inducible Caspase 9 (iCas9) is a protein produced by a human suicide gene that after administration of the small molecule AP1903 is activated and mediates caspase-9 apoptosis (Di Stasi et al., 2011). It’s important to bear in mind that the exploitation of suicide genes results in a genetic and permanent switch off, with a complete depletion of CAR T cells, thus forcing the end of the therapy.

Novel strategies that enable drug-controlled pausing or activation of CAR T cells could improve the feasibility, avoiding the permanent conclusion of the therapy. These approaches include OFF switch, such as with Dasatinib, which is a tyrosine kinase inhibitor that temporally interferes with CAR T cell signal transduction, through CD3 ζ chain (Mastermann et al., 2019). Temporal control of CAR T cell activity by clinically approved drugs can increase the safety profile of these cell products.

1.2.2 Clinical and biological determinants of CAR-T efficacy in solid tumors

As reported in previous paragraphs, the success of CAR T cell therapy has largely been observed in hematological malignancies, with the approval of six different CAR T cell products so far. However, despite extensive research, CAR T cell therapy for solid tumors has not been nearly as successful. Indeed, several obstacles in solid tumors must be overcome to reach desired efficacy, which can be summarized in three main categories: find an ideal target antigen, reach the tumor site and overcome the immunosuppressive tumor microenvironment (Martinez and Moon, 2019).

Starting from the first point, as stated above, finding a unique tumor associated antigen in solid tumor is challenging, since in most of cases targeted antigens are expressed also in normal healthy tissues. This is the case of CEA, HER2, EGFR, GD2, MUC1 and PSMA, frequently targeted antigens for solid tumors, but also present in normal cells with the increased risk of on-target off-tumor toxicity. Indeed, anti-HER2 CAR T cells lead to the death of a metastatic colon cancer patient after 5 days from CAR T cells infusion (Morgan et al., 2010). The cause of death was the expression of HER2 at low levels on epithelial cells of the lung, attacked by CAR T cells. Another example was found in neuroblastoma patient infused with anti-GD2 CAR T cells, in which the low antigen expression in the normal brain resulted in fetal encephalitis (Richman et al., 2018). These catastrophic events underline the importance to find safe tumor associated antigens, which even expressed at low levels on normal tissues, could result in significant toxicity.

Regarding this theme, another important issue in the context of solid tumors is antigen heterogeneity. Indeed, many tumors possess only a subset of cells that express the target antigen. In other tumors, where the antigen is uniformly expressed by tumor cells, there is the possibility of antigen escape or antigen loss. Antigen loss was largely observed also in hematological tumors with the anti-CD19 CAR T cells, but was also observed in a phase I study with an anti-EGFRvIII CAR-T to treat glioblastoma, where a single CAR T cell dose resulted in downregulation of EGFR/EGFRvIII receptor, leading to a reduced T cell efficacy (O'Rourke et al., 2017).

When target antigen is identified, CAR T cells have to reach the tumor mass. In hematological tumors, circulating CAR T cells in the blood have already reached their destination, while in solid tumors, CAR T cells have to overcome several barriers. The first crucial requirement for a successful tumor response is the trafficking of CAR T cells

from the bloodstream within the tumor mass. In this phase, extravasation is a crucial and limiting step due to the possible downregulation of adhesion molecules, such as ICAM-1, by tumor cells and to the possible reduced expression of the exact set of chemokine receptors by CAR T cells (Sacksterin et al., 2017; Dirksen et al., 2003). Additionally, physical barriers such as cancer associated fibroblast (CAFs) and abnormal vasculature at the tumor site may block T cell entry (Hanahan and Coussens, 2012).

Even once CAR T cell infiltrates the tumor, there is still a great barrier to overcome, the hostile and immunosuppressive tumor microenvironment. It poses several challenges to T cell fitness and survival, such as an extended collection of inhibitory signals that suppress T cell responses and a particularly harsh metabolic milieu that limits T cell effector function. The glycolytic metabolism of tumor cells (e.g. the Warburg effect) induces a hypoxic, acidic and with low nutrient environment which is enriched of inhibitory enzymes, such as IDO-1 (Gullino et al., 1964; Hornyák et al., 2018) and oxidative stress (Renner et al., 2017). In an inflammatory environment, tumor cells often upregulate ligands such as programmed cell death ligand 1 (PDL-1) and Galectin-9, which inhibit CD8⁺ T cells after binding with their inhibitory receptors (PD-1 and TIM3, respectively) (Acharya et al., 2020). The TME also includes stromal cells like cancer associated fibroblasts (CAFs) and suppressive immune cells, including myeloid-derived suppressor cells (MDSCs), regulatory T cells (Tregs), tumor associated neutrophils (TANs) and tumor associated macrophages (TAMs). These cells together with the tumor secrete soluble growth factors and cytokines, like vascular endothelial growth factor (VEGF) and transforming growth factor β (TGF- β), which favor tumor neo-angiogenesis and promote anti-inflammatory polarization of TAMs (Turley et al., 2015; Hanahan et al., 2012). Tumor associated macrophages are a plastic and dynamic population, which can both support tumor progression or eradication. In the TME, TAMs can be divided into two major phenotypes: M1 classically activated macrophages and M2 alternatively activated macrophages. M1 macrophages are polarized by pro-inflammatory stimuli (IFN- γ , TNF- α , GM-CSF, TLR ligands) and promote anti-tumor effects by activating Th1 response through the secretion of TNF- α , IL-6 IL-12, CXCL5, CXCL8-10 and the activation of interferon regulatory factors (IRF) (Wang et al., 2014). On the other hand, M2 macrophages polarization is driven by immunosuppressive stimuli, typically present in the TME, including TGF- β , IL-4, IL-10 and IL-13. M2 polarized-macrophages show

immunosuppressive phenotype by supporting the Th2 responses and releasing IL-10, TGF- β , CCL17, CCL18, CCL22 and CCL24. Moreover, M2 macrophages directly contribute to the tumor progression and metastases capacity through the secretion of VEGF and the expression of PDL-1 (Wang et al., 2014.; Jayasingam et al., 2010). In liver metastases from colorectal cancer (CRC) it was observed that an extracellular matrix (ECM)-related protein named Collagen Triple Helix Repeat Containing 1 (CTHRC1) secreted by CRC cells promoted liver metastases by increasing macrophages infiltration. In particular, CTHRC1 bound to TGF- β receptor II and III activates TGF- β signaling (Zhang et al., 2021). Moreover, in the same disease TAMs recruitment and polarization in liver metastases was correlated with an elevated expression of TCF4, a transcription factor which regulates CCL2-CCR2 axis (Tu et al., 2021). Another mechanism of resistance for the treatment of liver metastases was reported by Yu et al. The group has shown that diminished immunotherapy efficacy was due to hepatic myeloid cells, which induce apoptosis of activated T cells through the Fas-Fas ligand (FasL) pathway (Yu et al., 2021).

CAFs are stromal cells with the ability to degrade the extracellular matrix, induce angiogenesis, tumor growth and invasiveness. In the TME, epithelial cancer cells secrete factors such as hepatocyte growth factor (HGF), epidermal growth factor (EGF), TGF- β and platelet-derived growth factor (PDGF). All these molecules activate resident fibroblast, which through the secretion of other chemokines such as CXCL12/CXCR4 promote tumor growth, migration and angiogenesis (Kuzet and Gaggioli, 2016). Moreover, CAFs are directly involved in the killing and dysfunction of effector T cells through the expression of FasL, PDL-1 and PDL-2 and the release of TGF- β (Lakins et al., 2018; Cho et al., 2011). A specific subset of liver CAFs includes the hepatic stellate cells, which are physiologically quiescent exerting the role of Vitamin A and retinoic acid storage. However, in the TME, factors and cytokines secreted by tumor endothelial cells activate these stromal cells (aHepSCs), which transdifferentiate into tumor supporting myofibroblasts. Indeed, it was observed that *in vitro* treatment of hepatic stellate cells with TGF- β or with tumor conditioned medium induced the trans-differentiation into aHepSCs. Phenotypic changes include expression of α -smooth muscle actin (α -SMA), increased motility, proliferation and production of growth factors (Kang et al., 2011). These released factors support the tumor growth and progression in the liver, neo-

angiogenesis, and induce immunosuppressive anti-tumor responses. Indeed, activated hepatic stellate cells are able to inhibit T cell proliferation and this is mediated by the binding between PDL-1 expressed by aHepSCs and PD-1 expressed by T cells (Yu et al., 2004; Chen et al., 2006). Finally, the active role of aHepSCs in metastases formation was recently observed in the context of breast cancer-liver metastases. The exit from dormancy of breast cancer cells was followed by a reduction of NK cells with an accumulation of HepSCs and the invasion of tumor cells into the liver (Correia et al., 2021).

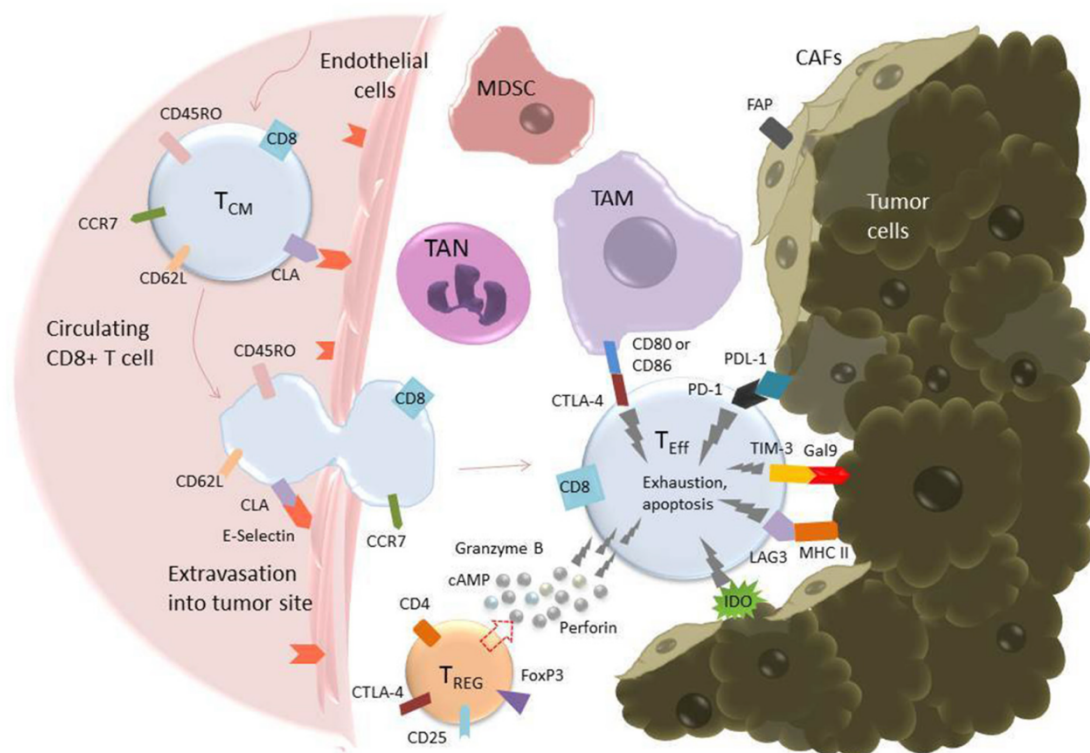


Figure 1.2 | Solid tumors obstacles for T cells fitness and functions.

T cells in solid tumors may overcome several challenges to reach the tumor site, persist and maintain their effector functions. T cells should be able to enter in the tumor site through the extravasation via binding with adhesion molecules such as VCAM-1, ICAM-1 P- and E-selectins. Once in the tumor, there is the suppressive TME with TAMs, TANs, MDSCs, Tregs and CAFs which express together with tumor cells inhibitory molecules, such as PDL-1 and Gal-9 and promoting T cell exhaustion characterized by the upregulation of PD-1, TIM-3, LAG-3, TIGIT. VCAM-1, vascular cell adhesion molecule-1; ICAM-1, intercellular adhesion molecule-1; TME, tumor microenvironment; TAMs, tumor-associated macrophages; TANs, tumor-associated neutrophils; MDSCs, myeloid-derived suppressor cells; Tregs, regulatory T cells; CAFs, cancer-associated fibroblasts; PDL-1, programmed death ligand-1; Gal-9, galectin-9; PD-1, programmed

cell death protein-1; TIM-3, T-cell immunoglobulin and mucin-domain containing-3; LAG-3, Lymphocyte activating-3; TIGIT, T cell immunoreceptor with Ig and ITIM domains).
From Martinez M. and Moon E.K., 2019 *Front. Immunol.*

1.2.3 Approaches to enhance CAR T cells therapeutic index against solid tumors

Improving the therapeutic index of CAR T cell therapy in the field of solid tumors is required to extend their applications beyond hematological tumors. As mentioned in 1.2.2, several challenges are present in solid tumors, regarding T cells migration to the tumor site, T cells invasion in the solid mass and T cells fitness and persistence in the hostile immunosuppressive tumor microenvironment.

In solid tumors, there are multiple barriers that CAR T cells have to overcome to reach the tumor site. The presence of abnormal vasculature has an important role in blocking the infiltration of T cells into solid tumors. Indeed, anti-angiogenic therapies targeting VEGF or endothelin B receptor have been demonstrated to normalize the abnormal tumor vascularization and could be used in combination with CAR T cells (Yang et al, 2018). Moreover, mismatching of tumor-secreted chemokines and T cells expressed chemokine receptors is an important obstacle for CAR T cell trafficking to tumors. In this light, different strategies have been exploited to improve the ability of T cells to reach the tumor mass. Several groups engineered CAR T cells to express chemokines receptors such as CXCR1, CXCR2, CCR4 and CCR2 enhancing CAR T cells trafficking and efficacy in glioblastoma, ovarian cancer, pancreatic cancer and Hodgkin lymphoma (Di Stasi et al., 2009; Bear et al., 2010). Moreover, cytokines are also necessary to achieve optimal activation of CAR T cells. To provide such signal, transgenic-based strategies to deliver IL-18, IL-21, IL15 or IL-12 have been employed. This 4th generation of CAR T cells, known as TRUCKs, demonstrated superior and long-lasting anti-tumor activity and capacity to overcome the tumor microenvironment in several preclinical solid tumors settings (Markley and Sadelain, 2010; Chmielewski and Abken, 2017).

Another promising approach to increase CAR T cell infiltration into tumor masses are CARs targeting tumor stroma. Indeed, CAFs create a physical barrier at the tumor site, which can block T cell entry. Fibroblast activation protein (FAP) is highly expressed on CAFs in over 90% of solid tumors and different groups developed anti-FAP CAR T cells,

enhancing the anti-tumor activity also in combination with T cells targeting TAAs, such as EphA2 (Kakarla et al., 2013). Another potential target within the tumor stroma is the extracellular matrix (ECM) itself. Indeed, Caruana and colleagues engineered CAR T cells to express heparanase (HPSE), an enzyme which degrades heparin sulfate proteoglycans in the ECM. This group reported that HPSE-expressing CAR T cells presented an enhanced capacity to degrade the ECM, thus promoting tumor T cells infiltration and anti-tumor efficacy (Caruana et al., 2015).

Apart from genetic tinkering of CAR T cells, a possible method to bypass the hurdle of T cell migration and infiltration into the tumor mass is the regional/local administration of the engineered cell product. In a xenograft mouse model of brain metastases from human breast cancer, intracranial administration of HER2-specific CAR T cells demonstrates an improved anti-tumor activity compared with intravenous delivery (Priceman et al., 2018.). Also, several clinical trials in patients with glioblastoma demonstrate a higher CAR T cell function upon intratumoral delivery, targeting different GBM-associated antigens (Brown et al., 2016; Keu et al., 2017). Similarly, intra-hepatic treatment with anti-CEA CAR T cells has demonstrated promising clinical results for the treatment of liver metastases (Katz et al., 2015; Katz et al., 2020).

Once CAR T cells find the way to enter into the tumor, the hostile tumor microenvironment represent another relevant barrier to T cell fitness and survival. The glycolytic metabolism of tumor cells creates a hypoxic, acid and nutrients poor environment, prone to oxidative stress (Renner et al., 2017). Activated-effector T cells generally rely on glycolysis to facilitate faster proliferation, while activated-memory T cells based their metabolism on oxidative phosphorylation (OXPHOS). However, both metabolic pathways are hampered in tumor infiltrating T cells, since glucose is depleted by tumor cells, reducing the capacity of glycolysis, but also OXPHOS is impaired, due to low oxygen concentration (Buck et al., 2015). Hypoxic condition in the TME provide challenges for memory T cells. To overcome this stress condition, engineering CAR T cells with 4-1BB costimulatory domain could be an efficient strategy. Indeed, BB ζ CAR T cells had an increased mitochondrial respiratory capacity compared to 28 ζ CARs, resulting in greater metabolic efficiency even in nutrient-poor and oxygen depleted environments (Kawalekar et al., 2016). Other than hypoxia, tumor cells upregulate ROS production, which sustain their proliferation, and also indoleamine 2,3 dioxygenase

(IDO), leading to T cell suppression and poor clinical prognosis (Ninomiya et al., 2015). The inflammatory and hypoxic TME induce the upregulation of tumor ligands, including PDL-1 and Galectin-9, that bind inhibitory receptors (IRs) on T cells, dampening their effector functions. PDL-1 and PDL-2 are expressed on a variety of tumor and stromal cells and the binding of PD-1 on T cells result in suppression of CD28-mediated signaling reducing T cell activation, proliferation and survival (Dong et al., 2002).

To improve CAR T cells in solid tumors, checkpoint inhibitors, such as antibodies targeting PD-1 and PDL-1, have been used in preclinical studies in combination with CAR T cells, showing promising results. In a breast cancer model, PD-1 blockade enhanced *in vitro* and *in vivo* tumor-control by CAR T cells (John et al., 2013). More recently, CRISPR/Cas9 technology has been used to knock out gene for inhibitory receptors (IRs) itself, which has been done for PD-1, CTLA-4 and LAG-3, either alone or in multiplex (Hu et al., 2019; Grosser et al., 2019). Not just tumor cells express PDL-1, but also TME cells such as myeloid derived suppressor cells. Indeed, to increase the efficacy of CEA CAR T cells against liver metastases, anti PDL-1 antibodies were used in combination with CAR-T (Burga et al., 2015). CAR T cells have also been engineered to secrete checkpoint inhibitor antibodies, such as anti-CAIX CAR T cells. This engineered product releases anti-PDL-1 antibodies and has shown significantly enhanced anti-tumor activity against renal cell carcinoma (Suarez et al., 2016).

Moreover, as mentioned before, in the hostile TME also several immunosuppressive signals released by stromal and tumor cells are present, such TGF- β and FasL (Turley et al., 2015; Motz et al., 2014). To avoid the immunosuppressive and apoptotic effect of these factors on T cells, some strategies have been employed. Tang et al., knock out the endogenous TGF- β receptor (TGFB2) in CAR T cells with CRISPR/Cas9 technology to prevent CAR T cell exhaustion in the TME, increasing their killing capacity *in vivo* (Tang et al., 2020). Other strategies aimed to increase T cell fitness in the TME include the knock-out of Fas receptor on these cells. Indeed, this receptor is highly expressed in patient derived T cells used for clinical adoptive T cell therapy and FasL is overexpressed within the majority of human TMEs. CAR T cells engineered with Fas variants prevent the ability to bind FasL on tumor cells avoiding T cell apoptosis, and also increasing T cells persistence and antitumor efficacy against both hematological and solid tumors (Yamamoto et al., 2019).

Other important key players in the solid TME are tumor associated macrophages, with a pro-tumor activity and immunosuppressive functions. Therapeutic approaches to deplete or repolarize TAMs are in clinical development (Mantovani et al., 2017; Weiskopf and Weissman, 2015; Weiskopf et al., 2013). To target this specific immunosuppressive population in the TME, anti-folate receptor β (FR β) CAR T cells have been developed. Indeed, FR β is expressed at high levels in an immunosuppressive subset of TAMs, with an M2-like profile. The elimination of this population enhances pro-inflammatory macrophages (M1-like), resulting in reduced tumor-progression and prolonged mice survival. Moreover, preconditioning of the TME with these specific CAR T cells improves the efficacy of anti-mesothelin CAR T cells. Interestingly, the enhanced effect was not observed when the two CAR products were infused together, suggesting the importance of TAMs-depleting before proceeding with the conventional immunotherapy (Rodriguez-Garcia et al., 2021). Outside the hostile tumor environment, macrophages are effectors and regulators of the innate immune response, capable of phagocytosis, secretion of pro-inflammatory cytokines and antigen presentation to T cells (Franken, et al., 2016). These key points were taken in consideration by the group of Gill at the University of Pennsylvania (UPenn), who genetically engineered human macrophages with CARs to redirect their phagocytic activity against tumors. They observed that CAR macrophages (CAR-Ms) sustained a pro-inflammatory M1-like phenotype and led to decreased tumor burden in two solid tumor xenograft mouse models (Klichinsky et al., 2020) This interesting engineered cellular product raised the interest to macrophages as direct effectors in solid tumor context, and not just target to be eliminated. In line with this, CAR-Ms in humanized mouse models have shown the capability to induce a pro-inflammatory tumor microenvironment to boost anti-tumor activity.

The modulation and reshaping of an immunosuppressive TME into a pro-inflammatory anti-tumor TME is now a novel research field also with CAR T cells. Indeed, this year two works have been published, showing the immunosuppressive role of TAMs-M2 macrophages and also MDSCs on CAR T cells functions. Yamaguchi and colleagues reported that CAR T cells inhibition induced by M2 macrophages was due to the overexpression of PDL-1 on these myeloid cells. PDL-1 blockade restores CAR T cells activity, reshaping M2 macrophages into a M1-like phenotype (Yamaguchi et al., 2022).

The other work by Luo et al. is focused not only on M2-TAMs, but also on MDSCs. They reported that with a combinatory strategy of CAR T cells and folate-targeted Toll-like receptor 7 agonist (FA-TLR7-1A), M2-TAMs and MDSCs are reactivated to a pro-inflammatory phenotype. With this combinatory approach, they modulated the TME, enhancing CAR T cells as well as endogenous T cells accumulation and activation, resulting in improved tumor control (Luo et al., 2022).

1.2.4 Preclinical models to test CAR T cells products for solid tumors: limits and solutions

To evaluate the clinical applicability of CAR T cells products, a deeper understanding of the intrinsic/extrinsic mechanisms and cell players contributing to the response is required. Currently available preclinical models often fail to accurately predict efficacy and especially toxicities observed in the clinic for several reasons. The main issues include the absence of endogenous human immune system and the inability to fully recapitulate human tumor microenvironment and tumor heterogeneity.

To evaluate CAR T cells antitumor killing capacity *in vitro*, T-cell-mediated cytotoxicity assays using co-culture of human tumor cell lines with CAR T cells are commonly used. This two-dimensional (2D) model lacks the TME compartment and usage of cell lines is not representative of the heterogeneity and the complex architecture of solid tumors (Guedan et al., 2022). To increase the complexity of the 2D model, tripartite co-cultures have been employed as an *in vitro* model to partially recapitulate key regulators of the TME. To take another step forward, spheroids and organoids are being now employed as 3D co-cultures to better predict CAR T cell efficacy *in vivo*. Spheroids are unicellular cell line-derived floating cultures and are used to validate CAR T cells cytotoxicity against a specific target antigen (Dillard et al., 2018). Organoids refer to complex multicellular cultures derived from tumor biopsies cultured *ex vivo* on a 3D scaffold. Patient derived organoids (PDOs) are extremely relevant since they retain the histological complexity and genetic heterogeneity of parental tumors, becoming a suitable *in vitro* model (Li et al., 2020). CAR T cells have been shown to infiltrate PDOs, expand, activate and kill the antigen-positive targets in various PDOs models (Jacob et al., 2020;

Yu et al., 2021; Schnalzger et al., 2019). Organoids can be successfully transplanted in mice and are more relevant than traditional cell lines, due to their better preservation of mutational burden and TME features (Jacob et al., 2020). There are various organoid culture methods to grow PDOs. The most commonly used is the submerged Matrigel culture, where dissociated PDOs are embedded in Matrigel and culture in a dish or plate with medium enriched in growth factors and cytokines. This is an easy method to enrich and expand PDOs, maintaining genetic and morphologic alterations of the original tumor. The limitation of this method is the lack of native immune and stromal components, since only epithelial tumor cells are maintained in the culture. However, to better recapitulate the TME, exogenous immune or stromal cells can be added to the culture (Vlachogiannis et al., 2018; Yuki et al., 2020). Another innovative and complex strategy includes the Air-Liquid Interface Culture (ALI), where fragments of PDOs are embedded in collagen exposed to air. The great advantage of this method is the possibility to culture native immune and stromal cells together with tumor cells. However, immune and stromal cells decline over 1-2 months in culture, so they cannot propagate long-term as tumor cells (Neal et al., 2018; Li et al., 2016).

Regarding *in vivo* models the majority of preclinical studies for the evaluation of the therapeutic potential have been performed in classical human cell line derived xenograft (CDX) models, in which tumor cell lines are infused in immune-deficient mice prior to CAR T cells administration. The most popular strain is the immune-deficient NOD/SCID/IL2Ryc^{-/-} (NSG) mouse, which is devoid of T, B and NK cells and retains defective dendritic cells and macrophages (Guedan et al., 2022). Aside from classical NSG mouse model, there are also other immune-deficient mouse strains, such as the Scid/Beige, that have been employed for efficacy studies with CAR T cells against both hematological and solid tumors (Drent et al., 2019 Koneru et al., 2015). This strain has a functional myeloid compartment that can partially mimic the role of myeloid cells in TME and inflammatory responses, restricted by species homologies (Giavridis et al., 2018). To recapitulate a multi-lineage human immune system and a milieu that better recreate the human tumor microenvironment, humanized mouse models were developed. In this models immune-deficient mice are engrafted with human hematopoietic stem cells (HSPCs) to support the human hematopoiesis *in vivo* (Siegler et al., 2018). To better reconstitute a human immune system, in particular focusing on the myeloid compartment,

NSG mice knocked-in with human genes for specific cytokines have been generated, called SGM3 mice. These mice are triple transgenic for the expression of human stem cell factor (SCF), granulocyte-macrophage colony stimulating factor (GM-CSF) and IL-3. This mouse model was first applied to study CAR-related toxicities, including CRS. Indeed, it revealed the crucial role of monocytes in driving CRS and neurotoxicity, as they represent the major source of IL-1 and IL-6 (Norelli et al., 2018; Arcangeli et al., 2022). The presence of myeloid cells is essential for toxicities studies, but it is relevant as well for efficacy studies. Indeed, these cells on one hand can support CAR T cells anti-tumor activity, increasing their expansion (Norelli et al., 2018). On the other hand, they might be helpful for establishing a more representative human TME, which is lacking in classical NSG mouse models and highly relevant for clinical translation, particularly in solid tumors. For this reason, humanized SGM3 mice (*huSGM3*) have been employed to study the antitumor activity of CAR T cells against solid tumors, with the evaluation of the immunosuppressive TME (Klichinsky et al., 2020). Unfortunately, this model still lacks the stromal component, so novel strategies have to be developed to fill this gap. Some groups have started to work on this aspect, trying to implement the classical NSG mouse model with the introduction of the human stromal compartment. With tissue engineering techniques, scaffold have been used to culture cancer associated fibroblast, which were implanted in a xenograft model together or prior of tumor cell lines injection (Guerrero-Aspizua et al., 2020). However, these models have not been employed with immunotherapies approaches yet.

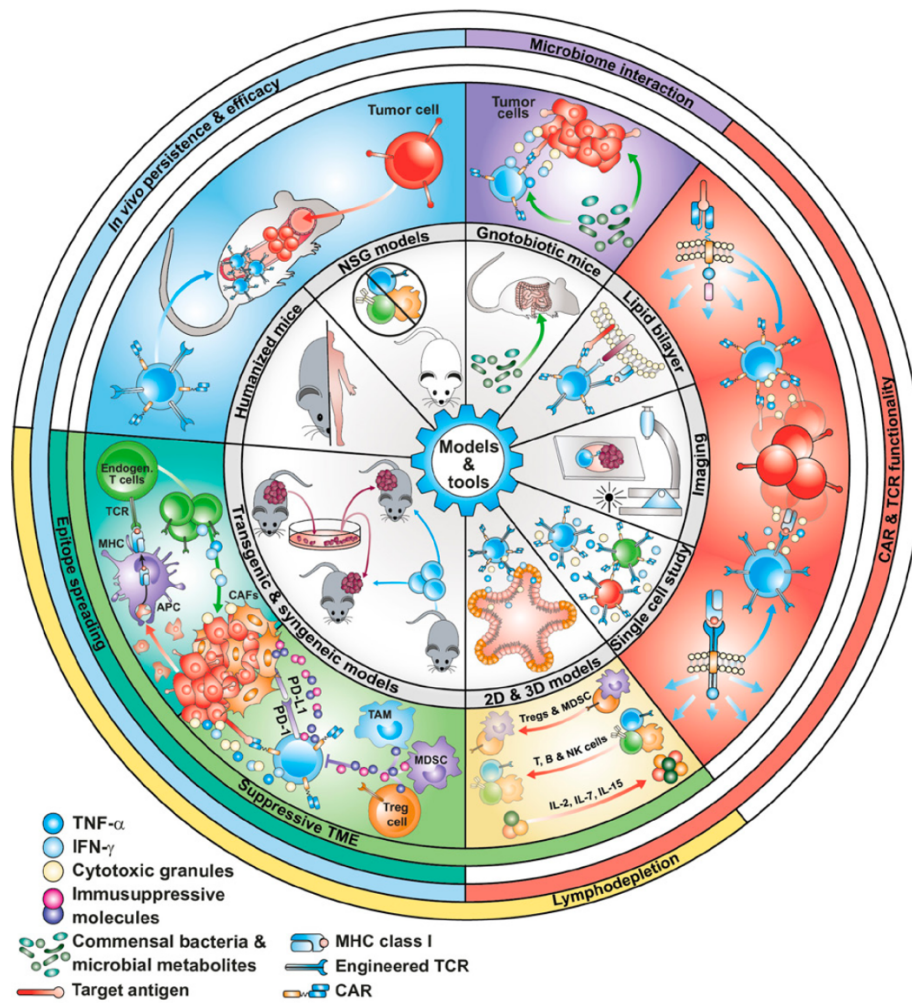


Figure 1.3 | Models and tools to test efficacy and toxicity of CAR T cells.

Currently typical preclinical models include 2D cultures assays and xenograft models in NSG mice. These methods present limits to assess and predict the efficacy of CAR T cells products in clinical trials. 3D model, such as spheroids or organoids, and humanized mouse models that better recapitulate tumor heterogeneity and the complex immunosuppressive TME are being developed. These new models together with analytical tools and imaging techniques help in the prediction of clinical efficacy of new CAR T cell products.

2D, two-dimensional; NSG, NOD/SCID/IL2Ryc^{-/-} mouse; 3D, three-dimensional; TME, tumor microenvironment.

From Guedan S., Luu M., Ammar D., *et al.*, 2022 *Jitc*

Of note, in all these *in vivo* models both xeno-and allo-reactions may be observed. First, CAR T cells generated from human donors and infused in mice can show xenoreactivity against murine tissues, causing the so-called xenogenic GvHD, which can lead to the death of animals (Kaneko *et al.*, 2009). Moreover, CAR T cells can potentially react

against human allogenic tumor and immune cells that develop from HSPCs (Norelli et al., 2018). To reduce the risk of these reactions, gene editing technologies to disrupt the endogenous TCR (T Cell Receptor Alpha Constant, TRAC or T Cell Receptor Beta Constant, TRBC locus) have been employed (Torikai et al., 2012; Mastaglio et al., 2017).

1.3 Glycosylation in health, tumor and tumor microenvironment

Glycosylation is a common post translational modification of proteins or lipids. Tumor cells display an abnormal glycosylation profile, which changes through disease stages and cellular metabolism. Glycans have multiple roles in cellular physiology, but also in cancer cells. Indeed, glycans increase tumor heterogeneity, promote proliferation and allow dissemination, thus being involved in metastases formation. At the same time, glycans also drive immunosuppression in the tumor microenvironment (TME) by masking tumor cells from antibody targeting and promoting immunosuppressive capacity of TME cells.

1.3.1 N-glycosylation in health and tumor

Glycans are saccharide or glucose chains that can be found freely or attached to proteins or lipids to form glycoconjugates. The majority of glycans is attached on the extracellular surface of cells. Among many glycan types that can be generated, glycoproteins are made through the conjugation of sugars to proteins, including the addition of N-linked glycans and O-linked glycans.

N-glycosylation, in particular, refers to the binding of N-acetylglucosamine (GlcNAc) to the amino group of Asn within polypeptide chains by a β -1N linkage at the consensus motif Asn-X-Ser/Thr. Each N-glycan is composed by a core structure comprising two GlcNAc and three mannose residues, to which other monosaccharides can be linked, defining the structure as high-mannose or hybrid or complex N-glycan. The N-glycosylation process starts in the endoplasmic reticulum (ER) and continues in the Golgi apparatus. There, mature carbohydrate can become a complex or hybrid N-glycan through the attachment of GlcNAc, galactose, sialic acid and fucose (Varki and Cummings).

As previously mentioned, glycans play a crucial role in healthy cells and they are involved in several functions. In the context of the immune system, immune receptors recognize pathogen associated molecular patterns (PAMPs), such as LPS, dsRNA, non-methylated CpG, but also specific glycan structures that are normally absent from mammals. Moreover, peculiar glycosylation patterns are required for the correct interaction between endothelial cells and leukocytes, crucial for T cell trafficking and migration. Inflammatory cytokines can modify surface N-glycans of endothelial cells, which in turn regulates their functions (Hakomori and Kannagi, 1983; Kannagi et al.,

2008). In addition, immunoglobulin isotypes differ in the prevalence and type of glycosylation residues in the heavy chain. In fact, immunoglobulin glycosylation can determine whether an antibody is pro-inflammatory, such as the absence of galactose in IgG N-glycans, or anti-inflammatory, such as sialic residues on N-glycans (Chacko et al., 2011; Scott et al., 2013).

As already now well known, tumors display a wide range of glycosylation alterations, which confer them several advantages in terms of growth, invasion and metastases. Aberrant glycosylation, which characterizes tumor cells, can consist in the incomplete synthesis of physiological glycosylated proteins or in the synthesis of new abnormal glycoconjugates (Hakomori and Kannagi, 1983). This process in tumor cells can depend on several factors, including abnormal expression of tumor glycosyl-transferases and changes in availability and abundance of sugar precursors or transporters (Kannagi et al., 2008; Pinho et al., 2012; Hatano et al., 2011). As result from all these deregulated processes, the most frequent cancer-related modifications in glycosylation include i) over-branching of N-glycans, ii) truncation of O-glycan, iii) increased sialylation and iv) altered fucosylation (Hakomori, 2002; Arnold et al., 2008). Focusing on branched N-glycans, increased activity of acetyl-glucosaminyltransferase 5 (GnT-V), due to the overexpression in many cancers of MGAT5 gene, promotes β 1-6 N-glycan branching on tumor cells (Dennis et al., 1987). Glycans have been involved in several crucial processes in cancer, including cell-cell adhesion, cell-matrix interaction, cancer cell signaling and metabolism (Zhao et al., 2008; Dennis et al., 2009). GnT-V overexpression determines the addition of branched N-glycans to E-cadherins, which lead to its functional impairment by compromising cell-cell adhesion and promoting metastases formation (Pinho et al., 2009). Changes in N-linked β 1-6 N glycans occur not only in cell-cell adhesion, but also in cell-matrix adhesion, by inhibiting the clustering of integrin and the signal transduction pathway. Indeed, the deregulation of integrins, due to an increased expression of branched N-glycans, impairs cell-matrix adhesion and increase tumor cell migration and signal transduction (Pochee et al., 2013). In addition, the level of glycan branching modifies the signaling and membrane localization of several cell surface proteins. Receptors that stimulate cell proliferation, growth and oncogenesis have more N-glycan sites, while growth-arrest receptors have less N-glycans sites. Metabolic changes affect the stability of cell surface receptors by modulating the interaction of

branched N-glycans and galectin-3, which regulates receptor endocytosis and signaling. Hence, the more N-glycan site, the more β 1-6 branching structures are added, which are linked to galectins, precluding endocytosis while increasing signal transduction (Lau et al., 2007). Indeed, MGAT5^{-/-} transgenic mice bearing a mammary carcinoma are less responsive to growth factors signals compared to wild-type mice, demonstrating reduced galectin-3 binding and internalization of receptors from cell membrane to endosomes (Partridge et al., 2004). Overall the nutrient flux which regulates complex N-glycans biosynthesis determines cellular response of tumor cells including growth, invasion and metastases capabilities (Dennis et al., 2009).

Since aberrant N-glycosylation helps tumor growth and metastases formation, some studies exploited the usage of N-glycosylation inhibitors, such as Swainsonine and tunicamycin. Swainsonine is an indolizidine alkaloid and an inhibitor of α -mannosidase II, an enzyme involved in the complex glycans biosynthesis. The inhibition of this enzyme replaced complex-type glycans with hybrid-type N-glycans. In 1986 was first reported that Swainsonine treatment of two different melanoma cell lines reduces their organ colonization potential when cells are injected intravenous in syngeneic mice (Dennis, 1986). In the next work from the same group, they demonstrated that Swainsonine reduced tumor growth and inhibited the expression of complex N-glycans (Dennis et al., 1990). Swainsonine has been shown to reduce tumor cell metastases, enhance cellular immune responses and reduce solid tumor growth in mice. However only one phase I study was performed, since significant toxicities including edema, elevated serum aspartate aminotransferase (AST), fatigue and dyspnea occurred in more than 20% of patients (Goss et al., 1997). Tunicamycin is another N-glycosylation inhibitor. It is a nucleoside antibiotic, which inhibits the first step of the N-glycans biosynthesis. Several reports have shown that tunicamycin, by inhibiting N-glycosylation, produces marked radio-sensitization in cancer cell lines (Contessa et al., 2010), enhances the susceptibility of lung cancer cells to Erlotinib (Ling et al., 2009), potentiates cisplatin-induced cytotoxicity in human cell lines (Xu et al., 2012), inhibits angiogenesis in nude mice by decreasing VEGF expression (Banerjee et al., 2011) and enhances anti-tumor activity in combination with Trastuzumab against HER2-positive breast cancer cells (Han et al., 2015).

Inhibition of N-glycosylation induces the unfolded protein response (UPR), due to presence of mis-folded proteins, which are retained in the endoplasmic reticulum (ER). As result of UPR activation, synthesis of new proteins is inhibited and degradation of aberrant proteins is increased leading to ER stress, which can either be solved or if prolonged in time can lead to cell apoptosis. Under ER stress, the three-major activated UPR branches are: PERK, IRE1 α and ATF6. PERK through eIF2 α activates ATF4 which regulates the transcription of UPR target genes involved in amino acid biosynthesis, anti-oxidative response, autophagy and apoptosis. IRE1 α through TRAF and XBP1s activates the transcription of genes involved in inflammation, autophagy, protein folding and secretion. Finally, ATF6 activates ATF6p50 leading to the activation of protein folding and secretion (Hetz et al., 2020). Tunicamycin, in particular, since it inhibits the first step of N-glycosylation, induces ER stress which is followed by UPR and eventually leads to ER-stress related cell apoptosis (Shu et al., 2019; Wu et al., 2018).

Another N-glycosylation inhibitor, which can also lead to UPR, is 2-deoxy-D-glucose (2DG), a glucose/mannose analogue in which the C-2 hydroxyl group is replaced by hydrogen (Qin et al., 2010). 2DG competes with mannose for the assembly into lipid-linked oligosaccharides (LLO) chains, inhibiting the pathway of N-glycans biosynthesis (Kurtoglu et al., 2007). 2DG is not only an N-glycosylation inhibitor but also a glycolysis inhibitor, and it is well-known for this second function. Indeed, 2DG competitively inhibits glucose uptake, since both molecules are transported within cells through glucose transporters (GLUTs). Once in the cytoplasm, 2DG is phosphorylated in position 6 by hexokinase (HK) to form 2-Deoxy-D-glucose-6-phosphate (2DG-6P), which cannot be further catabolized and accumulates in the cell. This results in the inhibition of glycolysis with a decrease of ATP production, cell cycle arrest and inhibition of cell growth (Rasler et al., 1998; Kurtoglu et al., 2007). 2DG was tested in several preclinical models of human tumor xenografts and was used in combination with chemotherapeutic agents and OXPHOS inhibitors, showing the ability to induce tumor cell death (Maschek et al., 2004). It was also tested in humans to conduct a deeper safety evaluation and phase I clinical trials indicate that the administration of 2DG alone or in combination with chemotherapy or radiotherapy is well tolerated and non-toxic in normally oxygenated tissues (Raez et al., 2005; Singh et al., 2005; Raez et al., 2013). However, as mentioned before, many studies underline the specific effect of N-glycosylation inhibition, and not

glycolysis, by 2DG in selected tumor cell types (Xi et al., 2011). Moreover, very recently in our Unit, Greco et al. have demonstrated that disrupting N-glycan expression on tumor cells, both with genetic knock-out of MGAT5 and also with 2DG treatment, CAR T cells efficacy against solid malignancies is increased. Indeed, it was shown that inhibiting N-glycosylation CAR T cells killing against different carcinomas is enhanced, such as pancreatic ductal adenocarcinoma, lung, ovary and bladder cancer. Moreover, removal of cumbersome N-glycans leads to improved immunological synapse formation, increased killing activity as well as cytokine release, and decreased binding of co-inhibitory molecules between CAR T cells and tumor cells. This effect was observed with different CAR T specificities, both CD44v6 and CEA, hinting to the potential broad application of this approach to improve immunotherapies against solid malignancies (Greco et al., 2022).

1.3.2 The role of N-linked glycosylation in the tumor microenvironment

Glycosylation is strictly involved in the regulation of the tumor microenvironment. Indeed, despite the majority of studies are focused on glycosylation implications on tumor cells, a more emerging research field explores how tumor glycosylation affects the function of immune cells within the TME. In this context, several reports show that tumor glycans can bind lectin receptors on immune cells, such as sialic acid-binding immunoglobulin-like lectins (SIGLECs), macrophage galactose-specific lectin (MGL) and dendritic cell (DC)-specific ICAM3-grabbing non-integrin 1 (DC-SIGN). These interactions guide TME immune cells towards an anti-inflammatory state, characterized by increased secretion of anti-inflammatory cytokines that inhibit NK cells activity, while promoting T cells polarization into T helper 2 and regulatory T cells, tuning down the immune response (Gringhuis et al., 2014; Van Vliet et al., 2013; Rodriguez-Garcia et al., 2021). Furthermore, tumor cells secrete galectins, which bind to specific glycans on immune cells resulting in impaired T cell functions, dampening of NK cells and induction of suppressive myeloid cells (Toscano et al., 2007; Méndez-Huergo et al., 2017). Hence, altered glycan structures within the TME contribute to shape a glycol-code that drives innate and adaptive immune suppression. Interestingly, glycosylation can also affect the

structure of checkpoint molecules on tumor cells, modulating their function. Indeed, it was reported that N-glycosylation of PDL-1 on different solid tumors is necessary for its interaction with PD-1 receptor, enabling signal transduction and T cells exhaustion (Li et al., 2018; Greco et al., 2022). Another negative regulator of T cell response is the cytotoxic T-lymphocyte protein 4 (CTLA-4), which presents two N-glycosylation sites that modulate its cell surface expression on T cells. Also, lymphocyte-activating gene 3 (Lag-3) and mucin-domain-containing molecule-3 (Tim-3) are modulated by glycans expression (Pereira et al., 2018). Moreover, galectins expressed by tumor cells could become ligands for these co-inhibitory receptors. Indeed, galectin-3 binds N-glycans on CTLA-4 maintaining the inhibitory signals, as well as to Lag-3 on the surface of CD8⁺ T cells, suppressing their effector function (Lau et al., 2007; Kouo et al., 2015). Finally, galectin-9 inhibits CD8⁺ T cells function through its N-glycosylation dependent binding to Tim-3 (Zhu et al., 2005; Oomizu et al., 2012).

Within the TME, TAMs express several lectins which bind glycans on tumor cells enhancing the immune escape mechanism. It was observed that the binding of Siglec-9 with MUC1-ST increase the secretion of IL-10 and the expression of CD163, CD206 and PDL-1 corroborating TAMs immunosuppressive phenotype. Moreover, binding of Siglec-10 on macrophages with CD24, a highly sialylated glycoprotein expressed on tumor cells, activates a “don’t eat me” signal, inducing an immune escape mechanism by tumor cells. Indeed, the blockade of CD24 in the breast cancer MCF-7 cell line promotes higher phagocytosis by human macrophages both *in vitro* and *in vivo*. (Beatson et al., 2016; Park et al., 2020; Barkal et al., 2019).

All these studies report the impact of tumor glycosylation on TME cells, while less is known about the specific and direct role of N-glycans expressed by TME cells. Indeed, in the tumor microenvironment glucose and glutamine are involved in the hexosamine biosynthetic pathway (HBP), which produces UDP-GlcNAc, a building block for protein and lipid glycosylation, that is emerging not only as a critical metabolic pathway involved in cancer cells, but also in some TME cells, such as macrophages. In activated macrophages glucose is phosphorylated to glucose-6-phosphate, which can enter into glycolysis pathway or into the oxidative branch of pentose phosphate pathway (PPP). Moreover, the majority of fructose-6-phosphate (F6P), an intermediate of glycolysis reaction, can proceed to generate 2 molecules of pyruvates, which enter in the

tricarboxylic acid cycle to generate ATP. Another part of F6P can enter into the HBP to generate donor substrates for the production of glycoproteins and glycolipids. Glutamine can also enter in the HBP to generate at the end of the process UDP-GlcNAc (Rodriguez-Mantuano et al., 2019).

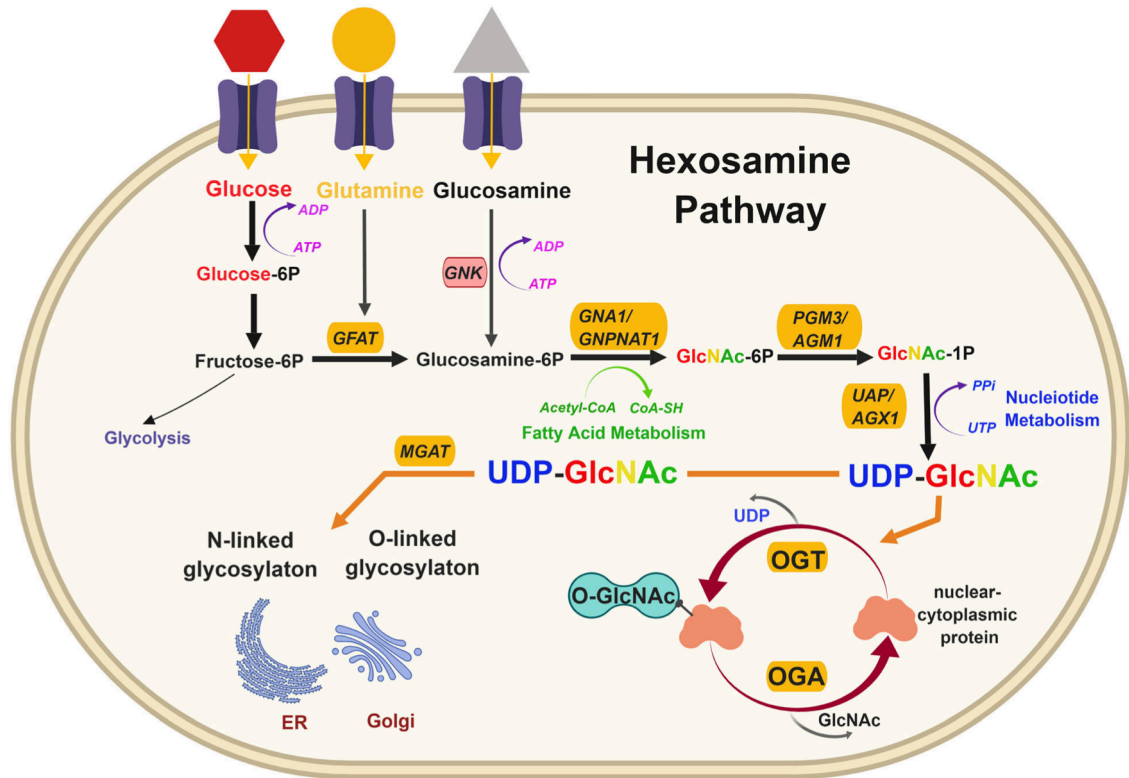


Figure 1.4 | The hexosamine biosynthetic pathway (HBP).

Glucose enters the cell and is converted to fructose-6P, which for the 95% precedes into the glycolysis pathway while around the 3-5% is converted to glucosamine-6P by the enzyme GFAT, using glutamine enters the cell. GNA1/GNPAT1 then converts glucosamine-6P (also made by glucosamine entering the cell) into GlcNAc-6P, converted to GlcNAc-1P by PGM3/AGM1 and further to UDP-GlcNAc, utilizing UTP from the nucleotide metabolism pathway. UDP-GlcNAc is used for N-linked and O-linked glycosylation in the ER and Golgi.

Fructose-6P, fructose-6-phosphate; glucosamine-6P, glucosamine-6-phosphate; GFAT, glucosamine-fructose-6-phosphate amidotransferase; GNA1/GNPAT1, glucosamine-6-phosphate N-acetyltransferase; GlcNAc-6P, N-acetylglucosamine-6-phosphate; GlcNAc-1P, N-acetylglucosamine-1-phosphate; PGM3/AGM1, phosphoglucomutase; UDP-GlcNAc, uridine diphosphate N-acetylglucosamine; ER, endoplasmic reticulum

From Akella N.M., Ciraku L. and Reginato M.J. 2019 *BMC Biology*

The imbalanced HBP in macrophages is still not well characterized; recently few studies have shown the importance of HBP in M2 macrophages. Indeed, Jha et al. identified many transcriptional-metabolic changes during M1 and M2 macrophages polarization (Jha et al., 2015). Glutamine catabolism and UDP-GlcNAc were activated during M2 polarization but not M1, and the absence of glutamine decreased M2 polarization while its addition up-regulates specific M2-like markers (Mazzone et al., 2018). Indeed, inhibition of glutamine synthase reverses M2-polarized macrophages to M1-like phenotype, avoiding metastases progression (Palmieri et al., 2017). Moreover, it was observed that only in hypoxic conditions, typical of tumor environment, HIF-1 α induces the transcription of GFAT in macrophages, enhancing glutamine routing towards UDP-GlcNAc synthesis and inducing M2 rather than M1 polarization (Manzari et al., 2007). UDP-GlcNAc is involved in the formation of extracellular glycoconjugates and the addition of a β -GlcNAc to asparagine residues initiates N-glycosylation. This has an important role in M2 macrophages, since when this pathway is blocked with a specific N-glycosylation inhibitor tunicamycin, several M2-like markers, such as CD206, CD301 and Relma, are downregulated in *in vitro* polarized murine macrophages. Moreover, this effect was observed only in M2 macrophages, while in M1 macrophages tunicamycin only mildly reduces inducible nitric oxide synthase (iNOS) protein expression and M1-like cytokines (Jha et al., 2015). These findings suggest that N-glycosylation is required for the appropriate synthesis of proteins that are crucial for M2-polarized macrophages functions.

Furthermore, N-glycans present at the surface of macrophages, containing β -galactose, can bind galectins. The binding of Galectin-3 (Gal-3) with CD98 stimulates M2 activation and using a specific Gal-3 inhibitor the M2 activation induced by IL-4 is blocked (MacKinnon et al., 2008). Finally, also sialic acid present in several glycoconjugates regulates several functions and sialylation is quite often upregulated in tumor cells. However, as N-glycosylation, also sialylation of TME immune cells has not been deeply investigated yet. It was observed that sialic acid decreases during the differentiation process from monocytes to macrophages and it is higher in M2 activated macrophages in comparison to M1-like. Recently, it was reported that targeting Siglec-sialic acid interaction in the tumor microenvironment, using an antibody-sialidase conjugate, increases anti-tumor immunity and arrests tumor progression in mice models. Through

single-cell RNA sequencing (scRNAseq), it was also observed that sialic acid inhibition repolarizes tumor-associated macrophages into a pro-inflammatory M1-like status, and thus, without sialylation blockade, M2 macrophages show their immunosuppressive phenotype expressing high levels of CD206. In mice treated to block sialylation, tumors contain few immunosuppressive TAMs, which display an M1 phenotype, expressing IL-1 β , TNF and CD80 (Stanczak et al., 2021).

As previously reported, another important TME component are stromal cells. The role of N-glycosylation is still not clear also regarding this population. Focusing on the specific population of liver stromal cells, HepSCs, there are evidence that show that activated HepSCs present a different glycosylation profile in comparison to quiescent cells (Qin et al., 2012). Moreover, the study of Wu et al. demonstrates the role of N-glycosylation in the migration and activation capacity of these cells. Indeed, they observed that Neuropilin-1 (NRP-1), which is a glycosylated receptor expressed by HepSCs, binds Galectin-1 (Gal-1) in a N-glycosylation dependent manner. Blocking N-glycosylation with Swainsonine or through genetic knock-out of MGAT5 gene, no more interaction with Gal-1 is observed and HepSCs maintain their quiescent phenotype (Wu et al., 2017).

2. AIM OF THE WORK

T cells redirected with chimeric antigen receptors (CARs) represent an innovative and sophisticated way of treating cancer. Although this approach has proven its value targeting CD19 and BCMA in hematological malignancies, the same results have not yet been reached for solid tumors. In this context, unique challenges need to be overcome, including poor trafficking at the tumor site, inadequate tumor recognition and strong immunosuppression within the tumor microenvironment (TME).

Previous work in our Unit has identified N-glycosylation inhibition in tumor cells as a mean to increase CAR T cells efficacy against different solid malignancies. It has been demonstrated that blocking N-glycan synthesis in cancer cells improves immunological synapse formation and ameliorates CAR T cell exhaustion, resulting in increased CAR T cells efficacy (Greco et al., 2022).

In this work, we aimed at investigating the effect of N-glycosylation blockade on TME cells, with the final goal of improving the therapeutic potential of CEA CAR T cells in the context of liver metastases from pancreatic adenocarcinoma (PDAC) and colorectal cancer (CRC). More specifically, this work aimed at:

- i) analyzing the consequences of N-glycosylation inhibition on the immunosuppressive functions of M2 macrophages and hepatic stellate cells, from a phenotypic, transcriptional and functional point of view;
- ii) developing a xenograft mouse model of intra-hepatically injected tumors, where the presence of a human immune system allows a more accurate investigation of CEA CAR T cell efficacy and toxicity profile;
- iii) exploiting the humanized animal model to evaluate whether N-glycosylation blockade can modulate the immune TME, thus improving CEA CAR T cells antitumor responses.

3. RESULTS

3.1 2DG increases CEA CAR T cells killing of CRC and PDAC cell lines

3.1.1 CEA is expressed by CRC and PDAC cell lines and CRC patient-derived liver metastases

Several clinical trials have been focused on the carcinoembryonic antigen (CEACAM5, CEA), considered a suitable target antigen for CAR T cell therapy in a wide range of solid tumors. This antigen in healthy tissue is expressed only in the apical surface of cell membranes that faces the luminal part of the colon. This polarized expression renders this antigen invisible to CAR T cells, but still detectable by TCR redirected T cells, leading to severe inflammatory colitis, as shown in clinical trial (Parkhurst et al., 2011). Interestingly, in tumor cells the apical-basal polarity is lost and CEA acquires a homogeneous expression on the cell surface, becoming visible to circulating immune cells (Nap et al., 1988; Saeland et al., 2012). This peculiar feature characterizes CEA as a safe antigen to be targeted with CAR T cell therapy. Indeed, CEA CAR T cells have been investigated in clinical trials for the treatment of liver metastases from gastrointestinal carcinomas, which represent a crucial unmet clinical need due to the absence of an effective therapeutic option nowadays. Regional administration of CEA CAR T cells into the hepatic artery has shown encouraging signs of clinical activity in a heavily pretreated population (Katz et al., 2015; Katz et al., 2020). Another trial, however, also reported acute respiratory toxicity possibly due to low CEA expression on normal lung epithelium (Thistlethwaite et al., 2017). For these reasons, much must be done in order to improve the therapeutic index of this CAR T cell approach in the context of liver metastases from colorectal cancer (CRC) and pancreatic adenocarcinoma (PDAC).

To confirm the relevance of this antigen in this context, we first evaluated CEA expression on a panel of human PDAC and CRC cell lines. This screening revealed that most of them express the antigen, albeit at not so high levels. Among all, BxPC3 and LoVo cell lines showed the highest expression, both in terms of percentage of positive cells and antigen density (fig 3.1a). Subsequently, we analyzed CEA expression in 25 primary samples of CRC liver metastases retrieved from patients undergoing surgical resection at San Raffaele Hospital. All tumor samples showed CEA positivity, while

expression in the peri-tumoral tissue was minimal, supporting the favorable safety profile of this antigen (fig 3.1b).

Overall, these data confirm that the CEA antigen represents a suitable target for CAR T cell therapy of CRC and PDAC liver metastases.

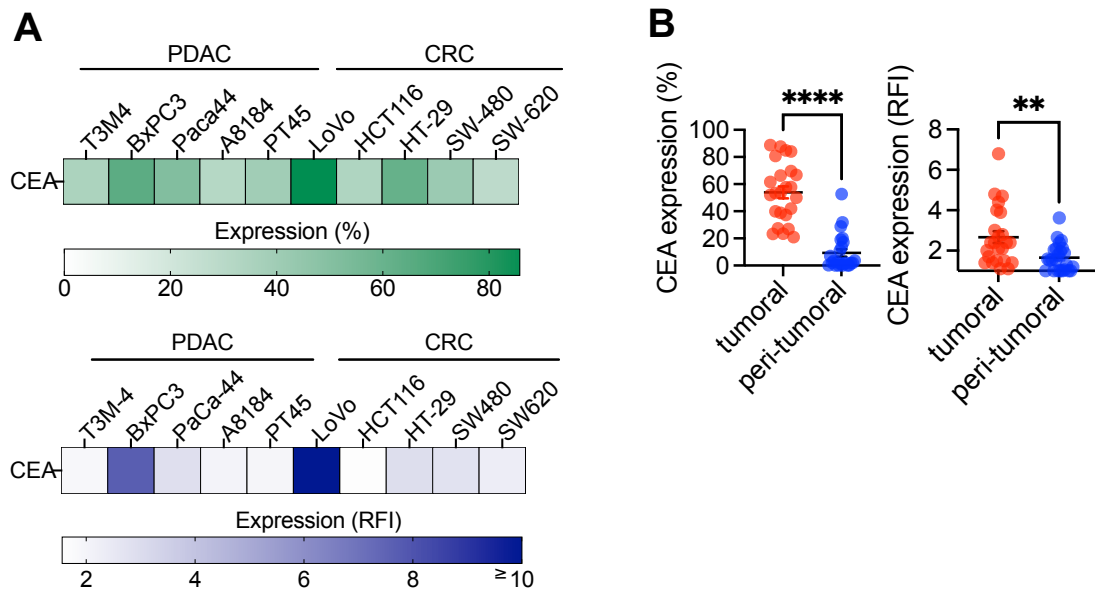


Figure 3.1 | CEA is expressed by CRC and PDAC cell lines and CRC patient-derived liver metastases. A) CEACAM5 (CEA) protein expression by FACS in different CRC and PDAC cell lines (% above; RFI below). (B) CEA protein expression by FACS in primary liver metastases (% left; RFI right) (n=25 CRC patient-derived liver metastases). Results from t-test are indicated when statistically significant (B) (**P ≤ 0.01; ****P ≤ 0.0001).

3.1.2 N-glycosylation blockade unmasks the CEA antigen to antibody recognition and increases susceptibility to CEA CAR T cells

Compared to healthy cells, solid tumors display a higher amount of cumbersome surface N-glycans, which support their invasion and metastases capability. Recently in our Unit, we observed that disrupting N-glycans expression on tumor cells can increase CAR T cell targeting, by improving immunological synapse formation and inhibiting the interaction between inhibitory receptors and their ligands. (Greco et al., 2022).

To evaluate the N-glycosylation status of PDAC and CRC cell lines, we used PHA-L, a lectin that binds over-branched N-glycans. The majority of these cell lines were found to express high levels of these sugar structures, which were significantly reduced after treatment with 2DG, a potent inhibitor of N-glycan synthesis (fig 3.2a). This effect was more evident in some cell lines, possibly since they express higher levels of GLUTs channels through which 2DG enters the cells.

Several membrane molecules are masked by cumbersome N-glycans. For example, N-glycans attached to PDL-1 have been reported to interfere with binding to PD-1 (Li et al., 2018; Greco et al., 2022). Since also CEA is highly N-glycosylated, we evaluated if treatment with 2DG renders it more visible to mAb staining, thus predicting a better recognition by CEA CAR T cells. Interestingly, we observed that upon N-glycosylation inhibition with 2DG, CEA become more visible to mAb targeting. Of notice, this effect was CEA-specific, since increased expression was not observed for other common epithelia markers, such as CD44 or EPCAM (fig 3.2b). To ensure that incremental antibody binding was due to an unmasking effect rather than gene induction, we performed real-time PCR analysis on both BxPC3 and LoVo cell lines, treated or not with 2DG. Importantly, we observed no changes in mRNA expression levels (fig 3.2c), supporting the conclusion that removing N-glycans from CEA renders this antigen more visible to antibodies.

To evaluate whether this translates into increased susceptibility to CEA CAR T cells, we performed co-culture experiments in which BxPC3 and LoVo cells were pre-treated or not with 2DG. Importantly, using a CD28 endo-costimulated anti-CEA CAR, we observed significantly increased tumor elimination when both cell lines were pre-treated with 2DG (fig 3.2d).

Overall, these data suggest that CEA CAR T cell therapy of PDAC and CRC tumors may benefit from combination with de-glycosylating agents.

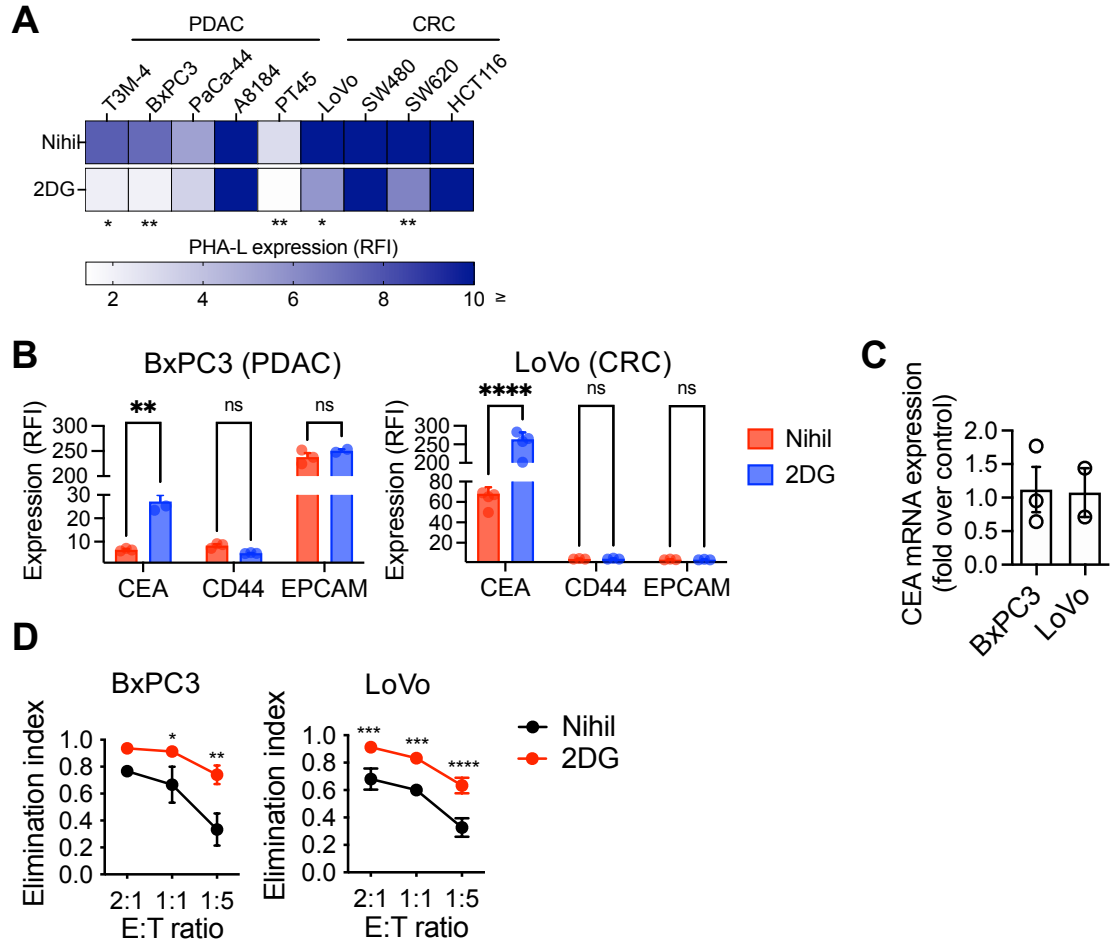


Fig. 3.2 | N-glycosylation blockade unmasks the CEA antigen to antibody recognition and increases susceptibility to CEA CAR T cells. (A) PHA-L expression level (RFI) by FACS in PDAC and CRC cell lines before and after 2DG treatment (4mM for 48 hours). (B) CEA, CD44 and EPCAM expression level (RFI) by FACS in BxPC3 and LoVo cell lines, in the presence or absence of 2DG treatment. (C) CEA mRNA expression after 2DG treatment (fold over control) assessed by real-time PCR in BxPC3 and LoVo cell lines. (D) BxPC3 (left) and LoVo (right) were exposed to 4mM 2DG for 48 hours before being co-cultured with CEA.28z CAR T cells or control CD19.28z CAR-T at 2:1, 1:1, 1:5 effector-to-target ratio (E:T ratio). After 48 hours (for BxPC3) or 24 hours (for LoVo) killing was analyzed by bioluminescence (Tristar 3), thanks to the expression of luciferase (Luc) by cell lines. Killing was expressed as elimination index (see “Materials and Methods”) (n=3 donors). Results from t-test (A, C), two-way ANOVA (B) and one-way ANOVA (D) are indicated when statistically significant (* $P \leq 0.05$; ** $P \leq 0.01$; *** $P \leq 0.001$; **** $P \leq 0.0001$). Data are represented as means \pm SEM.

3.2 Glycosylation blockade reduces immunosuppressive activity of cells within the tumor microenvironment and increases CEA CAR T cells function *in vitro*

3.2.1 De-glycosylated tumors dampen M2 macrophages polarization

In literature, it is very well reported that N-glycosylation is required and necessary for tumor growth, invasion and metastases (Pinho et al., 2009). Moreover, N-glycans expressed by malignant cells are crucial for their interaction with the tumor microenvironment (TME). This axis, which engages lectins such as SIGLECs expressed on immune cells, promotes tumor growth by inhibiting immune response. Therefore, we evaluated the effects of inhibiting N-glycosylation in tumor cells on the polarization of a specific and common TME population, M2 macrophages.

We differentiated primary M2 macrophages (M2-M) from PBMCs of healthy donors. Briefly, we sorted CD14⁺ cells, differentiated them with human monocyte-colony stimulating factors (M-CSF) for 5-7 days and human interleukin-4 (IL-4) for additional 48 hours to finally obtain M2 macrophages (fig 3.3a). To check if we succeeded in generating M2-M, we analyzed by FACS the expression of typical M2 markers. Pro-inflammatory M1 macrophages (M1-M), polarized *in vitro* with LPS for 48 hours, were tested in comparison. The mannose receptor CD206 and the folate receptor beta (FR β) expressed by immunosuppressive M2-like tumor associated macrophages (TAMs) (Rodriguez-Garcia et al., 2021) showed a higher expression in M2-M in comparison to M1-M (fig 3.3b).

To evaluate the impact of glycosylated versus de-glycosylated tumors on M2 macrophages, we performed *in vitro* co-culture experiments. When the tumor was fully glycosylated, M2-M maintained high levels of CD206 and CD200R, another M2-M specific marker (Koning et al., 2010) (fig 3.3c). However, when tumor cells were de-glycosylated by pre-treatment with 2DG or tunicamycin, CD206 and CD200R expression in M2 macrophages was significantly reduced. The same results were obtained using tumor cells knocked-out of the gene encoding for a glycosyltransferase involved in the synthesis of branched N-glycans, MGAT5.

These results suggest that de-glycosylated tumors have a reduced capacity to sustain M2 macrophages polarization.

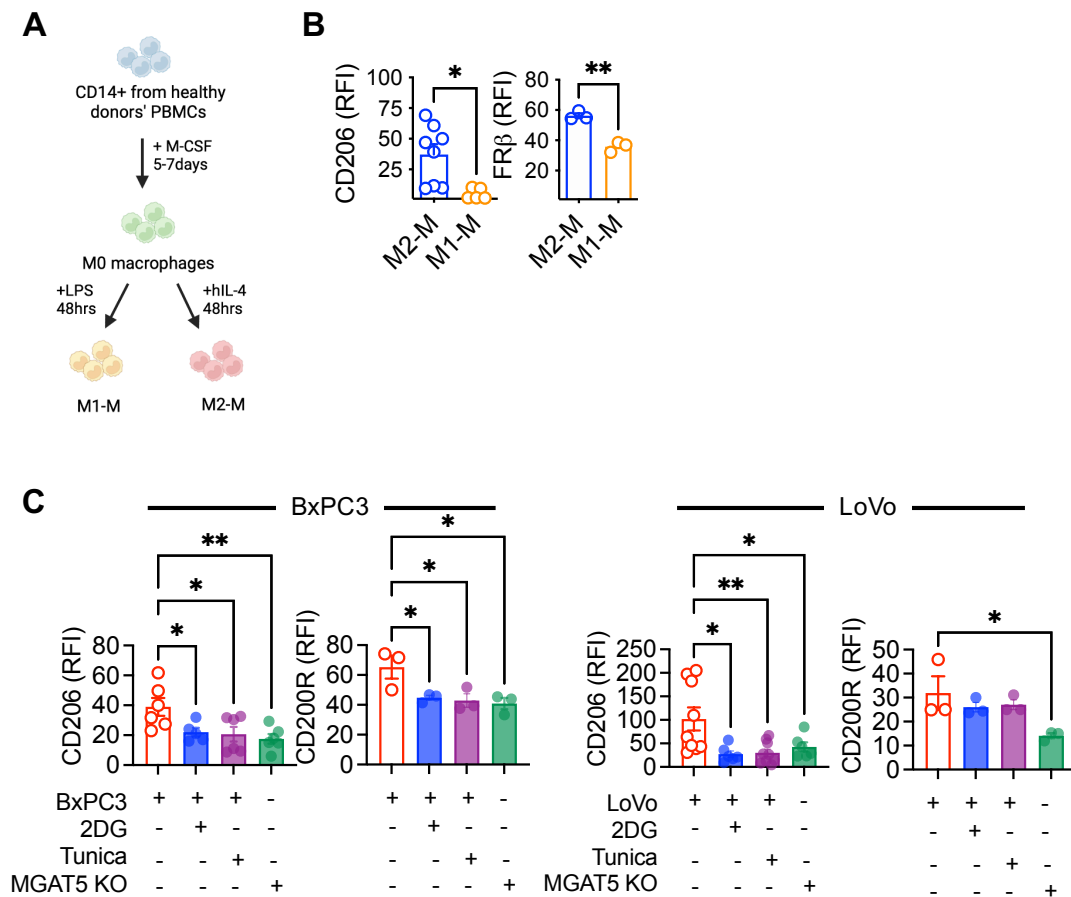


Fig 3.3 | De-glycosylated tumors dampen M2 macrophages polarization. (A) Schematic representation of protocol employed for primary macrophages differentiation and polarization is shown. CD14⁺ cells sorted from healthy donors' PBMCs were plated and cultured for 5-7 days in the presence of human M-CSF. Once obtained M0 macrophages, they were polarized in M2 macrophages (M2-M) with human IL-4 for 48 hours or in M1 macrophages (M1-M) with LPS for 48 hours (See "Material and Methods"). (B) Specific M2-M markers were analyzed by FACS in M1-M and M2-M polarized cells. The expression level (RFI) of CD206 and FRβ is shown. (C) CD206 and CD200R expression (RFI) of M2-M in co-culture with BxPC3 (left) or LoVo (right) pre-treated or not with 4mM 2DG, 100ng/ml tunicamycin or genetically knock-out for MGAT5. Results from t test (B) and one-way ANOVA (C) are indicated when statistically significant (*P ≤ 0.05; **P ≤ 0.01). Data are represented as means ± SEM. Schematics (A) was created with Biorender software.

3.2.2 THP-1 derived M2 macrophages lose their immunosuppressive activity upon N-glycosylation blockade

The role of glycosylated tumors in inducing an immunosuppressive microenvironment is well reported in literature. However, the direct role of N-glycosylation on TME cells is not well known. Therefore, we were interested in evaluating the effects of N-glycosylation inhibition on the immunosuppressive function of M2 macrophages.

We started by exploiting the monocyte-like cell line THP-1, which can be genetically modified through MGAT5 KO rather easily compared to M2 macrophages. THP-1 cells were differentiated *in vitro* with PMA for 24 hours (M0-like) and then exposed to IL-4 for 48 hours to obtain M2-like macrophages (M2-like, fig 3.4a). FACS analysis of these cells confirmed successful obtaining of M2-like THP-1 cells expressing higher levels of CD86 in comparison to M0-like, as reported in literature (Forrester et al., 2018) (fig 3.4b).

To test if the M2-like THP-1 cells show an inhibitory effect on CAR T cells, we set up tripartite co-cultures including BxPC3 cells, M2-like THP-1 and CEA CAR T cells. These assays revealed that CEA.28z CAR T cells displayed a reduced killing capacity in the presence of M2-like THP-1 cells. Strikingly, however, 2DG was able to abrogate this inhibitory effect, restoring potent elimination of BxCP3 also in the presence of M2-like THP-1 cells (fig 3.4c).

2DG is both a N-glycosylation and a glycolysis inhibitor. To analyze its impact on M2-like THP-1 cells, we performed PHA-L staining and analyzed lactate production as proxy of N-glycosylation and glycolysis, respectively. Interestingly, while we observed no difference in lactate production (fig 3.4e), a significant reduction in PHA-L lectin staining was detected after treatment with 2DG (fig 3.4d). These results suggest that 2DG preferentially inhibits the N-glycosylation pathway in M2-like THP-1 cells, at least at the dose we employed for these studies.

Then, to better assess the specific effect of N-glycosylation inhibition on M2-like THP-1 cells, we knocked-out MGAT5 in these cells. Successful gene knock-out was confirmed by PHA-L lectin staining (fig 3.4f) and tripartite co-cultures were performed to evaluate the functional impact of MGAT5 KO in M2-like THP-1 cells. Tumor killing at the 2:1 effector to target ratio was higher with M2-like MGAT5 KO THP-1 cells (fig 3.4g), supporting the notion that de-glycosylated M2-like THP-1 cells display lower immunosuppressive activity. In line with this observation, M2-like THP-1 cells inhibit

the proliferation of polyclonal-stimulated T cells, but treatment with 2DG or MGAT5 KO mitigated this negative effect (fig 3.4h).

Overall, these data suggest that N-glycosylation blockade reduces the immunosuppressive activity of M2-like THP-1 cells, thus leading to superior tumor elimination by CEA CAR T cells.

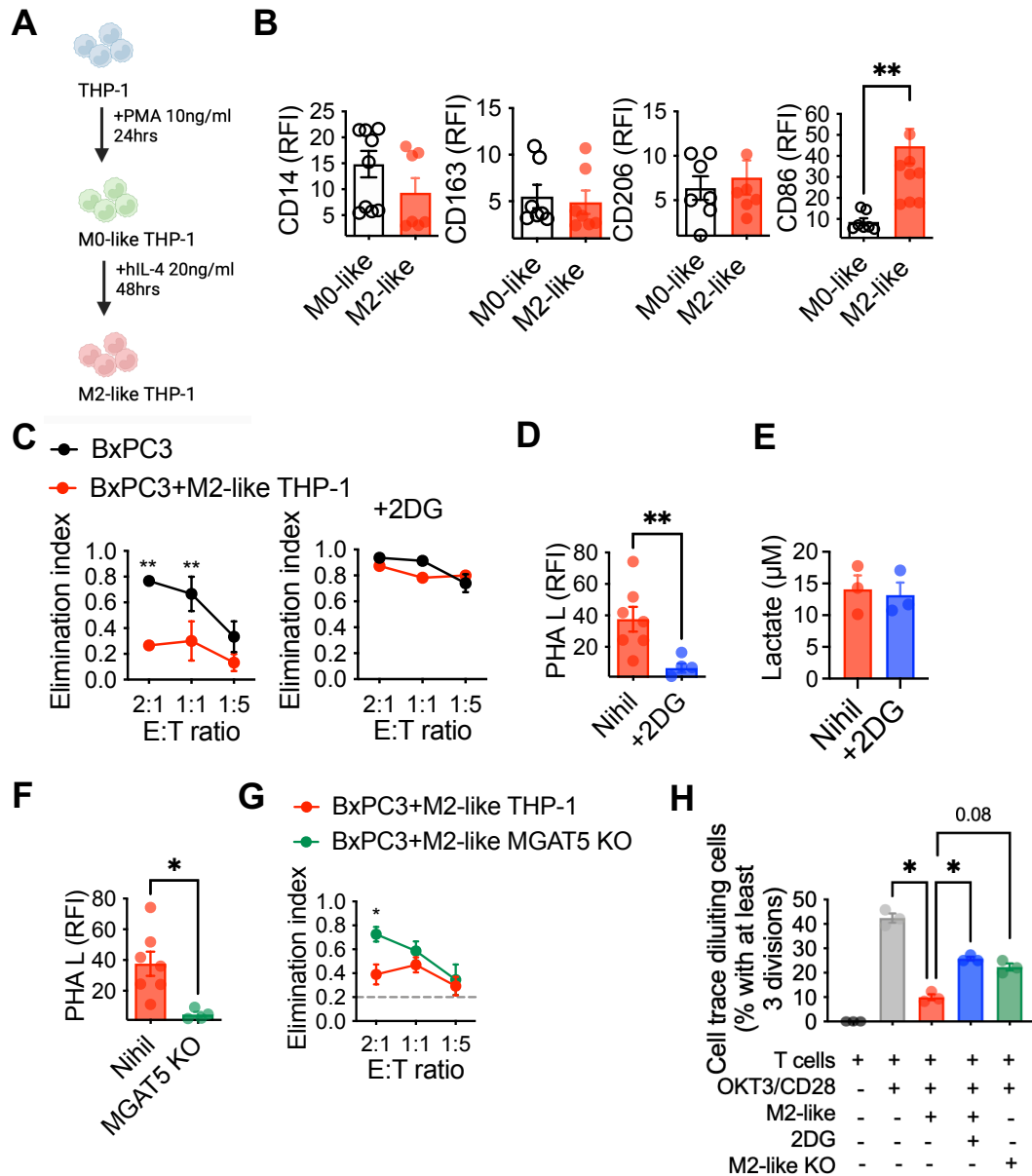


Fig. 3.4 | THP-1 derived M2 macrophages lose their immunosuppressive activity upon N-glycosylation blockade. (A) Schematic representation of protocol employed for THP-1 differentiation in macrophages (M0-like) and polarization in M2-like THP-1 is shown. THP-1 cell line was cultured for 24 hours with PMA. To polarize cells in M2 macrophages-like, M0-like

THP-1 cells were washed-out and cultured for 48hours with IL-4 (See “Material and Methods”). **(B)** THP-1 M0-like and M2-like expression markers analyzed by FACS (RFI) are shown. **(C)** Elimination index of BxPC3 after 48 hours triple co-culture with M2-like THP-1 and CEA.28z CAR-T in 2:1, 1:1 and 1:5 E:T ratio (left without previous 2DG treatment; right with 4mM 2DG pre-treatment to BxPC3 and M2-like THP-1 co-culture, washed-out before adding CAR T cells) (n=3 donors). **(D)** PHA-L expression level (RFI) by FACS of M2-like THP-1 with or without 2DG treatment is shown. **(E)** Lactate concentration in the medium of M2-like THP-1 culture, in the presence or absence of 2DG is reported. **(F)** PHA-L expression level (RFI) by FACS of M2-like THP-1 WT and MGAT5 KO is shown. **(G)** Elimination index of BxPC3 after 48 hours triple co-culture with M2-like THP-1 (WT or MGAT5 KO) and CEA.28z CAR-T in 2:1, 1:1 and 1:5 E:T ratio (n=3 donors) is reported. **(H)** T cells proliferation after 5 days co-culture with M2-like THP-1 (WT, treated with 2DG or MGAT5 KO) (n=3 donors). Results from t-test (B, D, E, F) and one-way ANOVA (C, G, H) are indicated when statistically significant (*P≤0.05; **P ≤ 0.01). Data are represented as means ± SEM. Schematics (A) was created with Biorender software.

3.2.3 Primary M2 macrophages are less immunosuppressive upon N-glycosylation inhibition

Once verified that inhibiting N-glycan synthesis in M2-like THP-1 cells reduces their inhibitory activity, we moved on to evaluate primary M2 macrophages. These cells were obtained from healthy donors' PBMCs, as described in section 3.2.1.

To characterize the effect of N-glycosylation blockade on M2 macrophages polarization, we first analyzed their phenotype after treatment with 2DG or tunicamycin. Interestingly, typical M2 markers such as CD206, CD209, CD200R, PDL-2 and FR β were strongly downregulated after treatment with both de-glycosylating agents (fig 3.5a). To enrich the phenotype characterization, we analyzed also the expression of markers involved in “don't eat me signal” mechanisms. In these pathways, tumor cells express specific ligands (e.g., CD24, CD47 and PDL-1), which bind their receptors expressed on M2 macrophages (namely Siglec10, SIRP α and PD-1), inhibiting their phagocytic capacity (fig 3.5b). Interestingly, upon N-glycosylation blockade, these receptors on M2 macrophages were downregulated, suggesting the inhibition of the “don't eat me” mechanism by tumor cells (fig 3.5c).

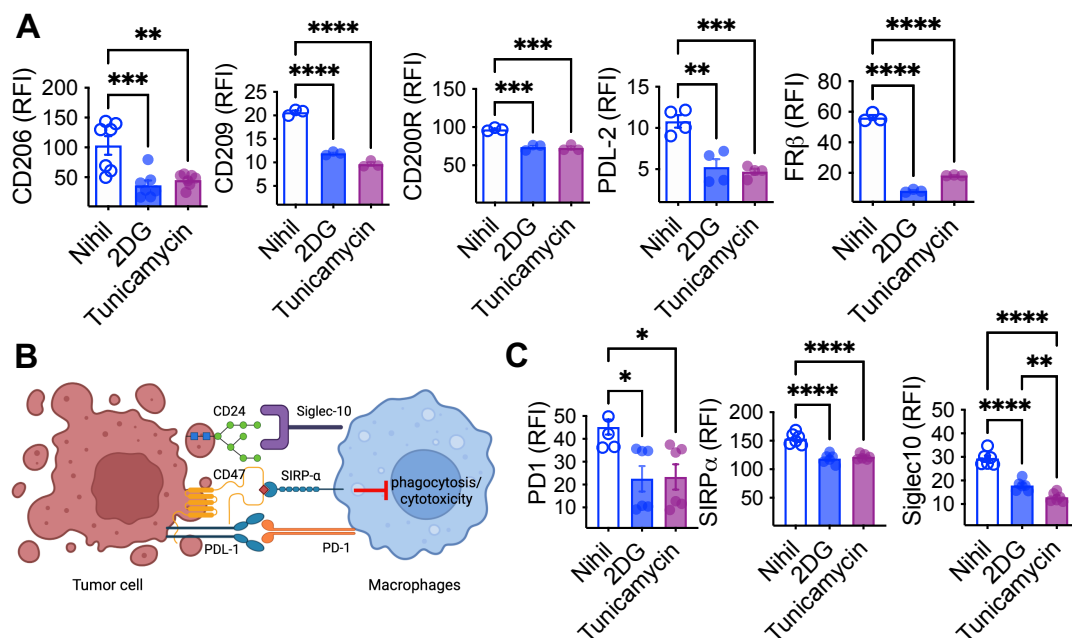


Fig. 3.5 | N-glycosylation blockade inhibits M2 macrophages polarization. (A) M2-M markers expression level (RFI) by FACS with or without 4mM 2DG or 100ng/ml tunicamycin treatment for 48 hours (CD206 n=7 donors; PDL-1 n=4 donors; other makers n=3 donors) (B) Schematic representation of “don't eat me” signals between tumor cells and macrophages is shown. (C) PD-

1, SIRP α and Siglec10 expression level (RFI) with or without 2DG or tunicamycin treatment (n=6 donors). Results from one-way ANOVA are indicated when statistically significant (*P \leq 0.05; **P \leq 0.01; ***P \leq 0.001; ****P \leq 0.0001). Data are represented as means \pm SEM. Schematics (B) was created with Biorender software.

To evaluate whether these phenotypic changes translate into functional differences, we analyzed cytokine release, phagocytic capacity and performed suppressive assays. Interestingly, both de-glycosylating agents completely abolished the ability of M2 macrophages to release IL-10, while promoting the production of pro-inflammatory TNF- α (fig 3.6a). In line with this, N-glycosylation blockade was also able to increase the phagocytic capacity of M2-M, bringing them closer to M1-M (fig 3.6b). These observations suggest that N-glycosylation inhibition not only hamper M2 polarization, but also promote the acquisition of features of pro-inflammatory M1 macrophages. Like M2-like THP-1 cells, also primary M2 macrophages were capable of inhibiting T cell proliferation in suppressive assays, but in the presence of 2DG this negative effect was significantly reduced (fig 3.6c-d). This effect was reverted by addition of mannose, which competes with 2DG in the N-glycosylation pathway, confirming that 2DG inhibits N-glycosylation by mannose mimicry. In line with this, we observed that 2DG treatment of M2 macrophages reduced PHA-L staining (fig 3.6e), without impacting on lactate production (fig 3.6f).

Altogether these results suggest that N-glycosylation blockade restrains the immunosuppressive activity of primary M2 macrophages, while inducing pro-inflammatory features.

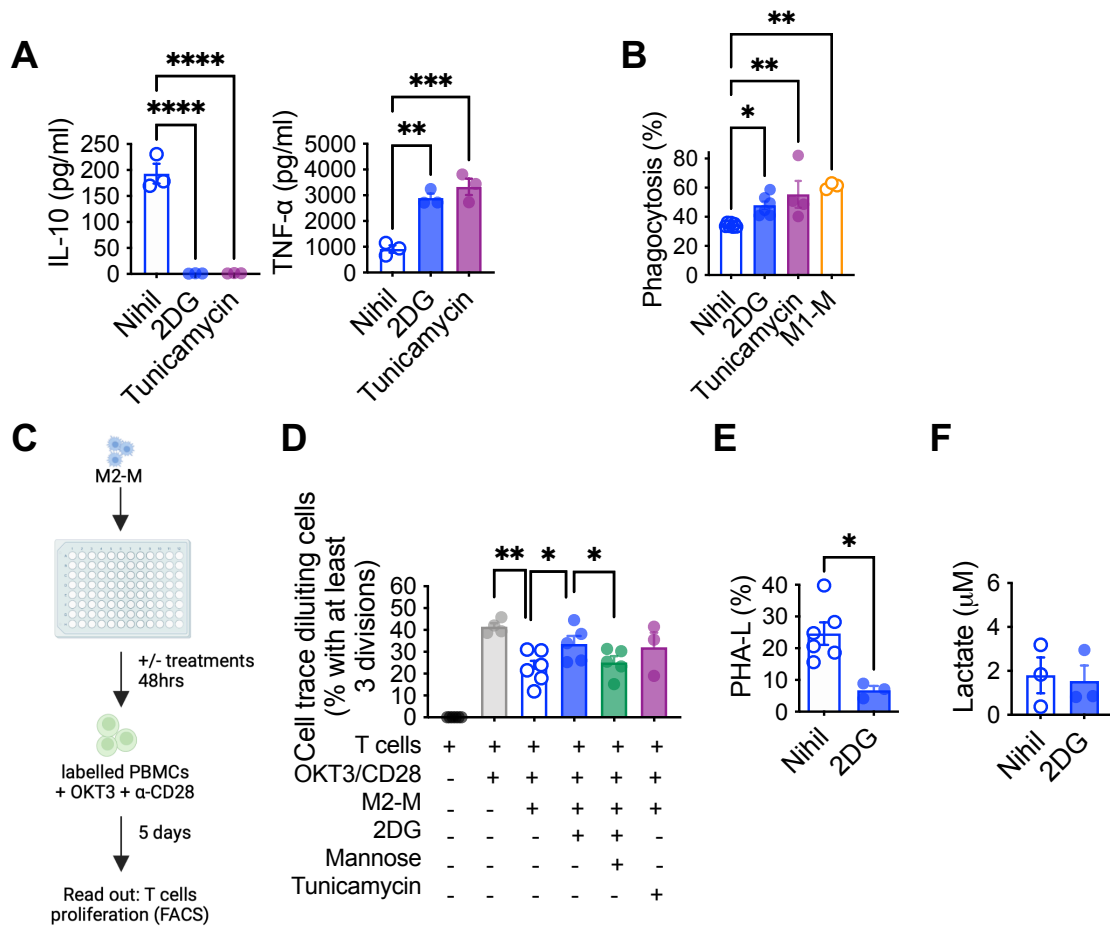


Fig. 3.6 | Primary M2 macrophages are less immunosuppressive upon N-glycosylation inhibition. (A) M2-M cytokines (IL-10 and TNF- α) concentration from supernatant, after 48 hours treatment with 4mM 2DG or 100ng/ml tunicamycin (n=3 donors). (B) Zymosan-based phagocytosis assay of M2-M (treated or not with 2DG or tunicamycin) and M1-M (Nihil n=7 donors; 2DG n=6 donors; tunicamycin n=4 donors; M1-M n=3 donors). (C) Schematic representation of suppressive assay with M2-M is shown. M2-M were plated in the presence or absence of different treatments (4mM 2DG, 4mM 2DG+1mM mannose, 100ng/ml tunicamycin) for 48 hours. Treatments were washed-out and labelled PBMCs from healthy donors, activated with OKT-3 and α -CD28 were added. After 5 days T cells proliferation was analyzed by FACS. (D) T cells proliferation after 5 days co-culture with M2-M. Treatments were washed-out before adding stimulated T cells (n=5 donors; n=3 donors in tunicamycin condition). (E) PHA-L expression (%) by FACS of M2-M before and after 2DG treatment (Nihil n=6 donors; 2DG n=3 donors). (F) Lactate concentration of M2-M culture medium in the presence or absence of 2DG (n=3 donors). Results from t-test (E, F) and one-way ANOVA (A, B, D) are indicated when statistically significant (*P \leq 0.05; **P \leq 0.01; ***P \leq 0.001; ****P \leq 0.0001). Data are represented as means \pm SEM. Schematics (C) was created with Biorender software.

3.2.4 N-glycosylation blockade downregulates immunosuppressive genes in M2 macrophages

To analyze more in depth the effect of N-glycosylation blockade on M2 macrophages, we performed transcriptome analysis of M2-M treated with de-glycosylating agents (2DG and tunicamycin) compared to untreated M2-M. M1 macrophages were also analyzed as comparison. From Pearson correlation analysis of transcriptional data, we observed similarity between the gene expression profile of both treated cells, which differ substantially from M2-M (fig 3.7a). To identify genes modulated after treatment, we performed a differential expression analysis of M2-M versus M2-M treated with 2DG or tunicamycin, separately, and we identified around 6000 genes classified in 7 clusters, using unsupervised hierarchical analysis (fig 3.7b). Cluster I and Cluster IV collect genes that are commonly down-regulated or up-regulated in treated versus untreated M2-M, while the others include genes specifically modulated by individual treatments. Enriched pathway analysis revealed that N-glycosylation blockade induces M2-M to downregulate genes involved in the inhibition of immune response, including PD-1 signaling and genes involved in the polarization and maintenance of M2-M, including IL-4 and IL-13 signaling. On the other hand, upregulated pathways include protein processing in the endoplasmic reticulum (ER) and the unfolded protein response (UPR), which are the expected consequences of N-glycosylation inhibition (Hetz et al., 2020) (fig 3.7c).

Analysis of specific genes extrapolated from Cluster I and Cluster IV revealed that many of the down-regulated genes are involved in immunosuppressive functions, while several of the up-regulated ones have a role in immuno-stimulating pathways (fig 3.7d). Among down-regulated genes, we highlight those reported in the dataset published by Martinez et al., described as M2-specific and down-regulated in M1-M, such as *Cd300a*, *Mrc1*, *Palld*, *Melff*, *Epb41l2*, *Ccl26* and *Cd209* (Martinez et al., 2006). Importantly, down-regulated genes also include some of those expressed by tumor associated macrophages, such as *Mpeg*, *Pdcd1lg2*, *Trem2*, *S100a9*, *Tgfb2*, *Mmp9* (Ma et al., 2022). Most of these genes play a crucial role in immunosuppressive functions, such as *S100a9* (Kwark et al., 2020), *Pdcd1lg2* (PDL-2) (Sumitomo et al., 2022) and *Trem2* (Katzenelenbogen et al., 2020), whose expression correlates with a poor prognosis in cancer patients. On the other hand, up-regulated genes include immunostimulating genes expressed by M1 macrophages, such as *Irf1* (Xie et al., 2016), *Irf7* (Yang et al., 2018),

Tnfsf9 (Wu et al., 2021), *Pagl* and *Cd55* (Martinez et al., 2006), which are expressed at high levels in M1 pro-inflammatory and anti-tumoral macrophages, as also reported from gene ontology.

Taken together these results, we can conclude that treating M2 macrophages with de-glycosylating agents induces profound transcriptional changes that appear to inhibit their immunosuppressive function. Interestingly, the treatment also results in the up-regulation of immune-stimulating genes, suggesting possible remodeling towards a pro-inflammatory state.

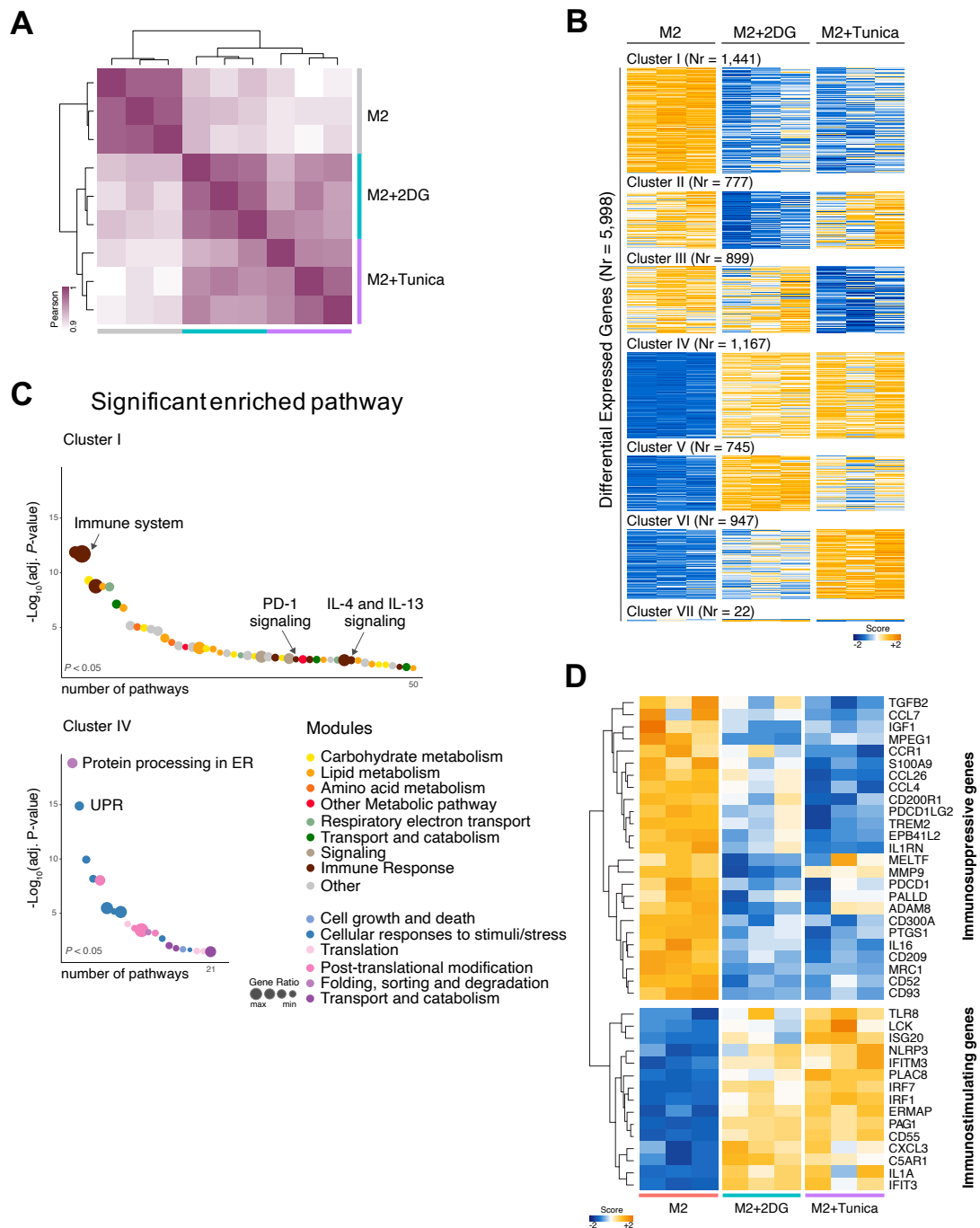


Fig. 3.7 | *N*-glycosylation blockade downregulates immunosuppressive genes in M2 macrophages. (A) Pearson correlation heatmap showing separation of M2-M with M2-M treated with 2DG or tunicamycin. Darker regions represent high correlation and lighter regions represent low correlation. (B) Gene expression heatmap and unsupervised hierarchical clustering (by *maximum* distance and *complete* linkage) of 5,998 genes found to be differentially expressed (FDR ≤ 0.01 and Fold Change ≥ 1.5) between M2-M and 2DG or tunicamycin treated M2-M. (C) Balloon plot showing significant enrichment pathways associated with genes differentially expressed in the Cluster I (upper-panel) and Cluster IV (bottom-panel) identified in B. Pathways were colored according to the legend.

(D) Heatmap showing significant differential expression of immunosuppressive and immunostimulating genes collected from literature.

3.2.5 De-glycosylated M2 macrophages acquire M1-like features

In the previous subparagraphs, we described how M2 macrophages treated with 2DG or tunicamycin lose their immunosuppressive function and acquire immune-stimulating features.

To better characterize this last aspect, we compared the gene expression profile of M1 macrophages from the same donors to that of the other samples. Principal Component Analysis (PCA) showed a global similarity between M1-M and M2-M treated with de-glycosylating agents relative to PC-2, which is very different for untreated M2-M (fig 3.8a). Differential expression analysis revealed 717 and 604 genes commonly up-regulated and down-regulated in M1-M and treated M2-M compared to untreated M2-M (fig 3.8b). These data already suggest the strong transcriptional similarity between de-glycosylated M2-M and M1-M.

To investigate which pathways are commonly overexpressed or down-regulated, we performed an enrichment analysis of de-regulated genes (fig 3.8c). Interestingly, the pathways commonly up-regulated in M1-M and treated M2-M are principally involved in epigenetic modification and positive regulation of immune response, including response to type I interferon and activation of interferon-regulatory factors (IRFs) by tumor necrosis factor receptor associated factors (TRAFs) (Dhillon et al., 2019). There are some evidences in literature regarding the role of epigenetic regulation in determining macrophages polarization. It's reported that overexpression of specific methyl transferases, such as DNMT3B and DNMT1, prevents M2 polarization, increasing TNF- α and IL-6 production by M1-M (Yang et al., 2014; Cheng et al., 2014). Acetylation is also known to control macrophages phenotype. In particular, H3 acetylation is reported to induce TNF- α and IL-6 expression in M1-M (Feng et al., 2010), while histone deacetylases 3 (HDAC3) is described as a negative regulator of M2 macrophages, able to repress IL-4 signaling and TGF- β production and to promote M1 polarization (Chen et al., 2012).

On the other hand, pathways downregulated in M1-M and treated M2-M compared to untreated M2-M comprise negative regulation of immune response, like IL-4 and IL-13 signaling, and metabolism, in particular respiration and Tricarboxylic acid cycle (TCA cycle). TCA cycle in M1-M is usually impaired, since it is broken in two different steps, after citrate and after succinate, thus resulting in the accumulation of specific metabolites,

such as citrate, succinate and itaconate, which exerts antibacterial function (Jha et al., 2015). M1-M are also characterized by reduced oxidative phosphorylation (OXPHOS), since they principally rely on glycolysis, crucial for their pro-inflammatory functions including phagocytosis, ROS production and secretion of inflammatory cytokines (Freemerman et al., 2014; Viola et al., 2019). Differently, in M2-M the TCA cycle is intact and their metabolic activity is characterized by enhanced fatty acid oxidation (FAO) and OXPHOS (Jha et al., 2015). These results suggest that N-glycosylation blockade can shape M2-M also in terms of metabolism that, after treatment become more similar to M1-M.

Overall, these findings support the concept that, besides inhibiting immunosuppressive behavior, N-glycosylation blockade also induces M2-M to acquire a M1-like pro-inflammatory phenotype, from a functional, metabolic and epigenetic point of view.

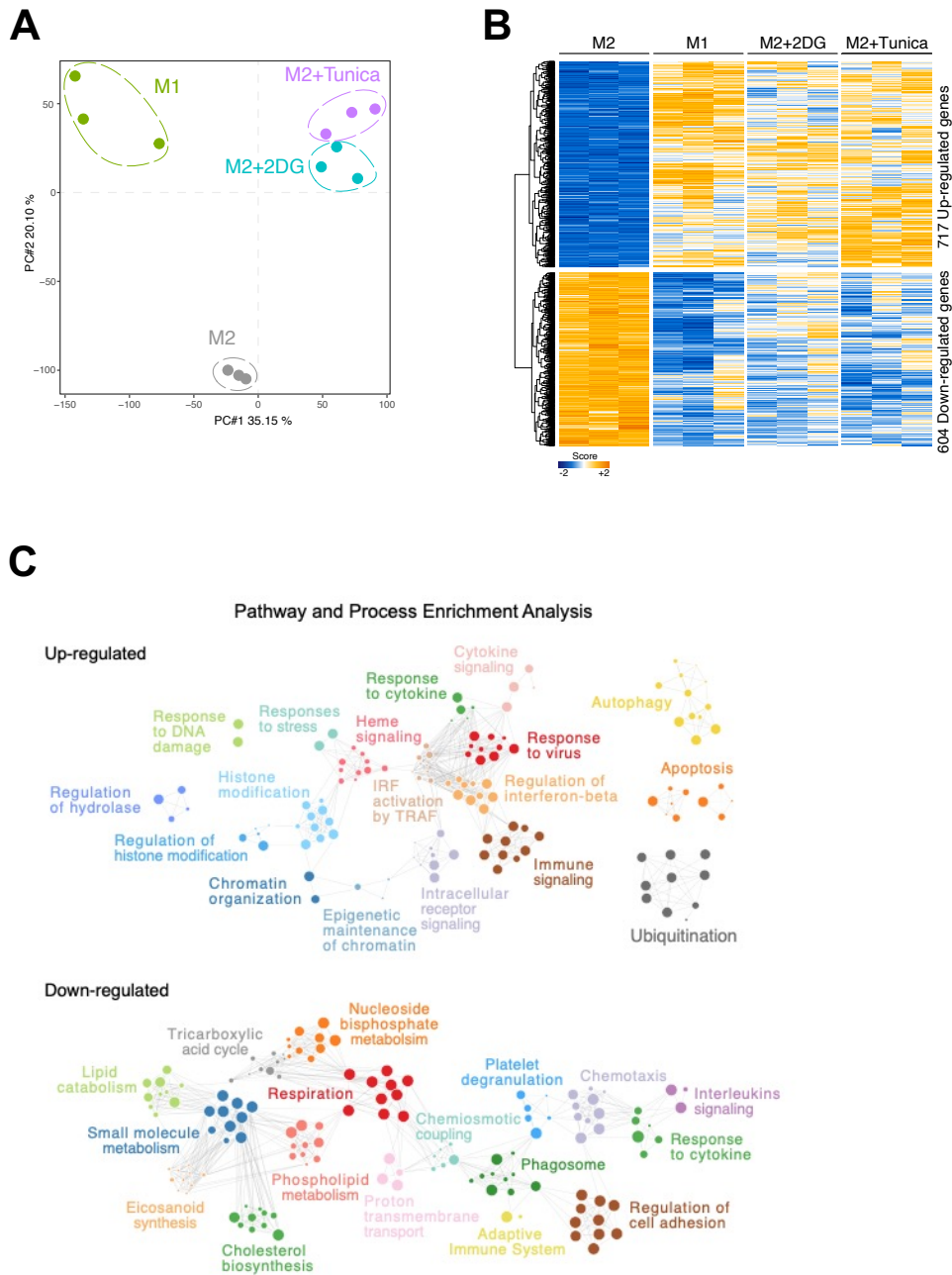


Fig. 3.8 | De-glycosylated M2 macrophages acquire M1-like features. (A) Principal component analysis (PCA) of RNAseq data. M1-M and M2-M (treated or not with 2DG or tunicamycin) were obtained from three individual PBMCs' donors upon differentiation with M-CSF and polarization with LPS (for M1-M) and IL-4 (for M2-M). (B) Gene expression heatmap and unsupervised hierarchical clustering (by *maximum* distance and *complete* linkage) of 1,321 genes found to be differentially expressed (FDR ≤ 0.05 and Fold Change $\geq |1.5|$) between M2-M versus M1-M macrophages samples. Gene expression of 2DG or tunicamycin treated M2-M are also shown. (C) Enriched processes associated with genes up-regulated (upper-pannel) and down-regulated (bottom-pannel) resulted by M1-M versus M2-M comparison. Terms with $P < 0.01$ were considered significant and two terms (nodes) with a similarity > 0.3 are linked by edges.

3.2.6 N-glycosylation inhibition reduces hepatic stellate cells activation

In the context of liver tumors and metastases, hepatic stellate cells (HepSCs) represent a crucial population of the TME, which support tumor progression and metastases formation. These cells are normally quiescent (qHepSCs), working as storage for vitamin A and retinoic acid droplets. However, in the context of tumors they become activated (aHepSCs) and support cancer progression by secreting growth factors and cytokines (Kang et al., 2011).

The contact of HepSCs with culture-treated plates renders HepSCs activated, as provided by manufacturer's data sheet (Lonza). aHepSCs are characterized by increased proliferation and high contractility with expression of pericellular matrix proteins, such as α -smooth muscle actin (α SMA) and specific markers, including platelet-derived growth factor β (PDGFR- β). On the other hand, qHepSCs are characterized by lipid droplets in cytoplasm to store vitamin A and retinoic acid, which is their main function (Shang et al., 2018). We analyzed the expression of these markers by immunofluorescence (α SMA and lipid droplets) and FACS (PDGFR- β). Upon N-glycosylation blockade, aHepSCs reduce their activation by downregulating the expression of PDGFR- β and α SMA (fig 3.9a-b). On the other hand, the inhibition of N-glycosylation increases the amount of lipid droplets, suggesting reshape towards a quiescent state (fig 3.9b).

The PD1/PDL-1 axis is a well-known mechanism of tumor immune escape, able to inhibit antitumor activity of T cells. It has been demonstrated that this binding requires N-glycosylation. In particular, N-glycans prevent PDL-1 degradation and ensure proper binding to PD-1, a feature shared with other co-inhibitory molecules but not with stimulatory pairs (Li et al., 2016; Li et al., 2018). Similarly, also PD-1 in T cells is extensively N-glycosylated and this is critical for its stability on the cell surface interaction with PDL-1 (Sun et al., 2020). Accordingly, abrogation of the PD-1/PDL-1 axis is one of the mechanisms responsible for improved antitumor activity of CAR T cells in combination with de-glycosylating agents (Greco et al., 2022). Interestingly, we observed that also aHepSCs bind a PD-1 chimera, and this interaction is reduced when the cells are de-glycosylated with 2DG or tunicamycin (fig. 3.9c).

To evaluate the functional consequences of N-glycosylation blockade, we performed suppressive assays like those performed with M2-M and observed that also aHepSCs are

capable of inhibiting T cell proliferation. Importantly, treatment with 2DG or tunicamycin was sufficient to abrogate their immunosuppressive function, paralleling the observation made with M2-M (fig 3.9d). Mannose supplementation to the condition with 2DG restored the inhibitory capacity, suggesting the specific role of N-glycosylation blockade in the observed phenomenon. In line with this, we observed that 2DG inhibits N-glycosylation (fig 3.9e) but not glycolysis (fig 3.9f) in aHepSCs.

Altogether, these evidences suggest that N-glycosylation blockade reduces HepSCs activation and abrogates their immunosuppressive functions.

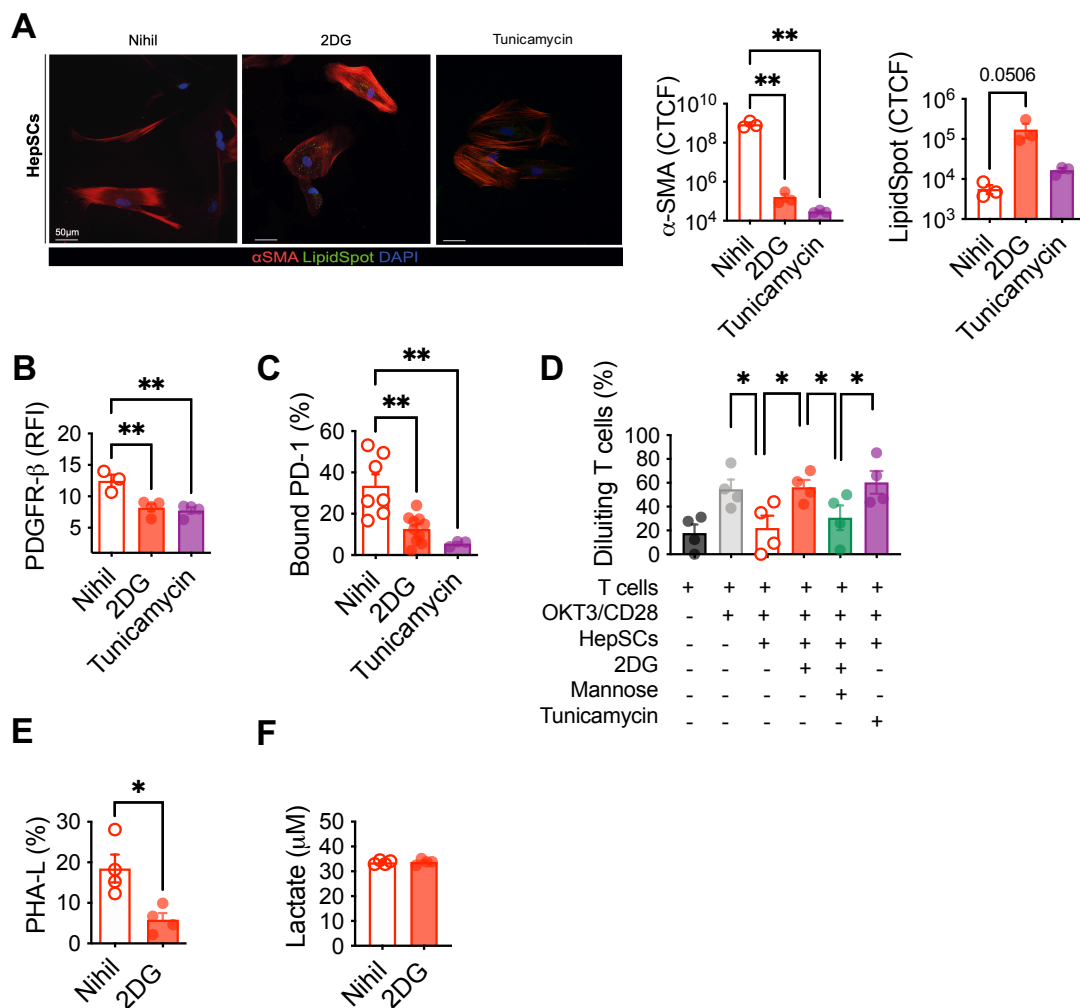


Fig. 3.9 | N-glycosylation inhibition reduces HepSCs activation. (A) Representative immunofluorescence images of HepSCs (treated or not with 2DG or tunicamycin) stained for α -SMA (red) and LipidSpot (green). Scale bars: 50µm. Below: ROI-based analysis of α -SMA and LipidSpot expression. (B) PDGFR- β expression level (RFI) in HepSCs (with or without 2DG or tunicamycin treatment). (C) PD-1 Fc binding to PDL-1 (%) in HepSCs treated or not with 2DG

or tunicamycin. **(D)** T cells proliferation after 5 days co-culture with HepSCs. Treatments were washed-out before adding stimulated T cells (n= 4 donors). **(E)** PHA-L expression (%) by FACS of HepSCs treated or not with 2DG. **(F)** Lactate concentration of HepSCs culture medium in the presence or absence of 2DG. Results from t-test (E, F) and one-way ANOVA (A, B, C, D) are indicated when statistically significant (* $P \leq 0.05$; ** $P \leq 0.01$). Data are represented as means \pm SEM.

3.2.7 N-glycosylation blockade increases CEA CAR T cells functions despite the presence of TME cells

Once evaluating the general effect of N-glycosylation blockade on M2 macrophages and hepatic stellate cells, we analyzed its specific effect in the context of CAR T cell therapy. To this aim, we performed tripartite co-cultures with TME cells, CEA CAR T cells and tumor cells, with or without 2DG treatment (fig 3.10a).

Of notice, CEA CAR T cells showed a reduced ability to kill BxPC3 cells in the presence of HepSCs, but 2DG completely reverted this negative effect (fig 3.10b, right). Differently, M2 macrophages failed to inhibit tumor cell killing (fig 3.10b, left), suggesting a milder inhibitory effect of this population in comparison to HepSCs. In general, targeting of LoVo cells was less influenced by both TME cells. However, a clear trend towards reduced killing in the presence of HepSCs was observed, but 2DG proved able to revert the effect (fig. 3.10c, right). Interestingly, in a suppressive assay with irradiated tumor cell lines, TME cells and CEA CAR T cells, M2-M demonstrated an inhibitory effect on CEA.28z CAR T cells proliferation in the presence of both BxPC3 (fig 3.10d, left) and LoVo cell line (fig 3.10e, left). This inhibitory mechanism was completely reduced upon treatment with 2DG or tunicamycin. HepSCs, however, resulted less prone to inhibit CEA CAR T cells proliferation in the presence of LoVo cell line (fig 3.10e, right), while showed strong suppression with BxPC3 cell line (fig 3.10d, right).

Altogether these data suggest that TME cells can inhibit CEA CAR T cells activity *in vitro*, both in terms of killing and/or proliferation, but treatment with de-glycosylating agents can restore their full functionality.

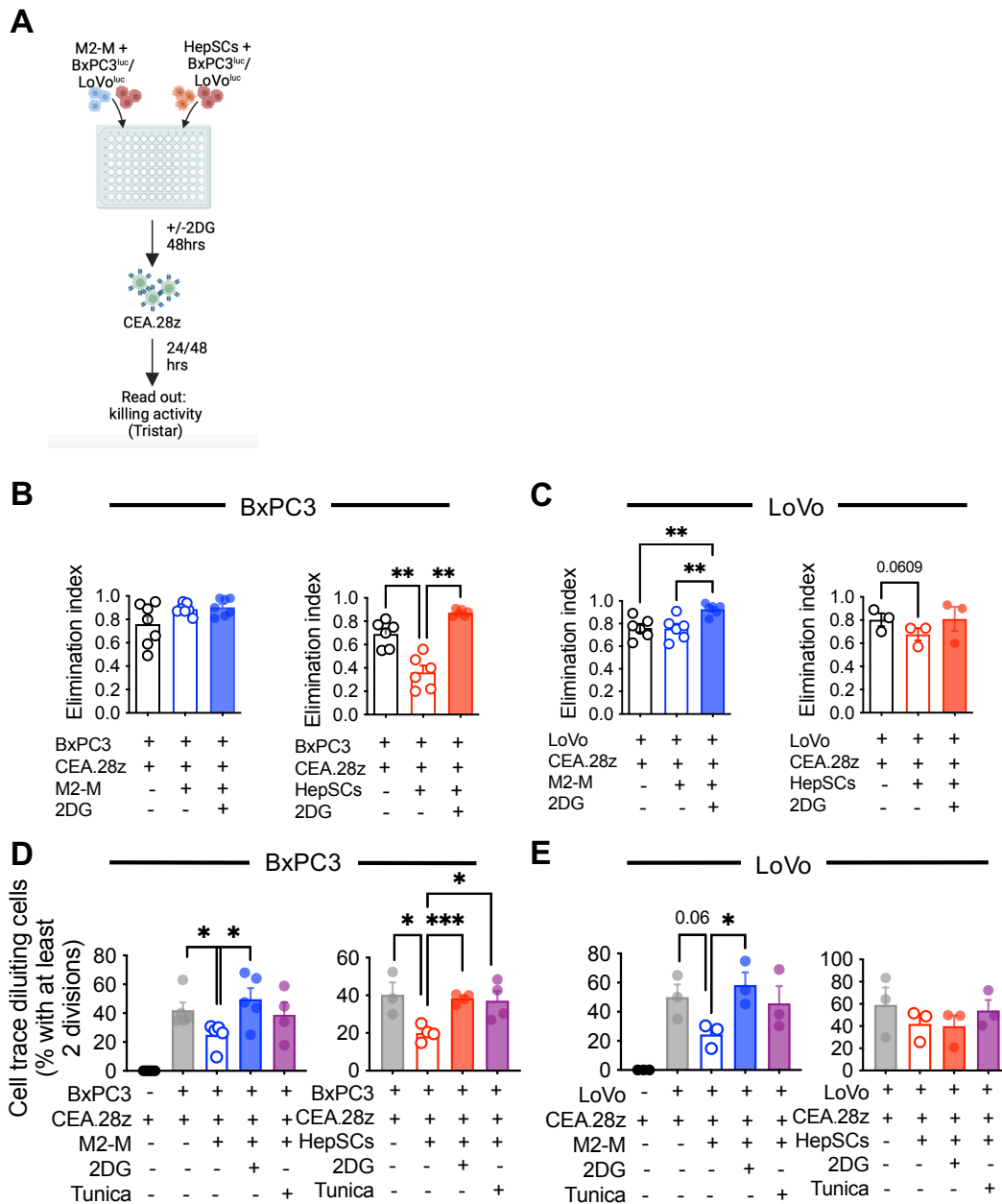


Fig. 3.10 | N-glycosylation blockade increases CEA.28z CAR T cells functions despite the presence of TME cells. (A) Schematic representation of triple co-culture with tumor cells (BxPC3 or LoVo), TME cells (M2-M or HepSCs) and CEA.28z CAR T cells is shown. BxPC3 Luc⁺ or LoVo Luc⁺ were plated together with M2-M or HepSCs and treated or not with 4mM 2DG for 48 hours. After treatment wash-out, CEA.28z were added in a 1:1 E:T ratio. After 24 hours, supernatant was collected for cytokine analysis. After 24 hours for LoVo and 48 hours for BxPC3, killing was analyzed by Tristar. (B) Elimination index of BxPC3 after 48 hours triple co-culture with M2-M (left) or HepSCs (right) in a 1:1 E:T ratio (n=6 donors). (C) Elimination index of LoVo after 24 hours triple co-culture with M2-M (left) or HepSCs (right) in a 1:1 E:T ratio (n=6 donors for M2-M and n=3 donors for HepSCs). (D) CEA.28z CAR T cells proliferation after 5 days co-culture with irradiated BxPC3 and M2-M (left) or HepSCs (right) (n=5 donors left; n=4 donors right). (E) CEA.28z CAR T cells proliferation after 5 days co-culture with irradiated LoVo

and M2-M (left) or HepSCs (right) (n=3 donors). Results from one-way ANOVA are indicated when statistically significant (*P \leq 0.05; **P \leq 0.01; ***P \leq 0.001). Data are represented as means \pm SEM. Schematics (A) was created with Biorender software.

3.2.8 2DG increases CEA CAR T cells killing capacity against PDOs from CRC-liver metastases

In the previous subparagraph, we described how 2DG restrains the immunosuppressive activity of TME cells, increasing CAR T cell reactivity against tumor cell lines. To understand if this potential is maintained in a more relevant context, in collaboration with Giovanni Tonon's group, we performed the same *in vitro* triple co-culture with organoids generated from liver metastases of CRC patients. Metastatic lesions were resected and processed to obtain a single cell suspension that was plated to generate organoids in the presence of Matrigel and specific medium (see "Material and Methods"). For the assay, PDOs were plated with TME cells and CEA.28z CAR T cells, with or without 2DG. After 72 hours CEA CAR-T killing activity was analyzed (fig 3.11a).

Clearly, PDOs are more resistant to CAR T cells than cell lines (fig 3.11b,c). Indeed, the elimination index (see "Materials and Methods") was only 0.5 with PDOs, while it reached 0.7 and 0.8 with BxPC3 and LoVo, respectively (see section 3.2.7). However, the presence of M2-M demonstrates a stronger inhibitory effect in comparison to HepSCs (fig 3.11b,c). Importantly, 2DG was able to increase targeting of PDOs both in absence and presence of either M2-M or HepSCs. Interestingly, the same behavior was observed analyzing tumor killing with bioluminescence (based on PDO's luciferase expression) and counting viable PDOs from microscope images.

Altogether, these data suggest that the N-glycosylation blockade can increase CAR T cell targeting of patient-derived tumor organoids despite the presence of TME cells.

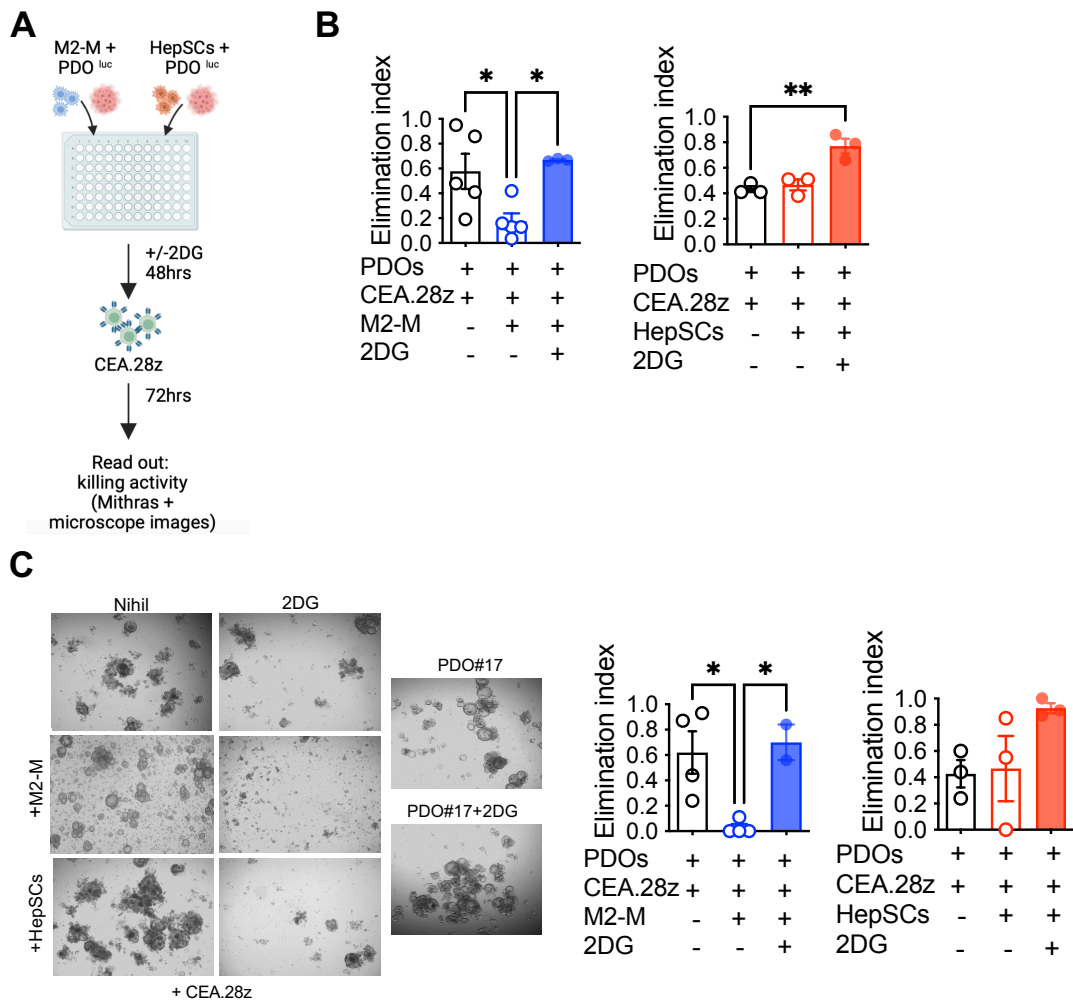


Fig. 3.11 | 2DG increases CEA CAR T cells killing capacity against PDOs from CRC-liver metastases. (A) Schematic representation of triple co-culture with PDOs, TME cells (M2-M or HepSCs) and CEA.28z is shown. PDOs Luc⁺ were plated with M2-M or HepSCs for 48 hours with or without 4mM 2DG treatment. After treatment wash-out, CEA.28z were added to the co-culture in a 1:1 E:T ratio. After 72 hours killing activity was analyzed with Tristar and with Axio Vert inverted microscope. (B) Elimination index of different PDOs (n=3) after 72 hours triple co-culture with M2-M (left) or HepSCs (right) in a 1:1 E:T ratio (n=3 donors with M2-M and n=5 donors with HepSCs). (C) Representative microscope images of triple co-culture of CEA.28z CAR-T, PDO#17, TME cells and with or without 2DG are shown. On the right elimination index of 3 PDOs was calculated from microscope images, by counting live PDOs in each condition normalized to PDO alone, without CAR-T. Results from one-way ANOVA are indicated when statistically significant (*P≤0.05; **P ≤ 0.01). Data are represented as means ± SEM. Schematics (A) was created with Biorender software.

3.3 Human TME *in vivo* modeling in the context of liver metastases

3.3.1 Intra-liver injection of CEA CAR T cells outperforms the intravenous one

In the previous paragraph, we observed *in vitro* the relevance of N-glycosylation to determine the immunosuppressive phenotype of M2 macrophages and hepatic stellate cells. Even if *in vitro* systems are useful to easily answer to specific questions, they are unable to recapitulate the complexity of cell interactions in a structured environment.

Therefore, we decided to set up an orthotopic xenograft mouse model for CEA CAR T cell therapy of CRC and PDAC liver metastases. First, we evaluated the feasibility of surgically injecting BxPC3 into the liver of immunodeficient mice and verified that the procedure permits the development of hepatic tumor masses. For the easy monitoring of tumor growth, cancer cells were engineered with a secreted luciferase that can be analyzed in blood samples. Second, we verified whether localized infusion of CEA CAR T cells at the tumor site was advantageous over systemic infusion (fig 3.12a). Indeed, once injected intravenously, CAR T cells have to overcome physical barriers to reach the tumor site, such as stromal cells and abnormal vasculature, that limit CAR T cells entry (Sacksterin et al., 2017; Hanahan and Coussen, 2012). Moreover, intravenously administered T cells do not usually infiltrate non-inflamed tumor tissues and can be sequestered within other organs, such as the lungs. These obstacles can be overcome by injecting CAR T cells directly at the tumor site. This administration route may also result in lower cytokines levels in the peripheral blood, reducing the risk to develop CRS and cytokine-mediated organ damage. Finally, regional delivery offers a way to bypass normal tissues, thus reducing on-target off-tumor toxicity (Cherkassky et al., 2022). Regional/local CAR-T administration has been investigated in different clinical trials, in the context of both brain tumors with anti-Her2 CAR T cells (Brown et al., 2016; Keu et al., 2017) and liver metastases with anti-CEA CAR T cells (Katz et al., 2015; Katz et al., 2020). Here, we observed that at the early time points, i.e., until day 7 from CAR T cells infusion, intra-liver injection was superior in tumor control compared to systemic delivery. However, in subsequent time points tumor control was lost also in the mice that received CAR T cells intra-liver (fig 3.12b).

It has been recently reported that liver metastases restrain immunotherapy efficacy due to hepatic myeloid cells, which induce apoptosis of activated T cells (Yu et al., 2021).

Hence, to better understand if the liver could be an obstacle *per se* due to its suppressive environment, we changed the tumor injection site. We compared CEA CAR T cells efficacy in the intra-liver (i.l.) and intra-peritoneum (i.p.) settings, where both tumor and CAR T cells were infused in the same site (fig 3.12c). Although a trend towards increased antitumor activity in the i.p. setting was observed, this advantage was rapidly lost (fig 3.12d), suggesting that independently from tumor location CEA CAR T cells are not sufficiently potent to counteract tumor growth.

Overall, these data suggest that hepatic CAR T cell delivery is superior to intravenous infusion, even if its efficacy remains low.

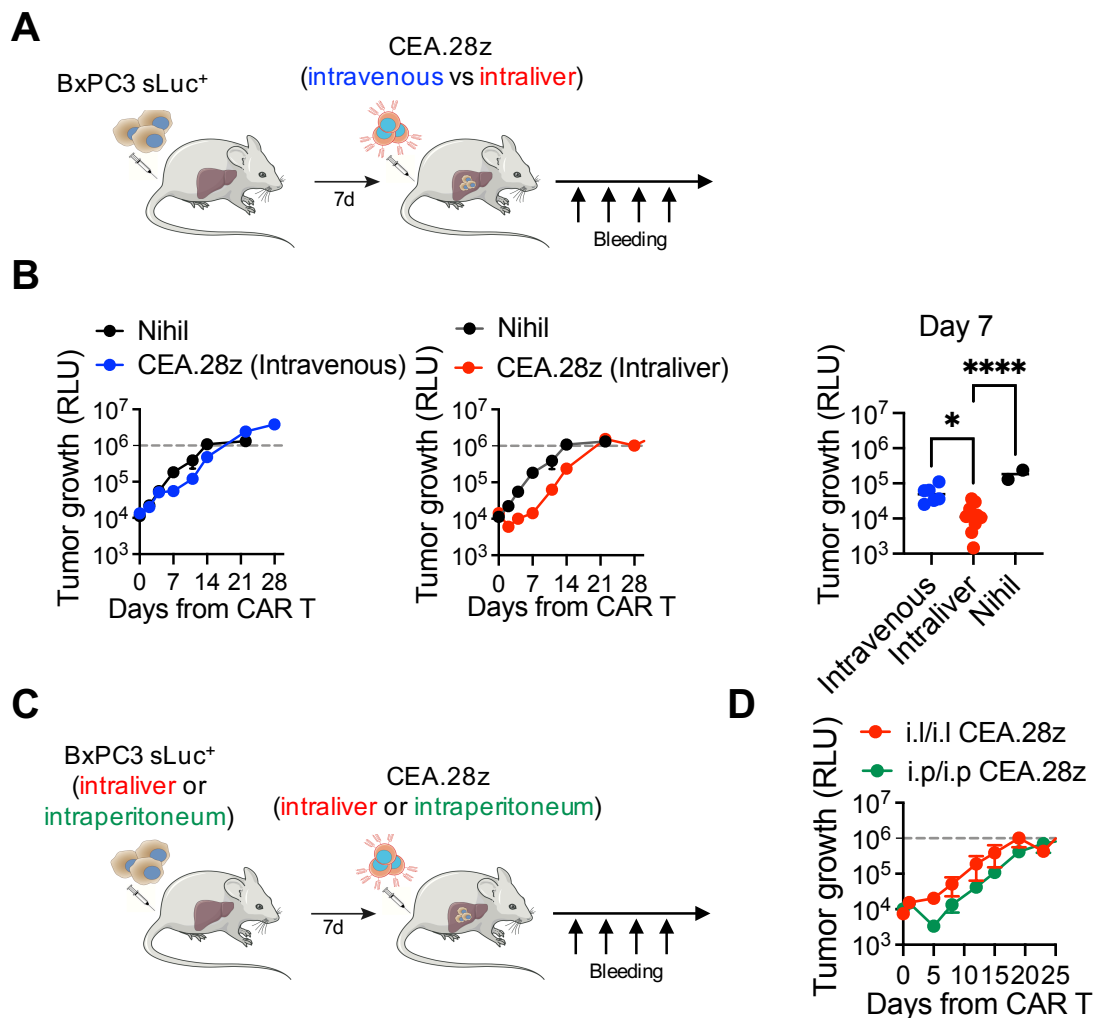


Fig. 3.12 | Intra-liver injection of CEA CAR T cells outperforms the intravenous one. (A) Schematic representation of pancreatic BxPC3 cell line injected intra-liver in SGM3 mice, treated with 10×10^6 CEA.28z CAR-T intravenous (i.v.) or intra-liver (i.l.) is shown. Tumor growth was

followed by bioluminescence analysis from blood samples, thanks to secreted luciferase (sLuc) expression by tumor cell line (Nihil, n=2 mice; CEA.28z i.v., n=6 mice; CEA.28z i.l., n=10 mice). **(B)** Tumor growth was measured from blood samples and reported as RLU, relative light unit. On the left RLU of i.v. infused CEA.28z treated group versus untreated group are shown. In the middle RLU of i.l. injected CEA.28z treated group versus untreated group are shown. On the right RLU at day 7 of i.v CEA.28z, i.l. CEA.28z and untreated groups are shown. **(C)** Schematic representation of BxPC3 injected i.l. or intra-peritoneum (i.p.) in SGM3 mice, treated with CEA.28z CAR-T i.l. or i.p. is shown (i.l/i.l CEA.28z, n=5 mice; i.p/i.p CEA.28z, n=5 mice). **(D)** Tumor growth reported as RLU of i.l. treated or i.p. treated mice is shown. Results from one-way ANOVA (B right) and two-way ANOVA (B left and middle, D) are indicated when statistically significant (* $P \leq 0.05$; **** $P \leq 0.0001$). Data are represented as means \pm SEM.

3.3.2 Humanized mice recreate a human immune tumor microenvironment

Even though classical xenograft mouse models are useful to answer questions regarding CAR T cell reactivity against tumor cells, they are limited by the absence of functional murine and human immune cells, which are crucial to support CAR T cell function, recreate a human immune tumor microenvironment and exacerbate CAR-related toxicities (Norelli et al., 2018; Giavridis et al., 2018). The presence of immune cells increases the complexity of xenograft mouse models, allowing to better profile CAR T cells efficacy and toxicities.

Therefore, for this project, we exploited a humanized mouse model in which immune-deficient mice are infused with human hematopoietic stem and progenitor cells (HSPCs) to reconstitute a functional human immune system. To this aim, we used a triple transgenic mouse strain (SGM3), which express human stem cell factor (SCF), granulocyte-macrophage colony stimulating factor (GM-CSF) and interleukin-3 (IL-3). These mice better support human hematopoiesis compared to NSG mice and allow an improved reconstitution of the myeloid compartment, which has a crucial role in modulating CAR T cell responses (Billerbeck et al., 2011; Norelli et al., 2018).

First, we set up the model in the context of tumors within the liver, injecting BxPC3 directly in the liver of humanized SGM3 (*huSGM3*) (fig 3.13a). In a first experiment, we analyzed tumor growth and human hematopoiesis in humanized versus not humanized mice. Tumor growth didn't differ in the two conditions (fig 3.13b), suggesting that humanization *per se* does not inhibit liver tumor progression. Similarly, no differences were observed in total human CD45+ cell counts and in specific immune populations,

including monocytes, NK cells and B cells (fig 3.13c), suggesting that the presence of tumor cells within the liver does not interfere with human hematopoiesis.

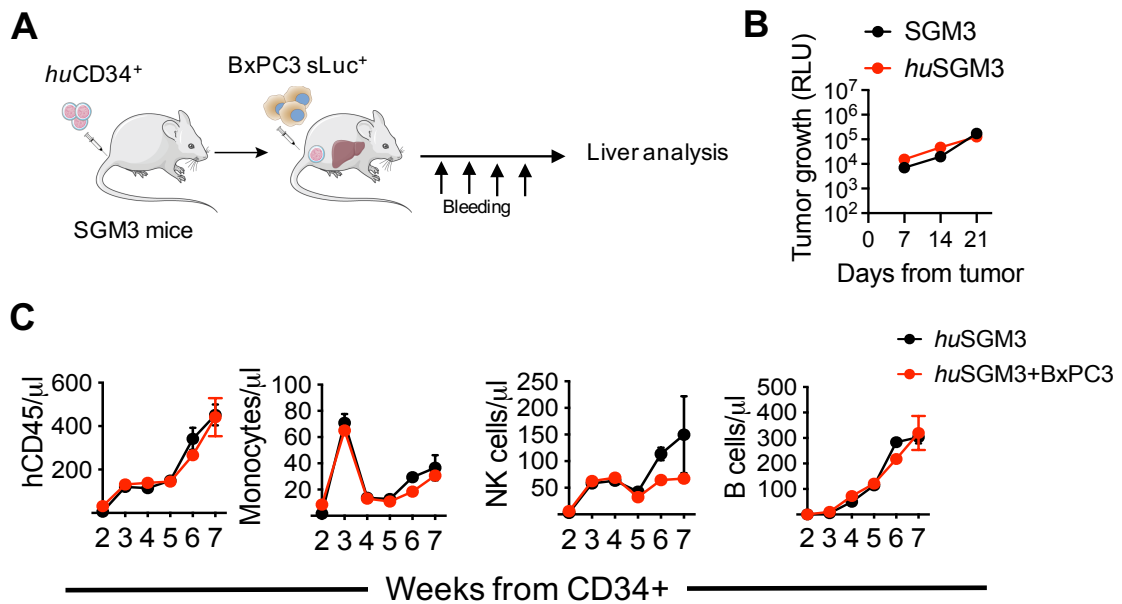


Fig. 3.13 | Tumor engraftment does not impair human immune reconstitution in humanized mice. (A) Schematic representation of intra-liver injected BxPC3 in *huSGM3* mice is shown. SGM3 mice were reconstituted with human CD34⁺ cells infused i.v. After BxPC3 i.l. injection, mice were treated or not with 2DG (500mg/Kg) infused i.p. every day, with two days wash-out. From blood sampling, human immune reconstitution was analyzed by FACS and tumor growth was measured by Mithras Reader as RLU. When tumor level was at cut-off, mice were euthanized and liver was analyzed by FACS. (B) Tumor growth (RLU) was measured every week from BxPC3 injection in *huSGM3* (n= 8 mice) vs SGM3 mice (n= 9 mice). (C) Human reconstitution in peripheral blood was analyzed by FACS. Concentration of hCD45, Monocytes, NK cells and B cells was calculated by FACS, in *huSGM3* (n= 3 mice) and in tumor-bearing *huSGM3* mice (n= 8 mice). Results from two-way ANOVA are indicated when statistically significant. Data are represented as means ± SEM.

In a second experiment, we treated tumor-bearing *huSGM3* mice with 2DG to evaluate if N-glycosylation blockade could impair human hematopoietic reconstitution and/or influence the human liver TME. We didn't observe any effects on total circulating human CD45⁺ cells and on monocytes, NK cells and B cells (fig 3.14a).

Importantly, when we analyzed the livers at sacrifice, we observed a great representation of different human immune cell subsets, including B cells (CD19⁺), monocytes (CD14⁺), dendritic cells (CD11b⁺/CD11c⁺), neutrophils (CD15⁺/CD16⁺),

eosinophils (CD15+/CD16-), M1 macrophages (CD80+/CD86+) and M2 macrophages (CD163+/CD206+), supporting the potential of the humanized model to recreate the complex interactions between tumor and immune cells (fig 3.14b). Accordingly, we observed that the frequency of M2 macrophages was increased in tumor-bearing mice and, in line with our *in vitro* data, 2DG treatment was able to reduce this immunosuppressive cell population (fig 3.14c).

Altogether, these data suggest that humanization does not impair tumor growth but allows tumor cells to coexist with other human immune cell populations. Interestingly, 2DG was able to reduce the frequency of M2 macrophages that was increased in the presence of the tumor.

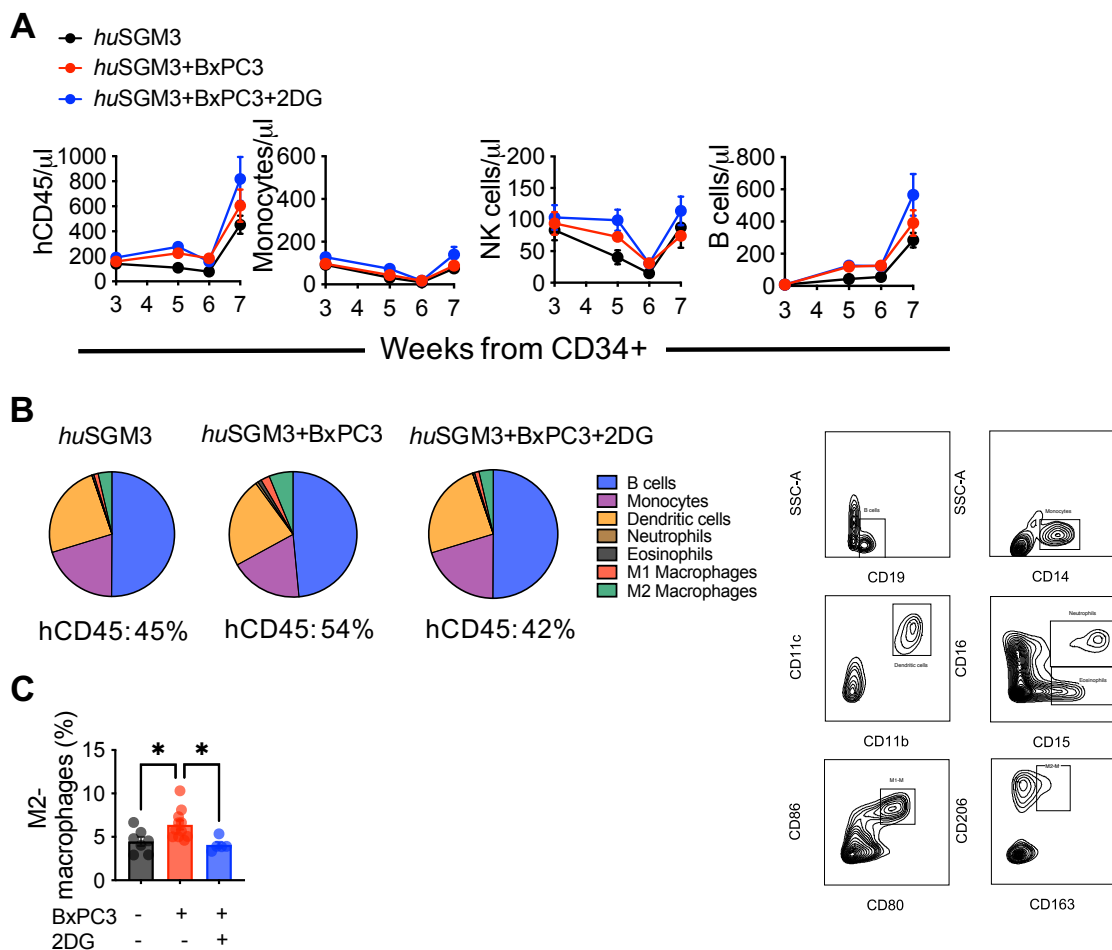


Fig. 3.14 | 2DG reduces the frequency of liver M2 macrophages in tumor-bearing *huSGM3* mice. (A) Concentration of hCD45, monocytes, NK cells and B cells was calculated by FACS, in *huSGM3* (n=3 mice), in tumor-bearing *huSGM3* mice (n=5 mice) and in tumor-bearing *huSGM3* mice treated everyday with 2DG (n=5 mice). (B) Pie charts of human immune cells distribution

within livers of *huSGM3* mice (n=7 mice), in tumor-bearing *huSGM3* mice (n=11 mice) and in tumor-bearing *huSGM3* mice treated everyday with 2DG (n=5 mice). Percentage (%) of total liver hCD45 in each group was reported (left). Representative FACS plots of human populations shown in pie charts (right). (C) Liver M2-M frequency (%) in *huSGM3* mice (n=7 mice), in tumor-bearing *huSGM3* mice (n=11 mice) and in tumor-bearing *huSGM3* mice treated everyday with 2DG (n=5 mice) was reported. Results from one-way ANOVA (C) are indicated when statistically significant (*P≤0.05). Data are represented as means ± SEM.

3.3.3 Intra-liver administration of CEA CAR T cells better controls tumor growth in BxPC3-bearing huSGM3 mice

Once understood that *huSGM3* mice are a feasible and useful model for liver tumors, we aimed to evaluate CEA CAR T cells efficacy in BxPC3-bearing *huSGM3* mice.

First, we evaluated the best CAR T cells delivery route as already performed in not humanized mice (fig 3.15a). The results obtained confirmed the superiority of CAR T cells injection at the tumor site compared to intravenous infusion (fig 3.15b). Interestingly, antitumor activity was stronger in humanized than in not humanized SGM3. In fact, in *huSGM3* disease was kept under control until day 14, while in SGM3 after day 7 tumor control was lost. This result indicates the importance of human immune cells in supporting CAR T cells functionality *in vivo*. Unfortunately, the experiment was aborted prematurely since mice developed severe toxicity. In detail, around day 14, we observed an exponential increase of circulating T cells (fig 3.15c) and a significant weight loss (fig 3.15d), detectable in all experimental conditions including mice treated with untransduced T cells. These observations suggest the occurrence of a xenogeneic GvHD reaction rather than a CAR-related toxicity like CRS. To support this hypothesis, we also analyzed serum concentration of typical CRS cytokines, including IL-6, IL-8, MCP-1 and IP-10, and we did not observe significant elevations compared to control mice (fig 3.15e), confirming the occurrence of xeno-GvHD rather than CRS.

Since xeno-reactive T cell precursors are usually present at a low frequency, we investigated whether reducing CAR T cell doses could mitigate this toxicity and allow to follow the mice in the long term. The administration of half dose of CEA CAR T cells injected *in situ* was sufficient to significantly delay tumor growth (fig 3.15f) and to increase mice survival (fig 3.15g). Interestingly, we didn't observe any signs of CRS in these mice, neither weight loss (fig 3.15h) nor relevant cytokines elevations (3.15i).

Overall, these data suggest that human immune cells help CAR T cells control of tumor growth without CRS occurrence. However, xeno-GvHD might prevent long term monitoring especially at high CAR T cell doses.

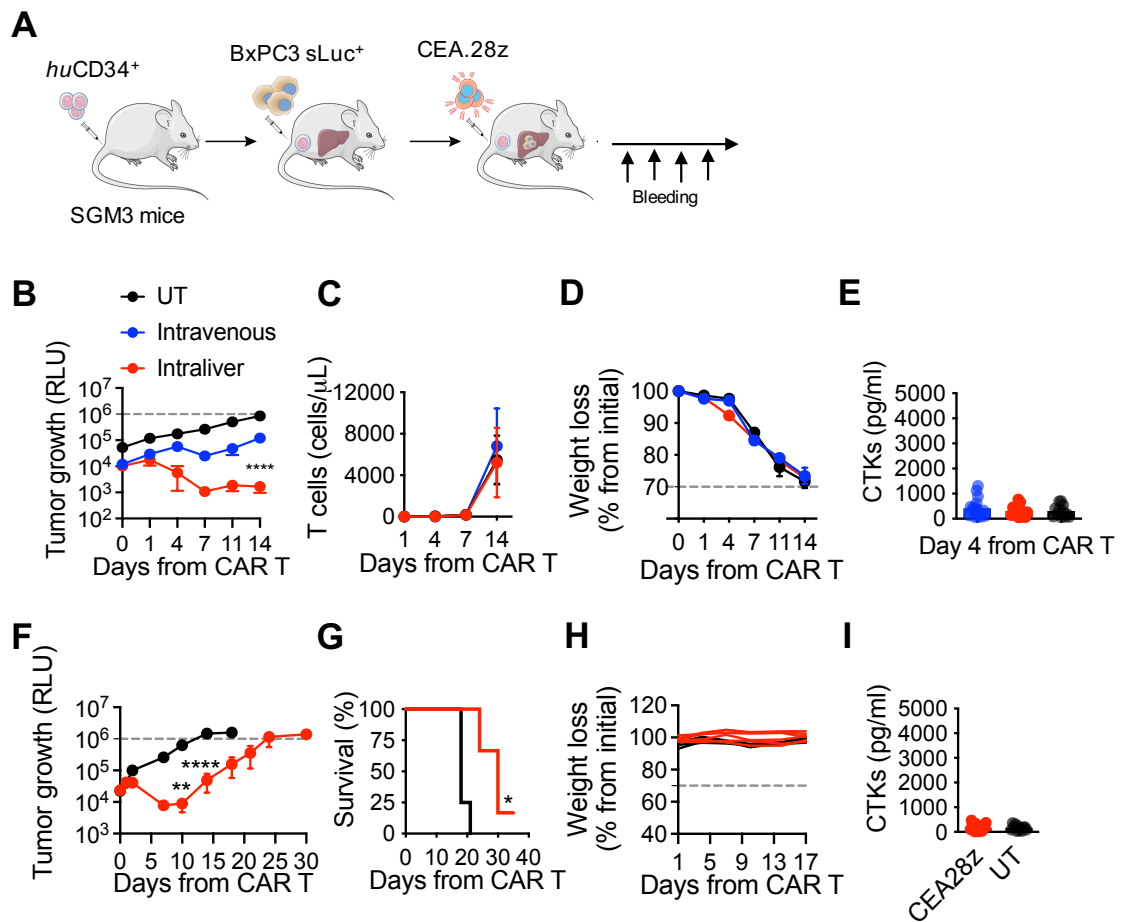


Fig. 3.15 | Intra-liver administration of CEA CAR T cells better controls tumor growth in BxPC3-bearing huSGM3 mice. (A) Schematics of intra-liver injected BxPC3 in huSGM3 mice treated with 10×10^6 CEA.28z is shown. SGM3 mice were reconstituted with human CD34⁺ cells infused i.v. BxPC3 were injected i.l. and after 7 days mice were treated with CEA.28z CAR-T i.v. or i.l. or with control untransduced T cells (UT, n=3 mice; CEA.28z i.v., n=4 mice; CEA.28z i.l. n=3 mice). (B) Tumor growth (RLU) was measured during time. (C) Peripheral blood T cells concentration is shown. (D) Weight loss from day 0 from CAR-T injection is shown. (E) Pooled IL-6, IL-8, MCP-1 and IP-10 concentration from serum collected at day 4 from CAR-T is reported. (F) Tumor growth (RLU) of 5×10^6 CEA.28z (n=4 mice) or UT (n=3 mice) treated mice was measured during time. (G) Kaplan-Meier survival plot of CEA.28z vs UT mice is shown. (H) Weight loss from day 0 from low-doses CEA.28z injected i.l. is shown. (I) Pooled IL-6, IL-8, MCP-1 and IP-10 concentration from serum collected at day 4 from low-doses CEA.28z injected i.l. is reported. Results from one-way ANOVA (E, I) two-way ANOVA (B, C, D, F, H) and log-rank Mantel-Cox test (G) are indicated when statistically significant (* $P \leq 0.05$; ** $P \leq 0.01$; **** $P \leq 0.0001$). Data are represented as means \pm SEM.

3.3.4 TCR knock-out CEA CAR T cells control tumor growth in LoVo-bearing huSGM3 mice, without the occurrence of xeno-GvHD

BxPC3 cells derive from a primary human pancreatic adenocarcinoma and do not develop multiple hepatic lesions when injected intra-liver. To better recapitulate a liver metastases mouse model, we tested LoVo cells, which derive from lymph-node metastases of colorectal cancer and express higher CEA levels compared to BxPC3 (fig 3.16a). Importantly, once injected in the liver of SGM3 mice, LoVo cells were able to give rise to intra-hepatic metastatic lesions, visible by MRI (fig 3.16b).

For these reasons, we decided to develop a LoVo-based *huSGM3* mouse model, injecting these cells intra-liver and infusing CEA CAR T cells 21 days after (fig 3.16c). Considering that, independently from the cell dose, the occurrence of xeno-GvHD reaction can vary among different donors, we decided to produce CEA CAR T cells knocked out of the endogenous TCR, allowing long term monitoring of experimental animals. Using the CRISPR/Cas9 technology and in collaboration with Chiara Bonini's group, we produced CEA CAR T cells, with a high TCR knock-out (TCR^{ko}) efficiency. Mice treated with TCR^{ko} CAR T cells proved able to control tumor growth (fig 3.16d) and prolong the survival (fig 3.16e) compared to the control condition, although mice eventually succumbed to the disease. Around day 7 from CAR T cells administration, we observed the lowest tumor level, which was concomitant with CAR T cells peak of expansion in peripheral blood (fig 3.16f). It is also interesting that CAR T cells are present also in the peripheral blood even if they were administrated intra-hepatic. Loss of tumor control by CAR T cells was concomitant with their disappearance in peripheral blood. Additionally, also with this cell line, no mice showed signs of CRS toxicity, both in terms of weight loss (fig 3.16g) and cytokines peak at day 4 from CAR T cells (fig 3.16h). Liver analysis at sacrifice indicated a high frequency of total human CD45⁺ cells in treated mice (fig 3.16i left), mainly explained by the presence of CAR T cells (fig 3.16i middle). Moreover, mice receiving CAR T cell therapy showed a lower frequency of immunosuppressive M2 macrophages compared to untreated controls, suggesting that treatment *per se* is capable of modulating the human immune compartment (fig 3.16i right).

These data suggest that LoVo-bearing *huSGM3* mice could be a useful liver metastases mouse model to test the efficacy of approaches aimed at potentiating CAR T cell responses, without any sign of toxicities.

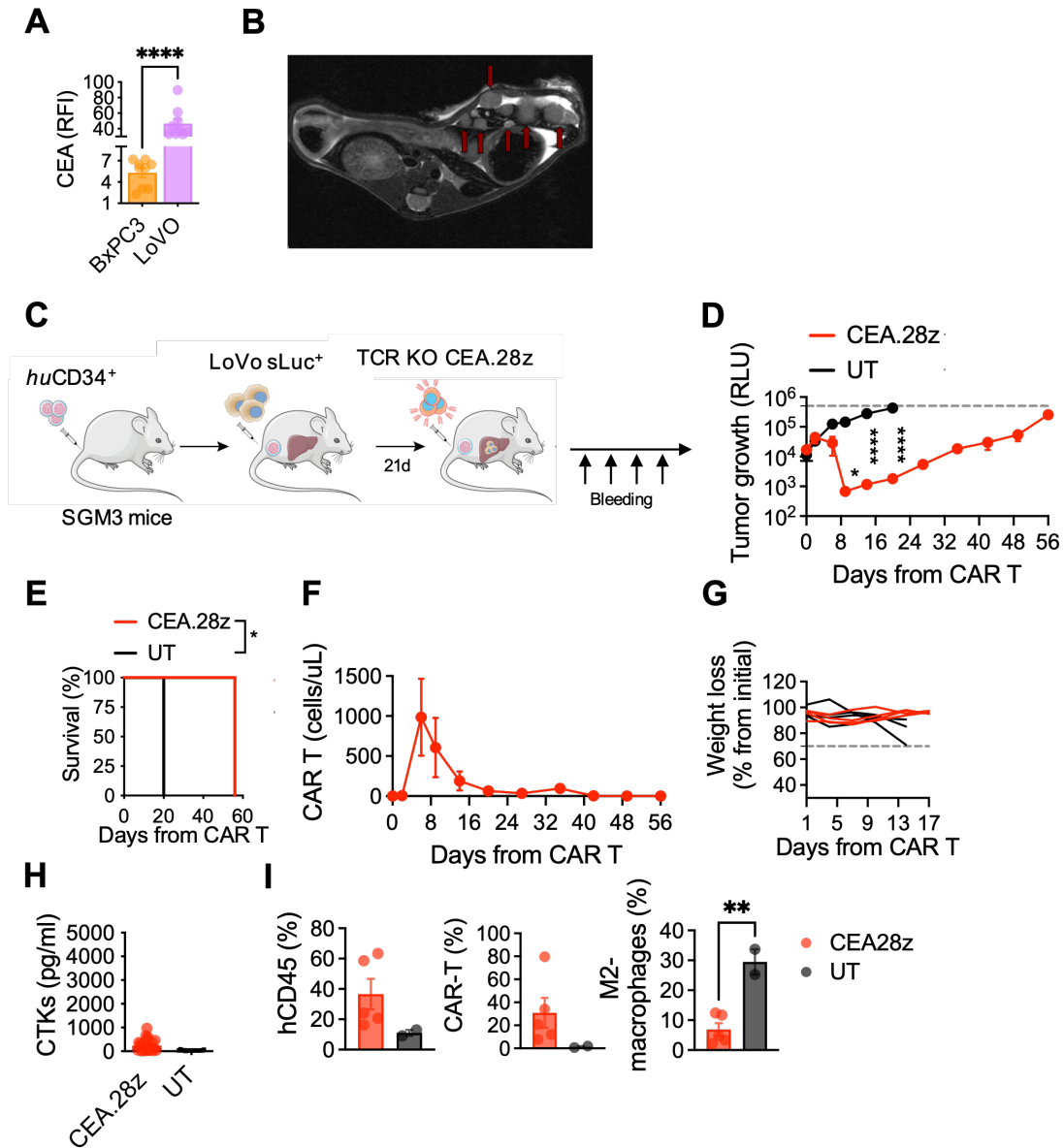


Fig. 3.16 | *TCR^{ko} CEA CAR T cells control tumor growth in LoVo-bearing huSGM3 mice, without the occurrence of xeno-GvHD* (A) CEA antigen expression (RFI) in BxPC3 and LoVo cell lines. (B) Representative MRI image of SGM3 mouse with metastatic lesions after 21 days from LoVo i.l. injection. (C) Schematic of LoVo-bearing *huSGM3* mice treated with 5×10^6 TCR^{ko} CEA.28z CAR-T is shown. After human reconstitution, LoVo were injected i.l. and after 21 days TCR^{ko} CEA.28z CAR-T (n=5 mice) or TCR^{ko} UT cells (n=3 mice, as control) were injected i.l. in *huSGM3* mice. Blood samplings were performed to follow the mice over time. (D) Tumor growth (RLU) was measured by blood sampling in treated vs control mice. (E) Kaplan-Meier of

survival plot of TCR^{ko} CEA.28z vs TCR^{ko} UT mice is shown. **(F)** Peripheral blood CEA.28z concentration is shown. **(G)** Weight loss from day 0 from CAR-T injection is shown in each experimental group. **(H)** Pooled IL-6, IL-8, MCP-1 and IP-10 concentration from serum collected at day 4 from T cells is reported. **(I)** Liver analysis at the sacrifice of human CD45+, CEA.28z CAR-T and M2-macrophages (%) in each experimental group is reported. Results from t-test (A, H, I), two-way ANOVA (D) and log-rank Mantel-Cox test (E) are indicated when statistically significant (*P≤0.05; **P ≤0.01; ****P ≤0.0001). Data are represented as means ± SEM.

3.3.5 Patient derived organoids from CRC-liver metastases develop metastatic lesions in the liver of huSGM3 mice

We developed tumor-bearing *huSGM3* mouse model, with both LoVo and BxPC3, to study CAR T cell therapy in the context of intra-hepatically injected tumor cells. In particular, we aimed to exploit the feasibility of the model and the efficacy of CEA CAR T cells in the presence of human immune cells. We observed that these cells strongly support CAR T cell function and seems to recreate a human immune TME.

To further improve the relevance of this model, we also exploited patient derived organoids (PDOs) from CRC-liver metastases (CRC-LM), which retain histological complexity and genetic heterogeneity of parental tumors.

Briefly, we injected CRC-LM PDOs intra-liver and evaluated the development of hepatic lesions by MRI and IVIS scan, since PDOs were transduced with firefly luciferase (Luc+) (fig 3.17a). We injected three different PDOs (#6, #17 and #54), which showed different engraftment capacity. PDO#6 failed to engraft, PDO#54 engrafted in 2 of 6 mice, while PDO#17 was the best one, with 7 of 9 mice developing lesions visible by both IVIS and MRI (Table 3.1). These three PDOs were derived from CRC-LM samples obtained after tumor resection. Primary CRC tumors were KRAS wild-type, excluding the one referred to PDO#17, which was mutated. Moreover, all the patients from which organoids were derived underwent chemotherapy before metastases resection.

In *huSGM3* mice, another variable is the cord blood (CB) donor. To evaluate its contribution, we injected PDO#17 in mice reconstituted with CD34+ cells from three different CB donors and observed a different engraftment capacity (Table 3.2). While none of the mice reconstituted with OSR 21CB/0011 developed metastases, all the mice developed metastatic lesions with OSR 21CB/0017 and CB39440 purchased from LONZA (fig 3.17b). These data underline the complexity of the model and the high variability of PDO engraftment, also influenced by CB donor.

Importantly, the architecture of metastatic lesions retrieved from mice was very similar to that of the primary lesion from which the organoid was derived (fig 3.17c). Indeed, the two slides show neoplastic glandular structures that recall intestinal origin and both of them show tumor necrosis.

When we challenged CEA CAR T cells against PDO#17 in *huSGM3* mice, we observed significant antitumor activity, both in term of luminescence signal (fig 3.17d) and

metastases formation (fig 3.17e). In particular, CEA CAR T cell treated *huSGM3* mice showed a reduced number of metastatic lesions (3.17e left) with decreased volume (3.17e right).

These data underline the complexity of the model but also suggest its potential for a wide exploitability for cancer immunotherapy.

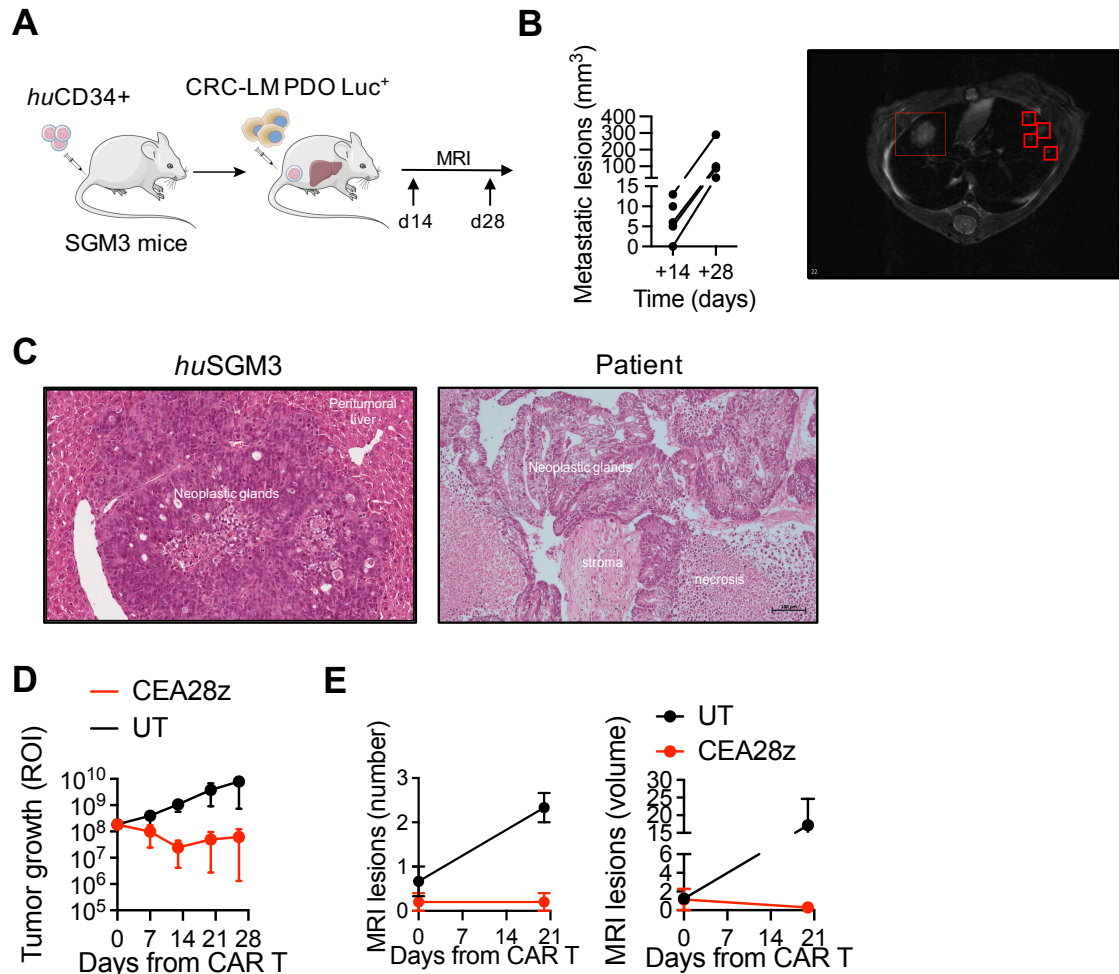


Fig. 3.17 | Patient derived organoids from CRC-liver metastases develop metastatic lesions in the liver of *huSGM3* mice. (A) Schematic of PDOs-bearing *huSGM3* mice is shown. After human reconstitution, PDO *Luc+* were injected i.l. and PDO growth was followed and analyzed by MRI and IVIS scan (n=5 mice). (B) Volume (mm^3) of metastatic intra-hepatic lesions in PDO-bearing *huSGM3* mice after 14 and 28 days from PDO injection (left). Representative MRI image of intra-hepatic metastatic lesions in PDO-bearing *huSGM3* mouse, engrafted with OSR 21CB/0017 (right). (C) Histological images of a metastatic intra-hepatic lesion from a representative *huSGM3* mouse (left) engrafted with CB39440 (LONZA) and injected with PDO derived from a patient, which lesion is shown in the right image. (D) Tumor growth, shown as ROI, of PDO in TCR^{ko} CEA.28z (n=4 mice) vs TCR^{ko} UT (n=4 mice). (E) Metastatic lesions from MRI images in TCR^{ko}

CEA.28z vs TCR^{ko} UT mice (left number; right volume). Results from two-way ANOVA (D, E) are indicated when statistically significant. Data are represented as means ± SEM.

#PDO	Engraftment	IVIS (ROI)	MRI (lesions)
PDO#6	0/5	ND	No
PDO#17	7/9	Mean: 1×10^9	Yes
PDO#54	2/6	Mean: 1×10^8	Yes

Table 3.1 | PDOs engraftment in huSGM3 mice.

CB donor	Engraftment	IVIS (ROI)	MRI (lesions)
OSR 21CB/0011	0/2	Mean: 1×10^5	ND
OSR 21CB/0017	4/4	ND	Yes
LONZA DON39440	3/3	Mean: 1×10^9	Yes

Table 3.2 | PDOs engraftment in huSGM3 mice infused with different cord blood (CB) donors.

3.4 N-glycosylation blockade inhibits immunosuppressive TME myeloid cells and increases CEA CAR T cells efficacy *in vivo*

3.4.1 N-glycosylation blockade increases CEA CAR T cells efficacy in LoVo-bearing huSGM3 mice

Once the *huSGM3* model was set up in the context of liver metastases, we used it to evaluate whether blocking N-glycosylation can increase the efficacy of CEA CAR T cell therapy by acting on both tumor and immune cells.

To this aim, we chose to start with tunicamycin because, differently from 2DG, it is a specific N-glycosylation inhibitor. LoVo-bearing *huSGM3* mice were treated with TCR^{ko} CEA CAR T cells with or without low doses of tunicamycin (0.02mg/Kg) injected i.p. twice a week (fig 3.18a), as reported (Han et al., 2015). Notably, the advantage of the group receiving tunicamycin was evident at all time points, with statistical significance reached at day 25 from CAR T cell infusion (fig 3.18b). At this time point, also the concentration of CEA CAR T cells in peripheral blood showed a higher trend in mice treated with the combined therapy (fig 3.18c). To analyze human liver populations in the two experimental groups, mice were euthanized at this time point. While we observed a reduction in the percentage of tumor cells and an increase in CAR T cells in mice receiving tunicamycin (fig 3.18d-e), no differences were observed in the proportion of dendritic cells, monocytes, M1 and M2 macrophages and FOXP3+Treg (fig 3.18e). To analyze the effect that N-glycosylation inhibition could have on the exhaustion profile of tumor-infiltrating lymphocytes (TILs), we also performed a SPICE analysis. Globally, no significant differences were observed (fig 3.18f left), but analyzing all the possible combinations of exhaustion markers such as PD-1, 2B4, TIM-3 and LAG-3, we noticed significant differences, supporting improved TILs phenotype, in mice treated with the combinatory strategy (fig 3.18f right). In particular, combination with tunicamycin resulted in a significantly lower frequency of CAR T cells expressing one or more exhaustion markers.

Although these results need to be confirmed, they suggest that N-glycosylation blockade increases CEA CAR T cells efficacy in *huSGM3* mice.

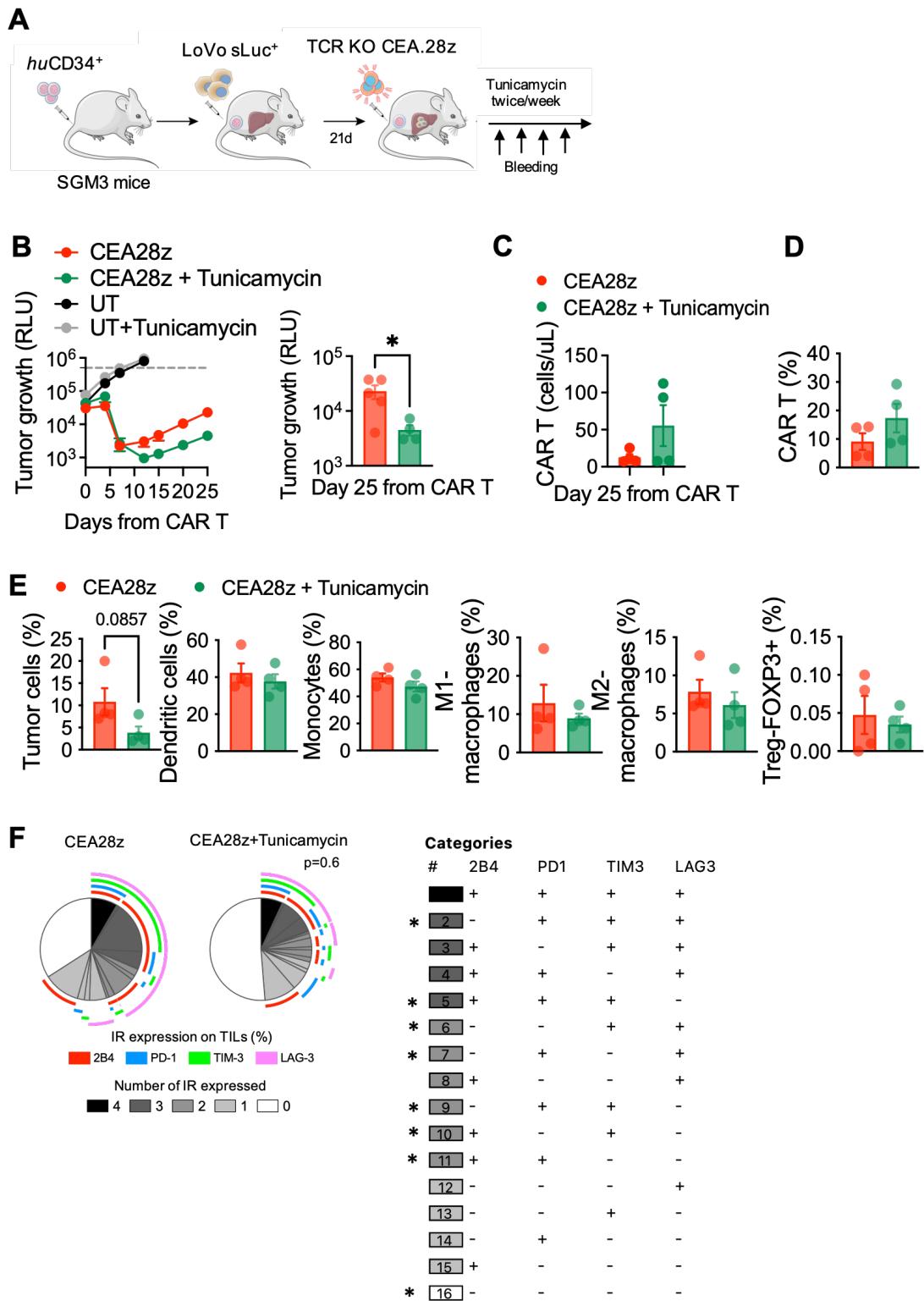


Fig. 3.18 | N-glycosylation blockade increases CEA CAR T cells efficacy in LoVo-bearing huSGM3 mice. (A) Schematic of LoVo-bearing huSGM3 mice treated with 5×10^6 TCR^{ko} CEA.28z CAR-T is shown. After human reconstitution, LoVo were injected i.l. and after 21 days TCR^{ko} CEA.28z or TCR^{ko} UT cells were injected i.l. in huSGM3 mice. A group of UT and

CEA.28z treated mice was also infused i.p. with 0.02mg/Kg tunicamycin twice a week for 3 weeks. Blood sampling were performed to follow the mice over time. **(B)** Tumor growth (RLU) was measured by blood sampling (left) in CEA.28z (n=5 mice) and CEA.28z + tunicamycin treated mice (n=5 mice) vs UT mice (n=5 mice) and UT + tunicamycin (n=2 mice). Right: Tumor growth (RLU) at day 25 from T is shown. **(C)** Concentration of peripheral blood CEA.28z CAR-T analyzed by FACS at day 25 from T. **(D)** Frequency (%) of CEA.28z CAR T cells were analyzed in tumor masses at sacrifice (day 25 from T). **(E)** Tumor analysis by FACS at day 25 when mice were sacrificed. Frequency of tumor cells, monocytes, dendritic cells, M1 macrophages, M2 macrophages and Treg-FOXP3+ are shown. **(F)** SPICE software analysis of TILs in CEA.28z mice vs CEA.28z + tunicamycin is shown (left). 2B4, PD-1, TIM-3 and LAG-3 expression between the two CEA.28z treated groups is reported in table obtained from SPICE software analysis (right). Results from t-test (B right, C, D, F right), two-way ANOVA (B left) and permutation test (F left) are indicated when statistically significant (*P≤0.05). Data are represented as means ± SEM.

3.4.2 N-glycosylation blockade downregulates myeloid immunosuppressive gene expression in *huSGM3* mice

To better characterize the effect of N-glycosylation inhibition on immune cells in the liver of tumor-bearing *huSGM3* mice receiving CAR T cell therapy, we performed a NanoString analysis on tumor-infiltrating human CD45+ cells.

Briefly, *huSGM3* mice were injected with LoVo cells subcutaneously and infused i.v. with CEA CAR T cells, in the presence or absence of tunicamycin (administered i.p. 2 days before and 2 days after CAR T cells infusion). After three days, mice were sacrificed and human CD45+ cells were isolated from tumor masses to perform NanoString analysis, using the human myeloid innate immune panel (fig 3.19a).

Strikingly, we observed that many genes were downregulated when tunicamycin was combined with CAR T cell therapy, as compared to CAR T cells alone. Interestingly, investigating from literature the role of these genes, we found that many of them are involved in M2 polarization and immunosuppressive features. For example, *ApoE* encodes for Apolipoprotein E that exerts potent anti-inflammatory effects and whose expression induces M2 macrophages polarization (Baitsch et al., 2011). *Trem2* is another gene expressed by M2 macrophages and recently its role in defining M2-TAMs with a potent immunosuppressive activity has been reported (Katzenelenbogen et al., 2020). In our results, we also observed the downregulation of typical M2-macrophages markers, such as *Mrc1* (CD206) and *Clec7a*, also known as *Dectin-1*, which promotes immune suppression in the TME inducing pancreatic carcinoma progression and peri-tumoral immune-tolerance (Daley et al., 2017). Specific M2-TAMs expressed genes are also *Fpr3* (Tan et al., 2020), *Marco* (Shi et al., 2021), *S100a8* (Li et al., 2020) and *Il4il* (Yue et al., 2015), which are associated with tumor progression and poor prognosis. In particular, *S100a8* and *Il4il* are also involved in immunosuppressive mechanisms, by promoting tumor escape and inhibiting effector T cells response (Li et al., 2020; Yue et al., 2015). In line with *in vitro* data, these results suggest that N-glycosylation blockade with tunicamycin inhibits the expression of immunosuppressive, tumor-promoting genes in *huSGM3* mice.

Despite the prevalence of down-modulated genes, we also observed the up-regulation of some immune-stimulating genes, such as *Il-3* (Chen et al., 2020) and *Edn1*, a toll-like receptor induced inflammatory gene (Dogan et al., 2019) (fig 3.19b). Moreover,

importantly, the expression of genes involved in Th1 activation and antigen presentation, such as *Ifng*, *Ifit1*, *Lamp3* and *Hla-dob* (NanoString Annotation v6), was similar in level as in the “only CAR” group and upregulated in both treated groups in comparison to control mice (fig 3.19c). These data underline the specific action of tunicamycin on the inhibition of immunosuppressive myeloid genes rather than a general inhibitory effect on gene transcription.

Altogether, these results suggest that N-glycosylation blockade could dampen immunosuppressive myeloid cells also *in vivo*.

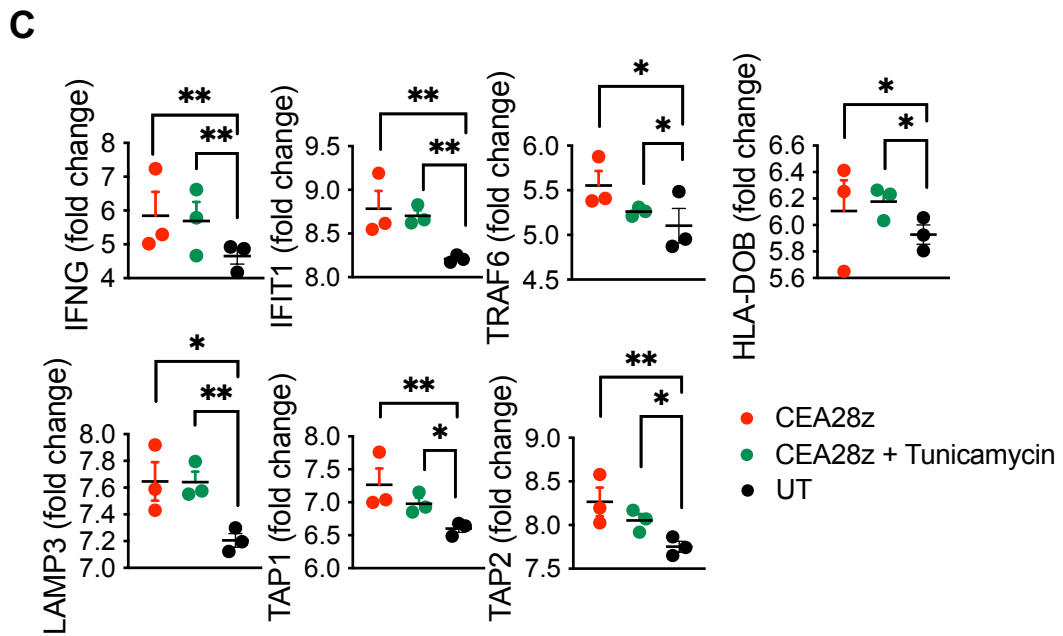
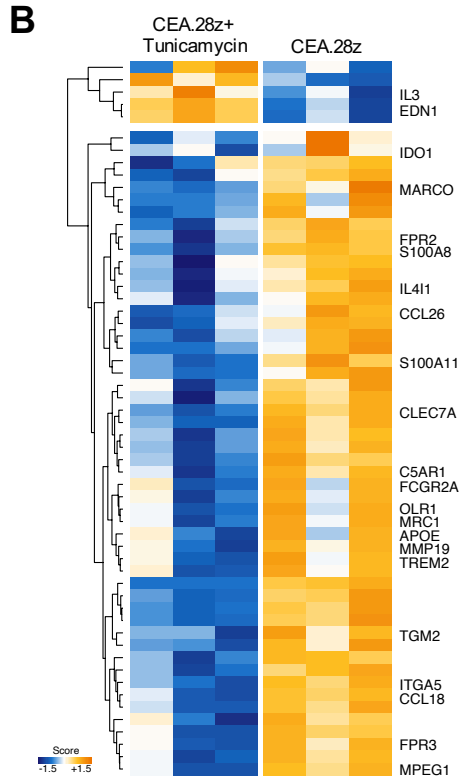
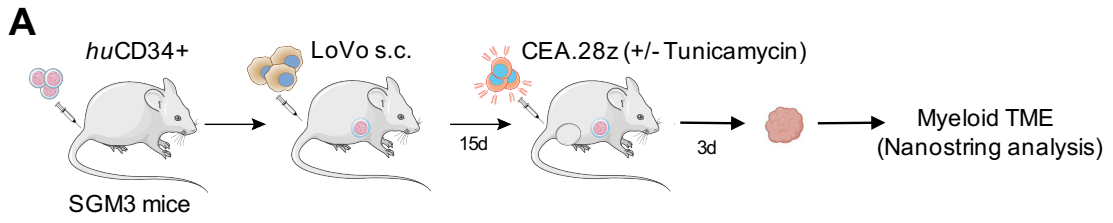


Fig. 3.19 | N-glycosylation blockade downregulates myeloid immunosuppressive gene expression in huSGM3 mice. (A) Schematic of NanoString myeloid TME analysis in *huSGM3* mice is shown. CD34⁺ cells were i.v. infused in mice and after human reconstitution, LoVo (5×10^5) were injected subcutaneously (s.c.) in the right flank. 15 days later mice were infused i.v. with (5×10^6) CEA.28z CAR-T (n=3 mice) or UT cells (n=3 mice), as control. A group of CEA.28z treated mice was also infused i.p. with 0.02mg/Kg tunicamycin two days before and two days after CAR-T infusion (n=3 mice). After three days from CAR-T, mice were sacrificed and tumor mass was collected, processed and hCD45⁺ cells were sorted. Myeloid NanoString panel was performed to analyze human myeloid TME. (B) Heat-map shows differentially expressed genes in CEA.28z + tunicamycin vs CEA.28z only, as reported from Rosalind Bio software analysis. (C) Normalized gene expression (fold changes) of genes involved in Th1 response and antigen presentation are shown. Results one-way ANOVA (C) are indicated when statistically significant (*P≤0.05; ** P≤0.01). Data are represented as means ± SEM.

4. DISCUSSION

CAR T cell therapy has demonstrated unprecedented clinical results in patients with refractory B-cell malignancies. As a consequence, four anti CD19 and one anti-BCMA CAR T cell products are now on the market, approved by both U.S. FDA and European Medicine Agency (EMA) (Haslauer et al., 2021). Moreover, in the U.S. a latest anti-BCMA CAR (CARVYKTY) has been recently approved for the treatment of adult patients with relapsed or refractory multiple myeloma (fda.gov). The exciting success achieved in hematological tumors propelled the development toward other highly lethal malignancies, such as solid cancers. Despite the enthusiasm, however, this task has met a number of hurdles. Indeed, clinical experience with solid malignancies revealed that the pharmacokinetics of CAR T cells in patients with solid tumors are quite different than those of B-cell malignancies. Indeed, in solid tumors CAR T cells must traffic to the tumor site, infiltrate within its stroma, engage the specific antigen on target cells and rapidly expand to mount an effective antitumor response (Martinez and Moon, 2019). Moreover, the highly immunosuppressive microenvironment typical of solid malignancies poses unique barriers to CAR T cell activity (Hou et al., 2021). Immunosuppressive cells and inhibitory ligands expressed on tumor cells restrain T cells fitness and functionality, allowing tumor escape mechanisms and limiting immune responses (Martinez and Moon, 2019).

Beyond the presence of a hostile TME, the first crucial requirement for a successful CAR T cell therapy is the efficient engagement of the target antigen, which have to be accessible to recognition. Most commonly, CAR T cells bind their antigen through a monoclonal antibody (mAb)-derived moiety. Importantly, it is well recognized that protein modifications, such as N-glycosylation, can impact on mAb binding. A typical example involves viruses; indeed, the envelope proteins of threat viruses, such as HIV-1, influenza virus and SARS-CoV-2 are strongly glycosylated. As reported, these glycans can hide an antigen epitope to mAb recognition, providing a convenient way for viruses to infect host cells and to promote immune escape (Li et al., 2021). Interestingly, glycosylation is also well described to be deregulated in solid malignancies. These tumors display a wide range of glycosylation alterations, which confer them many advantages in terms of growth, invasion, metastases formation and immune evasion. In particular, solid

tumors are characterized by the presence of truncated O-glycans, which are the result of an incomplete O-glycan synthesis that allows the exposure of sugar epitopes otherwise masked in healthy cells. A typical example of a truncated O-glycan in cancer is the tumor associated Tn-glycoform of Mucin 1 (MUC1). In 2016, the group of Carl June demonstrated that engineering CAR T cells with single chain fragment variable regions of a mAb targeting Tn-MUC1 (5E5) is an effective and safe strategy to eradicate pancreatic cancer and leukemia in mice (Posey et al., 2016). In the last few years, anti-Tn-MUC1 CAR T cells approaches have been reported also for the treatment of other solid tumors, including triple-negative breast cancer (Zhou et al., 2019) and cholangiocarcinoma (Supimon et al., 2021). While aberrant O-glycosylation generates truncated proteins exposing neo-antigens, N-glycosylation alterations are characterized by the overexpression of branched sugar chains on tumor cells. These cumbersome structures mask peptide epitopes on tumor cell surface, thus limiting CAR T cells recognition and killing.

Recently, our Unit demonstrated that inhibiting N-glycan synthesis can enhance CAR T cell targeting of different carcinomas, such as pancreatic ductal adenocarcinoma, lung, ovary and bladder cancer. Mechanistically, removal of cumbersome N-glycans leads to improved immunological synapse formation and reduced interaction between ligands-inhibitory receptors pairs, thus resulting in increased activation of anti-CD44v6 CAR T cells, higher cytokine release and improved target cell lysis (Greco et al., 2022). In the published work, the improved functionality was also observed with anti-CEA CAR T cells and, in this project, we have shown a potential unmasking effect of the CEA antigen upon 2-deoxy-glucose (2DG) treatment.

Several reports have also shown how tumor glycosylation could affect the function of immune cells within the TME. In fact, tumor N-glycans can bind lectin receptors on immune cells, such as sialic acid-binding immunoglobulin-like lectins (SIGLECs), macrophage galactose-specific lectin (MGL) and dendritic cell (DC)-specific ICAM3-grabbing non-integrin 1 (DC-SIGN). These interactions strongly promote the formation of immunosuppressive and anti-inflammatory environment, thus inhibiting the development of potent immune responses (Gringhius et al., 2014; Van Vliet et al., 2013; Rodriguez-Garcia et al., 2021). For instance, high abundance of sialic acid on tumor cells can dampen NK cell activation and favor polarization of immunosuppressive M2

macrophages upon binding to Siglec (Jandus et al., 2014; Rodriguez et al., 2021). Interestingly, it was recently demonstrated that targeting breast cancer with an anti-HER2 antibody-sialidase conjugate significantly improves tumor elimination in mice, by enriching CD8⁺ T cells and cytotoxic NK cells, while reducing Treg cells and CD206⁺ TAMs (Gray et al., 2020; Stanczak et al., 2021). In this work, we have also observed that tumor de-glycosylation reduces the polarization of immunosuppressive M2 macrophages, at least in term of CD206 and CD200R expression.

Most of the evidence report the impact of tumor glycosylation on the TME, while less is known about the direct role of N-glycosylation on TME cells. In this work, we aimed to evaluate this effect, investigating if N-glycosylation inhibition could modify the immunosuppressive TME and unleash the therapeutic potential of CAR T cell therapy. In particular, we focused our study on liver metastases of CRC and PDAC, which represent nowadays an important unmet clinical need. In this context, we analyzed the effect of N-glycosylation blockade on two liver TME populations, i.e., M2 macrophages and hepatic stellate cells, in which the role of N-glycosylation is still not clear. M2-M are immune cells recruited from the periphery and are a typical immunosuppressive population in the majority of solid tumors (Wang et al., 2014.; Jayasingam et al., 2010). On the other hand, HepSCs represent a liver resident stromal population that, once activated in the TME, support tumor progression and metastases formation (Kang et al., 2011).

Activated HepSCs show inhibitory effects on CEA CAR T cell proliferation and killing capacity. Interestingly, we found that treatment with de-glycosylating agents reverts their immunosuppressive effects, mitigates their activation status and reduces their binding to the co-inhibitory receptor PD-1. Moreover, treatment with de-glycosylating agents increases the formation of cytoplasmic lipid droplets, suggesting a reshape mechanism to quiescent HepSCs. These observations are supported by a report where it was shown that the use of Swainsonine, another N-glycosylation inhibitor, or the knock-out of MGAT5 gene reduce the activation of HepSCs and their migration capacity (Wu et al., 2017).

Focusing on M2 macrophages, we deeply analyzed the effect of N-glycosylation inhibition at the functional, phenotypic and transcriptional level. These cells share immunosuppressive functions with HepSCs, being able to suppress CAR T cell proliferation and killing capacity, in particular against PDOs from CRC-liver metastases.

Interestingly, this inhibitory effect was lost in the presence of both 2DG and tunicamycin, suggesting that N-glycosylation has a key role in their immunosuppressive functions. Accordingly, our *in vitro* characterization demonstrated that, upon N-glycosylation inhibition, M2-M down-regulate several surface markers, such as CD206, CD200R, FR β , CD209, PDL-2 and abrogate the secretion of IL-10. Interestingly, after treatment they also acquire pro-inflammatory M1-like features, including secretion of TNF- α and increased phagocytic capacity, comparable to that of M1-M. RNA-seq data confirm these results, showing the downregulation of immunosuppressive genes and inhibitory pathways, such as PD-1 and IL-4 signaling, after treatment with either 2DG or tunicamycin, concomitantly with the up-regulation of immune-stimulating genes, which are shared with M1-M. The reshape effect whereby M2 macrophages lose their polarization while acquiring features typical of M1 macrophages is supported by some evidence in the literature. It has been observed that tunicamycin induces the downregulation of specific M2-M markers, such as CD206, in murine macrophages (Jha et al., 2015) and that the removal of sialic acid repolarizes tumor-associated macrophages to a pro-inflammatory M1-like status (Stanczak et al., 2021). However, the mechanism by which N-glycosylation inhibition induces these wide modifications is still not clear. One hypothesis could be the activation of the unfolded protein response (UPR) pathway, which is a consequence of N-glycosylation blockade. Indeed, it has been shown that UPR modulates inflammation, activating the inflammasome response. Upon ER stress, cells express pro-IL1 β via NF-kB activation and after caspase-1 catalytic activity they secrete IL1 β , whose release depends on the activation of NLRP3 inflammasome (Kim et al., 2014; Li et al., 2020). The triggering of inflammation upon UPR and ER stress could explain the acquisition of pro-inflammatory features in M2-M upon de-glycosylating treatments. Another hypothesis could be the inhibition of binding between IL-4 and IL-4 receptor, which is crucial in determining M2 polarization in macrophages. It is known that N-glycans are required for the correct binding between different ligand-receptor pairs, such as PD-1/PDL-1 and TIM-3/Gal-9. N-glycans removal could also impair IL-4/IL-4 receptor binding, inhibiting M2 polarization. Furthermore, since N-glycans are involved in cell-cell contact and adhesion, N-glycosylation inhibition could alter these processes, impairing M2 polarization. It is known that M2-M are involved in wound healing and tissue regeneration and it was reported that the inhibition of cell adhesion

inhibits their polarization without affecting M1-M (McWhorter et al., 2013; Kang et al., 2019). This evidence supports our RNA-seq analysis on human macrophages, where we found that cell adhesion is a pathway down-regulated in de-glycosylated M2-M and in M1 macrophages. All these data allow us to hypothesize that N-glycosylation blockade dampens M2 polarization by interfering with cell adhesion and/or ligand-receptor interactions, and bring M2-M closer to pro-inflammatory M1-M, as a consequence of ER stress and UPR.

Standard xeno-graft NSG mouse models are not ideal to study the effect of N-glycosylation on the TME and its impact on CAR T cell function. Indeed, although they are useful to answer questions regarding CAR T cell reactivity against tumor cells, they are limited by the absence of a functional murine and/or human immune system. Indeed, immune cells are crucial to exacerbate CAR-related toxicities, such as CRS (Norelli et al., 2018; Arcangeli et al., 2022), but at the same time can support CAR T cell function by releasing chemokines and cytokines, enhancing killing activity and sustaining T cell proliferation. Accordingly, we observed increased antitumor efficacy of CEA CAR T cells in humanized versus not humanized mice. On the other hand, immune cells can be shaped by cancer cells to create an immunosuppressive microenvironment, a key barrier that need to be overcome in solid tumors. Interestingly, we observed that intra-hepatic injection of tumor cells allows to reconstitute a human immune TME in the liver of humanized mice. Indeed, we reported the presence of several human immune cells, including B cells, NK cells, dendritic cells, neutrophils, Tregs and M2 macrophages, which were increased in terms of frequency compared to *huSGM3* mice without tumor. To date we only evaluated the frequency of human immune cell subsets by FACS analysis, but we have planned to confirm these results and further characterize the model with advanced technologies, such as spatial transcriptomics and the MACSima imaging system (Miltenyi). In particular, we are interested in exploring the modulation of spatial and gene expression profile of different human immune cells in the presence of tumor before and after treatment with CEA CAR T cells.

As already mentioned, this sophisticated mouse model is appropriate to study not only CAR T cell efficacy, but also CAR-related toxicities, such as CRS. In our experiments with BxPC3, LoVo and PDOs, we didn't observe any sign of CRS. However, we didn't reach a robust efficacy with CEA CAR T cells, which has been proven to be crucial to

observe any CAR related toxicity. We have planned to perform specific experiments to exacerbate CRS, using high tumor burdens and CAR T cell doses, since this aspect is of great interest in solid tumor field. Indeed, even though CRS was principally observed in patients suffering from hematological tumors, clinical trials in solid tumors have also reported CRS symptoms, such as fever, hypotension and elevated IL-6 levels (Brown et al., 2016; O'Rourke et al., 2017). Very recently, in a clinical trial testing Claudin18.2 CAR T cells against gastrointestinal tumors, all treated patients experienced severe CRS (Qi et al., 2022). In perspective, we are also interested in investigating neurotoxicity (ICANS) that, as with CRS, was principally observed in the clinical experience with hematological tumors. However, this year, a phase I trial reported two cases of death for neurotoxicity in patients treated with armored anti-PSMA CAR T cells (Narayan et al., 2022). We reckon that the humanized mouse model may be a great tool to address these issues, since it is the only murine model in which the infusion of human CD19 CAR T cells induces the formation of brain hemorrhages (Arcangeli et al., 2022).

Despite *huSGM3* mice represent a bridge between xenograft and syngeneic animal models, they still present some limitations, such as the absence of human stromal compartment. In liver metastases, hepatic stellate cells play a key role in disease pathology, by supporting tumor progression and metastases formation. Therefore, we are evaluating the possibility to include this population in humanized mice in order to strengthen our results and increase the relevance of the model for testing approaches aimed at interfering with the TME, both immune and stromal.

Beyond the immunosuppressive TME, there are other challenges that CAR T cells have to overcome in solid tumors. Unlike hematologic malignancies, which are readily accessible to CAR T cells, solid tumors are surrounded by capsules that are difficult to infiltrate due to poor tumor vascularity and stromal barrier. To overcome these issues, regional delivery has been applied. Several pre-clinical studies have demonstrated that loco-regional administration of CAR T cells generates a robust local immune response and increases T cell persistence (Adusumilli et al., 2021; Cherkassky et al., 2022). In our work, we investigated intrahepatic injection of CEA CAR T cells, which granted enhanced control of tumor lesions residing in the liver in comparison to intravenous infusion. Another advantage of local CAR T cell delivery is the limitation of systemic release of cytokines, which can result in reduced cytokine-mediated organ damage.

Indeed, as previously mentioned, we never observed signs of toxicity in our *in vivo* experiments. On one hand this could be related to poor efficacy, but on the other it could represent an advantage of localized CAR T cell delivery. Nowadays, several clinical trials on solid tumors have exploited regional delivery of CAR T cells, especially in the context of brain tumors and liver metastases. Regarding the latter, phase I clinical trials testing CEA CAR T cells injected in the hepatic artery have shown promising results in terms of safety and efficacy against liver metastases from different carcinomas (Katz et al., 2015; Katz et al., 2020). In our model, we injected CEA CAR T cells directly into a liver lobe to gain insights on the advantages of local delivery. However, in perspective, we plan to implement intra-portal vein infusion to increase the translational value of the model.

The technical adaptation of the humanized mouse model to solid tumors has been instrumental for our purposes to evaluate the effect of combining CAR T cell therapy with de-glycosylating agents on the immune TME. Using tunicamycin, a specific N-glycosylation inhibitor, we observed increased tumor control by CEA CAR T cells. However, a first analysis performed by FACS did not reveal any change in the frequency of human immune cells in the liver. The only effect we observed was the presence of less exhausted tumor infiltrating CAR T cells, as already shown in our previous work with CD44v6 CAR T cells (Greco et al., 2022). Importantly, however, transcriptional analysis of a panel of myeloid genes on human CD45⁺ cells isolated from subcutaneous tumors revealed that combination with tunicamycin was associated with the downregulation of a wide panel of immunosuppressive genes. This beneficial effect could be either ascribed to a direct effect of N-glycosylation inhibition on immune cells, an indirect effect through tumor de-glycosylation, or both. To address this issue, we are planning to use glycosylation-deficient MGAT5 KO tumor cell lines or perform the same knock-out in CD34⁺ cells to obtain de-glycosylated human immune cells in mice. Finally, we have planned to perform single-cell RNA sequencing in a more relevant setting with PDOs, to perform a deeper characterization of each human immune cell subset in the TME and to analyze their modulation upon treatment with CAR T cells alone or with de-glycosylating agents.

In our *in vivo* experiments, we started by using tunicamycin because, differently from 2DG, it is a specific N-glycosylation inhibitor. This compound inhibits the first step of N-glycan biosynthesis and proved to be toxic in mice, rendering the translation of its

application to the clinic difficult to envisage. However, in several pre-clinical studies tunicamycin have shown great results in inhibiting tumor growth and improving cancer susceptibility to monoclonal antibodies, such as Erlotinib and Trastuzumab (Ling et al., 2009; Han et al., 2015). Moreover, at low doses (0.02mg/Kg) and with a temporary administration (twice a week for three weeks), tunicamycin did not prove to be toxic in mice (Han et al., 2015). Therefore, we used it under the same conditions and observed no toxic effects on the animals, as well as no direct impact on tumor growth when provided as a single agent. Differently, tunicamycin was able to synergize with CAR T cells and provided proof of concept that N-glycosylation blockade dampens immunosuppressive TME cells. Of course, we will also test the glucose/mannose analogue 2DG, a dose-dependent inhibitor of both glycolysis and N-glycosylation, which has proven effective in increasing CAR T cell efficacy in multiple xenograft mouse models of human carcinomas (Greco et al., 2022). From a safety point of view, this compound is interesting because it is expected to preferentially accumulate in tumor cells as a consequence of the Warburg effect (Raez et al., 2005; Raez et al., 2013). Accordingly, 2DG has shown good tolerability in human during clinical trials and a radiolabeled version of this compound is already approved for diagnostic purpose (PET-SCAN). However, even if tumor cells are greedier of glucose, it was recently demonstrated that 2DG uptake and accumulation is higher in CD45+ cells within the TME, rather than tumor cells (Reinfeld et al., 2021). On one hand, this suggests that 2DG could have a strong impact on myeloid immunosuppressive cells. On the other hand, it implies that it could accumulate in other effector cells inhibiting their function due to glycolysis inhibition. Therefore, besides efficacy experiments, we have also planned to perform single-cell RNAseq to analyze the effect of 2DG on the transcriptional profile of each single human population recreated in our *huSGM3* model. Importantly, alternative approaches could be pursued to safely and selectively block N-glycosylation in tumor and TME cells. For example, to avoid systemic administration of toxic de-glycosylating agents, local delivery through nanoparticles could be considered (Sasaki et al., 2021). Another approach could involve the generation of a single CAR T cell product armored to locally release a specific de-glycosylating factor, an approach that we are currently developing in our Unit.

In conclusion, several barriers need to be overcome to improve efficacy in solid tumors, including defective trafficking and tumor infiltration, poor tumor recognition and killing,

and strong immunosuppression within the tumor microenvironment. Most strategies currently under development tackle one barrier at a time, for example using anti-angiogenic therapies (Yang et al., 2018) to enhance T cells trafficking, targeting stromal compartment (Kakarla et al., 2013) or the extracellular matrix (Caruana et al., 2015) to increase T cells infiltration, or counteracting the immunosuppressive tumor microenvironment (Tang et al., 2020; Rodriguez-Garcia et al., 2021). The major advantage of N-glycosylation inhibition is the possibility to bypass several obstacles with a single approach. First, N-glycosylation inhibition allows to increase tumor killing by improving immunological synapse formation. Second, it has the potential to reduce CAR T cell exhaustion by impeding the interaction between immune checkpoint molecules like PD-1/PDL-1 (Greco et al., 2022). In this work, we also described a beneficial effect on the TME consisting in the inhibition of immunosuppressive activity of key players like M2 macrophages and hepatic stellate cells. Finally, it is important to underline that this strategy has the potential to be applied in multiple malignancies that up-regulate the N-glycosylation pathway and exploited with different CAR specificities, including but not limited to CD44v6 and CEA.

5. MATERIALS AND METHODS

5.1 Cells and Media

5.1.1 Primary cells

Buffy coats from healthy blood donors were obtained after written informed consent and Institutional Review Board (IRB) approval. Cord blood donors signed informed consent forms approved by the San Raffaele Hospital Ethics Committee (Protocol “34CB”, Milan, Italy), in accordance with the Declaration of Helsinki. Peripheral blood mononuclear cells (PBMCs) were isolated by Ficoll-Hypaque gradient separation (Lymphoprep, Fresenius) and used fresh or cryopreserved until use. PBMCs from cord bloods donors were sorted with CD34 Microbead Kit UltraPure human (Miltenyi) and CD34+ cells purity was checked by FACS. CD34+ cells were counted and cryopreserved until use. T lymphocytes from healthy donors’ buffy coats were cultured in RPMI 1640 medium (Euroclone), supplemented with penicillin (100 UI/ml; Pharmacia), streptomycin (100 UI/ml, Bristol- Meyers Squibb), glutamine (2mM, Gibco), 10% FBS (fetal bovine serum, BioWhittaker), MycoZap Plus (LONZA), IL-7 and IL-15 (5ng/ml, PeproTech). Primary human macrophages were obtained after sorting of CD14+ cells from PBMCs from healthy donors. CD14+ cells were cultured in RPMI 1640 medium, supplemented with penicillin, streptomycin, glutamine, 10% FBS, MycoZap Plus and human M-CSF (30ng/ml, Miltenyi). Macrophages were polarized in M1 macrophages with LPS (Lipopolysaccharides from Escherichia Coli O111:B4 100ng/ml, Sigma Aldrich) and in M2 macrophages with human IL-4 (20ng/ml, Miltenyi) for 48 hours. Primary human hepatic stellate cells were purchased from Lonza (#HUCLS) and cultured following manufacturer’s instructions in Human Stellate Cell Growth medium (#MCST250).

5.1.2 Generation of patient derived organoids (PDOs) from CRC-liver metastases samples

Tissue resections were obtained from patients undergoing surgery at San Raffaele Hospital, for the removal of clinically confirmed liver metastases from colorectal cancer (CRC-LMs). Human samples were obtained after written informed consent and IRB

approval (Protocol “Limet”, Milan, Italy). Tissue samples were kept in cold in Phosphate Buffered Saline (PBS) (Euroclone) until processing and for no more than 24 hours after surgery resection. Tissues were processed, by cutting them with scalpels in small pieces and incubating them with PBS + 5mM EDTA (Invitrogen). Tissues fragments were washed in PBS and then incubated for 1 hour at room temperature with a digestion solution, composed by PBS/EDTA 1mM + TrypLE 10X (Gibco) + 10X DNase I buffer + DNaseI (Roche). Dissociated cells were collected in Advanced DMEM/F12 medium (Gibco), pelleted and resuspended in 130µl of Growth Factor Reduced (GFR) Matrigel matrix (Corning) and seeded in single 24mws plate. After Matrigel solidification, complete human organoid medium was added to the plate. Basal medium was prepared using the following reagents: Advanced DMEM F/12 (Gibco) with the addition of 1% penicillin/streptomycin (100 U/ml, 0.1 mg/ml, Euroclone) and 1% Glutamine (2mM, Euroclone), 1x B-27 (Gibco), 1x N-2 (Gibco) and 0,1% BSA. Basal medium was complemented with the following additives: EGF (PrepoTech), Noggin (PrepoTech), R-Spondin-1 (PrepoTech), Gastrin (Sigma-Aldrich), FGF-10 (PrepoTech), FGF-basic (PrepoTech), WNT-3A (R&D Systems), Prostaglandin E2 (Tocris), Y-27632 (Stem Cell Technologies), Nicotinamide (Sigma-Aldrich), A 83-01 (Tocris), SB202190 (Sigma-Aldrich), HGF (PrepoTech). Additive solutions were prepared at 1000X concentration and freshly added to the basal medium.

To perform *in vitro* and *in vivo* functional assays, PDOs were transduced with Luciferase-expressing lentiviral vector and selected in puromycin. For the functional assays, PDOs were harvested by gently pipetted out of Matrigel using 1ml Cell Recovery Solution (Corning) per well and incubated for 45 minutes at 4°C. After the incubation, PDOs were collected in Falcon tubes, diluted five times in HBSS and centrifuged. Supernatant was discard and the pellet was resuspended in a 1:1 ratio Matrigel and basal medium (for *in vitro* co-cultures) or Matrigel and PBS (for *in vivo* infusion).

5.1.3 Cell lines

Tumor cell lines were kindly provided by several groups at San Raffaele Institute. THP-1, PDAC and CRC cell lines were all cultured in RPMI 1640 medium. 293T cells were kindly provided by Luigi Naldini’s group and cultured in IMDM. To differentiate THP-1 cell line in M2 macrophages, cells were cultured for 24 hours with phorbol 12-myristate

13-acetate (PMA, 10ng/ml, Sigma Aldrich) and then with human IL-4 (20ng/ml, Miltenyi) for 48 hours. All media were supplemented with penicillin, streptomycin, glutamine, FBS and MycoZap Plus as described in 5.1.1.

5.2 Viral vectors

5.2.1 CAR construct

CAR constructs were obtained by cloning the antigen-specific single chain fragment variable (scFv) into a CAR-encoding viral backbone containing an IgG1-derived hinge spacer, a CD28 transmembrane and co-stimulatory domain and a CD3 ζ endodomain (CEA.28 ζ). scFv specific for CEA was derived from BW431-26 variable heavy (VH) and variable light (VL) sequences. CAR constructs were expressed into a bidirectional lentiviral vector kindly provided by the group of Luigi Naldini (Amendola et al., 2005). In this vector, the expression of GFP as marker gene was substituted with NGFR by cloning. The LV CAR construct was employed for T cell transduction (see 5.3.3).

5.2.2 LV vector production and titration

To produce LV supernatants, 293T cells were co-transfected with the transfer vector, the packaging plasmid (pMDLg/pRRE, encoding for viral genes gag-pol; Addgene, Cambridge, MA), the REV plasmid (pRSV-Rev, encoding for the viral gene rev; Addgene) and the ENV plasmid (pMD2.VSV-G, encoding for G glycoprotein of the vesicular stomatitis virus pericapsis -VSV-G-; Addgene), using CaCl₂ precipitation. Supernatants containing lentiviruses were collected 48 hours later, ultracentrifuged and cryopreserved.

To titrate LV supernatants, 293T cells were transduced with different supernatant dilutions. After 6 days from the titration, 293T cells were analyzed by FACS and the titer of LV supernatants was calculated.

5.3 Cell-manipulation conditions

5.3.1 T-cell activation and expansion

Activation of T cells from healthy donors was performed with anti-CD3/CD28 immuno-conjugated magnetic beads (ClinExvivo CD3/CD28; Invitrogen) following manufacturer's instructions. Briefly, T cells were stimulated at 3:1 bead/T cell ratio and cultured in RPMI-1640 supplemented with 10% FBS, penicillin, streptomycin, glutamine, MycoZap Plus and IL-7 and IL-15. Magnetic beads were detached 6 days after T cell activation. Phenotypic analysis and functional testing were performed at day 20 from stimulation.

5.3.2 Generation of TCR knocked-out T cells

Stimulated human CD3⁺ cells were electroporated 48 hours after stimulation. Two million cells per condition were resuspended in P3 primary buffer (Lonza) and assembled Ribonucleoprotein Particles (RNPs), targeting the coding sequence of TRAC gene, were added to the cell suspension. Commercial crRNA (Alt-R® CRISPR-Cas9 crRNA, IDT) and tracrRNA (Alt-R® CRISPR-Cas9 tracrRNA, IDT) were purchased by Integrated DNA technology (IDT). crRNA:tracrRNA were mixed in equimolar concentrations and heated at 95°C for 5 min to form a duplex with a final 100µM concentration. crRNA:tracrRNA duplex and Cas9 enzyme were assembled in a 120:104pmol ratio for 20 minutes at room temperature, according to manufacturer's instructions. Then, 1µL of Enhancer (100µM; Alt-R® Electroporation Enhancer, IDT) was added to the reaction. Cells were electroporated using Nucleofector 4D (Lonza) according to manufacturer's instructions. 24 hours later, electroporated T cells were counted for transduction with CEA.28ζ LV vector.

5.3.3 T-cell transduction with LV vector

At day +2 after stimulation, activated T cells from healthy donor were collected, re-suspended, plated in a 24wells plate at the concentration of 1×10^6 cells/ml, 1 ml per well and transduced with LV vector (using µl of LV vector accordingly to viral titration, see 5.2.2). Transduction efficiency was measured by flow cytometry at day +9 before CAR⁺ T cell sorting at day +10.

5.3.4 Generation of MGAT5 knocked-out THP-1, BxPC3 and LoVo cell lines

The lentiviral vector plasmid encoding for MGAT5-specific gRNA and Cas9 protein was purchased from ABM good (K1298706). After lentiviral vector production, tumor cells were transduced and cultivated in puromycin-supplemented medium (3µg/ml Puromycin) for positive selection (Thermo Fisher). Knock-out efficiency was checked regularly by PHA-L lectin (EY-Lab) binding and evaluated by flow cytometry analysis.

5.4 Flow cytometry

5.4.1 Antibodies and procedures

Anti-human antibodies were purchased from BioLegend, eBioscience or Miltenyi. For staining, cells were washed with PBS containing 5% FBS. Data were analyzed with the FlowJo software (Tree Star Inc.) and relative fluorescence intensity (RFI) was calculated as follows: mean fluorescence intensity (MFI) of the sample stained with the mAb of interest / MFI of control sample.

5.4.2 Analysis of branched N-glycan surface expression

Cells were incubated with 50 mg/mL of biotinylated Phaseolus vulgaris Leukoagglutinin (PHA-L; EY-Lab) for 1 hour at room temperature, washed and incubated with PE-conjugated streptavidin and analyzed by flow cytometry.

5.5 In vitro functional assay

5.5.1 RNA extraction and qPCR analysis

Total RNA from BxPC3 and LoVo (cell lines treated or not with 4mM 2-deoxy-glucose, 2DG, for 48 hours) was extracted with RNAzol® RT (Sigma Aldrich). 500ng of RNA were retro-transcribed with High-Capacity cDNA Reverse Transcription Kit (Applied Biosystem), and real-time PCR was performed with StepOne™ Real-Time PCR

System (Applied Biosystem), according to the manufacturer protocol by using the human CEACAM5 Taqman probe (Hs00944025, Thermo Fisher) and the human GUSB Taqman probe (Hs00939627, Thermo Fisher) used to normalize CEACAM5 gene expression.

5.5.2 Lactate production assay

Lactate production was assessed 48 hours after 4mM 2DG treatment using the Lactate-Glo assay kit (Promega) according to the manufacturer's instructions.

5.5.3 Macrophages phagocytosis assay

To evaluate M2 macrophages phagocytic capacity upon de-glycosylating treatments, 1×10^5 /well M2 macrophages, *in vitro* differentiated from healthy donors' PBMCs, were plated in 48mws plate with or without de-glycosylating treatments (4mM 2DG or 100ng/ml Tunicamycin). After 48 hours, cells were stained with the Phagocytosis Assay Kit (Red Zymosan, Abcam), detached, stained also with PD-1, SIRP- α and Siglec-10 (Biolegend) and analyzed by flow cytometry.

5.5.4 PDL-1/PD-1 binding assay

To measure PDL-1/PD-1 protein binding, Hepatic stellate cells were fixed in 4% paraformaldehyde for 15 minutes at room temperature. HepSCs were then incubated for 1 hour with recombinant human PD-1 Fc chimera biotinylated protein (R&D Systems). Streptavidin-APC (BioLegend) antibody was used for detection by flow cytometry.

5.5.5 T cells proliferation assay

To analyze the proliferation, PBMCs or CEA CAR T cells were stained with CellTrace Violet Cell Proliferation Kit (Thermo Fisher). PBMCs were stimulated with anti-OKT3 (30ng/ml, Biolegend) and anti-CD28 (60ng/ml, Biolegend), while CEA CAR T cells with irradiated target cell lines (BxCP3 or LoVo). Then, T cells were plated on primary M2 macrophages or Hepatic stellate cells at 1:5 TME cells:T cells ratio. M2 macrophages and HepSCs were pre-treated for 48hrs with 4mM 2DG, 4mM 2DG+1mM Mannose or 100ng/ml tunicamycin and then washed with PBS before adding stained and stimulated PBMCs or CAR T cells. Frequency of cell-trace diluting T cells was evaluated by flow cytometry 5 days after initial stimulation.

5.5.6 M2 macrophages and tumor cell lines co-culture

BxPC3 or LoVo cell lines were pre-treated or not with 4mM 2DG or 100ng/ml tunicamycin for 48 hours. Then, these cells and also MGAT5 KO LoVo or BxPC3, were plated in 24mws plate in a 1:1 ratio with primary M2 macrophages, without any treatment. After 48 hours co-culture, cells were collected and analyzed by FACS. CD206 and CD200R expression (RFI) was analyzed as specific markers of M2 polarization.

5.5.7 CAR T cells killing assay

Anti-CEA CAR T cells from healthy donors were co-cultured in 96mws plate with target cells or in a 1:1 ratio with or without TME cells (M2-like THP1, M2-M or HepSCs) for 48 hours in the presence or absence of 4mM 2DG. After treatment wash-out with PBS, CEA CAR T cells or control T cells were added in 2:1, 1:1 and 1:5 E:T ratios, in the absence of IL-7 and IL-15. T cells either untransduced or CD19 CAR+ were used as control. Tumor killing was assessed after 24 hours (with LoVo) or 48 hours (with BxPC3) with luminescence using the Tristar 3 filter-based multimode plate reader (Berthold), thanks to the expression of luciferase by tumor cells. CAR T cell killing assay with PDOs was performed as follow. Five days before assay plating, PDOs were dissociated at single cell with TrypLE, counted and seeded 1×10^5 cells per well, in 24mws plate. After 3 days PDOs were harvested with Cell Recovery Solution to maintain their integrity and seeded with or without TME cells (M2-M or HepSCs) with Matrigel and PDOs medium, supplemented or not with 4mM 2DG. After 48 hours from 2DG treatment, co-culture assay was performed. PDOs were harvested with Cell Recovery Solution and collected in falcon tubes (around 6×10^4 PDOs/tube). CEA CAR T cells or either untransduced or CD19 CAR+ used as control were added to the tubes at different E:T ratio (2:1, 1:1, 1:5). Cells were centrifuged and then suspended in 1:1 ratio Matrigel + PDOs basal medium and seeded in 96mws white plate (Costar) for luminescence analysis with Tristar 3 after 72 hours. Triple co-culture with PDOs was also plated in transparent 96mws plate to obtain microscope images, with Axio Vert (Zeiss).

Specific target cell killing was expressed as elimination index and calculated as follows:
 $1 - (\text{number of residual target cells with experimental CAR T cells} / \text{number of residual target with control T cells})$.

5.5.8 Cytokine-release assay

To analyze M2 macrophages secreted cytokines, after 48 hours culture with 4mM 2DG or 100ng/ml tunicamycin, supernatants were collected and cryopreserved at -20°C. Cytokines level were determined using a LEGENDplex kit (BioLegend).

5.5.9 RNAseq analysis

Total RNA was extracted from *in vitro* differentiated M2 macrophages treated or not with 4mM 2DG or 100ng/ml tunicamycin for 48 hours, using ARCTURUS PicoPure RNA Isolation Kit (Thermo Fisher Scientific). Quality control (QC) check of all RNA samples was performed by TapeStation HS RNA. RNA samples were quantified with Qubit RNA HS Assay (Life Technologies) and their integrity was assessed using High Sensitivity RNA ScreenTape Assay on 4200 TapeStation System (Agilent Technologies). Libraries were prepared using TruSeq Stranded mRNA kit (Illumina) and then sequenced 2x100bp on the Illumina NovaSeq 6000 platform. RNA-seq analysis was performed as previously described (Balestrieri et al., 2018). Briefly, after the pre-processing steps (filtering, quality trimming, and adapter clipping), single-end reads were mapped to human genome build GRCh38/hg38 using STAR (version 2.5.3a) with default parameters (Dobin et al., 2015). Only properties paired mapped reads were retained. At the gene level, expression counts were measured using featureCounts (version 1.6.4) (Liao et al., 2014) summarized across all exons as annotated in GENCODE v39, with option –largestOverlap. Coding RNA genes with a minimum of 1 read count in at least three samples were retained for downstream analyses. Differential expression analyses were performed in paired using the EdgeR R package (version 4.0.5) (Robinson et al., 2010) with trimmed mean of M (TMM) normalization, generalized linear model, and likelihood ratio tests. Principal Components Analysis (PCA) were used to the comparison between M2 and M1 macrophages cells. Then, in both analysis genes were identified as DEGs when the following criteria were met: $\log_2(\text{FC}) > |0.7|$, false discovery rate (FDR) < 0.05 (Benjamini–Hochberg) and expression > 1 Transcript Per Million (TPM) in at least 70% of samples per condition.

Enrichment analysis were performed using g:Profiler (Raudvere et al., 2019) and resulting enriched GO terms and/or pathways were selected with FDR-adjusted $P < 0.05$.

Metascape was used to perform functional enrichment analysis (Zhou et al., 2019) using only terms with $P < 0.01$, minimum overlap of 3, and enrichment factor >1.5 .

5.5.10 Hepatic stellate cells immunofluorescence

Hepatic stellate cells were plated directly on fibronectin coated cover glasses (24mm, Zeus super) in a 6mws plate. Cells were treated or not with 4mM 2DG or 100ng/ml tunicamycin for 48 hours. After that, medium was removed and cells were fixed with 4% Paraformaldehyde (PFA; Sigma-Aldrich) for 15 minutes. For immunofluorescence staining, PFA was removed and cells were washed with PBS+0.1% Tryton-X 100 (PBS-T, Sigma), and then incubated 30 minutes with a blocking and permeabilization solution (PBS-T + 1mg/ml bovine serum albumin, BSA + 10% fetal bovine serum, FBS) at room temperature. Cells were first incubated with anti-human α -Smooth Muscle Actin (α SMA) primary antibody (Invitrogen), diluted 1:750 in blocking solution for 1 hour at room temperature. After 3 washes in PBS-T, cells were incubated with anti-mouse IgG Alexa Fluor 546 (Invitrogen) diluted 1:500 in PBS-T for 30 minutes at room temperature. After 3 washes cells were incubated with LipidSpot 488 Lipid Droplet Staining (Biotium), diluted in 1:500 for 10 minutes at room temperature. After 1 wash in PBS-T for 5 minutes, to visualize nuclei, cells were incubated with DAPI (Fluka), diluted 1:500 in PBS for 5 minutes at room temperature, followed by three washes in PBS-T. Slide mounting was performed with glycerol (Sigma) + milliQ H₂O (1:1 ratio).

Images were acquired using Axio Observer microscope. Digital images were acquired in separately scanned channels with no overlap in detection of emissions from the respective fluorochromes. Final image processing was performed with ImageJ software and Adobe Illustrator with minimal contrast and luminosity adjustment. ROI-based (3 sections per image) quantification analysis was performed with ImageJ software.

5.6 In vivo experiments

5.6.1 In vivo functional assays

For *in vivo* studies in standard xenograft mouse model, 6 to 8 weeks old NSGTgCMV-IL3 CSF KITLG1Eav/MloySzJ (SGM3) mice (Charles River), were injected intraliver (i.l.) or intraperitoneum (i.p.) with BxPC3 Lucia/NGFR⁺ cell lines (1×10^5 i.l.; 5×10^5 i.p.). After 1 week, mice were infused intravenous (i.v.), i.l. (in the i.l. tumor setting) or i.p. (in the i.p. tumor setting) with $5-10 \times 10^6$ CEA CAR T cells. The control group was represented by mice with only tumor (Nihil), or untransduced T cells (UT).

For *in vivo* studies with humanized mice, 6 to 8 weeks old SGM3 mice, were sublethally irradiated and infused i.v. with 1×10^5 human cord blood CD34⁺ cells, provided from Lonza or sorted in our laboratory from cord bloods. Upon reconstitution, *hu*SGM3 mice were injected i.l. with BxPC3 Lucia/NGFR⁺ (1×10^5), LoVo Lucia/NGFR⁺ (1×10^5) or with patient derived organoids luciferase positive (PDOs-Luc⁺, 4×10^4) from CRC-liver metastases patients. To evaluate human reconstitution in tumor bearing *hu*SGM3 mice and to analyze the reconstitution of human tumor microenvironment similar to human disease, mice did not receive CAR T cells, and a group was treated with 2DG (500mg/Kg) i.p. every day with 2 days of wash-out. In efficacy experiments, however, mice were also injected i.v. or i.l. with $5/10 \times 10^6$ CEA CAR T cells (TCR KO or WT) or untransduced T cells after 1 week (with BxPC3), 3 weeks (with LoVo) or 2-3 weeks (with PDOs).

In the combinatory treatment strategy with de-glycosylating agent, tunicamycin (0.02mg/Kg) was infused i.p. in mice at day -2 from T cells and then twice a week for 3 weeks (Han et al., 2015).

After CEA CAR T cells infusion, mice were followed with bleeding to check the tumor growth, thanks to the expression of secreted luciferase (Lucia/NGFR⁺) by cell lines. In the same sample of peripheral blood, FACS analysis were also performed to characterized human cells composition. For the PDOs experiment, the tumor growth was followed by IVIS Specturm (PerkinElmer), thanks to the expression of Luciferase (Luc), and by MRI analysis. Mice were sacrificed when relative light units (RLU) exceeded the threshold (1×10^6 with BxPC3; 5×10^5 with LoVo) or at specific time points, for end-point analysis. FACS liver analysis was performed to identify and deeply characterize the composition of human TME. For infiltrated CEA CAR T cells exhaustion phenotype analysis, SPICE

software was used. CAR-related toxicities, such as CRS, were evaluated by weight loss monitoring and analysis of the concentration of serum human cytokines (LEGENDplex).

5.6.2 MRI images

In vivo MRI experiments were performed on a 7-Tesla scanner for rodents, equipped for high resolution MRI/MRS (*Biospec*, Paravision 6.0.1 Software Bruker-Biospin), with 450/675 mT/m gradients (slew-rate: 3400-4500T/m/s; rise-time 140 μ s) and a circular polarized mouse body volume coil with an inner diameter of 40 mm. For each MRI exam, a mixture of IsoVet (isoflurane 1-2%) with oxygen was used to anaesthetize animals and breath rate was monitored to regulate the level of anaesthesia. Body temperature of mice was maintained through warm water circulating inside the bed where the animal was placed during the MRI exam. To display liver lesion, we used a hepatocyte-specific contrast agent, the Gd-EOB-DTPA (Bayer Schering Pharma, Berlin, Germany) known as gadoxetic acid (0.05 μ mol/g of body weight). Axial fat-saturated T2-weighted images (RARE-T2, Rapid Acquisition with Relaxation Enhancement, TR = 3000 ms, TE = 40 ms, voxel-size = 0.170 \times 0.120 \times 0.8 mm, averages = 4,) and axial fat-saturated T1-weighted sequences (RARE-T1: TR = 540 ms, TE = 7.2 ms, voxel size = 0.170 \times 0.120 \times 0.8 mm, averages = 4) acquired during the hepatobiliary phase of Gd- EOB-DTPA enhancement (10 minutes after administration).

Generated MRI images were analyzed by a single board-certified radiologist with a dedicated software, MIPAV (Medical Imaging Processing And Visualization, National Institutes of Health, Bethesda, Maryland, USA). Difficult findings or images were always discussed with a second senior radiologist. Images were analyzed in order to evaluate the number of liver metastases, their overall volume, the presence of extra-hepatic metastases and non-target lesions. Non-target lesions were defined as lesions too small to be measurable and non-measurable metastatic disease (e.g. presence of ascites). The number of hepatic metastases was visually assessed by the radiologist comparing T2 and T1 MRI sequences. The volume of the hepatic lesions was calculated by the software based on a manual segmentation of the lesion slice-by-slice and following the formula: area of the segmented region of interest (ROI) (mm²) x slice thickness (mm). The presence of extra-hepatic lesions or non-target lesions was communicated by the radiologist in a report.

5.6.3 Histopathological analysis

Livers from *huSGM3* mice were collected at sacrifice, fixed in buffered 4% formalin, embedded in paraffin, cut and stained in the Good Laboratory Practice (GLP) SR-TIGET Pathology laboratory following GLP principles. CRC-liver metastases samples were obtained after surgical resection and were fixed and embedded as for murine samples. Hematoxylin-and eosin-stained 3µm paraffin sections were blindly and independently examined for histopathological analysis by two pathologists. Images were taken using the AxioCam HRc (Zeiss) with the Axio-Vision System SE64 (Zeiss).

5.6.4 NanoString analysis

For NanoString analysis, SGM3 mice were infused i.v. with human CD34+ cells. After human reconstitution, mice were infused subcutaneously with 5×10^5 LoVo. After two weeks, tumors were visible and measurable with a caliper. Mice were treated i.v. with 5×10^6 CEA CAR T cells or untransduced T cells as control. tunicamycin treatment (0.02mg/Kg) was infused i.p. at day-2 and day+2 from CAR T cells infusion. At day +3 from CAR T cells, mice were sacrificed and tumors were collected. Tumors were processed by gentleMACS Octo Dissociator (Miltenyi) with human tumor dissociation kit (Miltenyi). Once obtained a single cell suspension, hCD45+ sorting was performed with human CD45 microbeads (Miltenyi). After sorting cells were count and the pellet was stored at -80°C. For NanoString technology, total RNA was extracted from cells samples using the Maxwell® RSC RNA FFPE Kit following manufacturer's instructions.

The NanoString™ nCounter® Myeloid Innate Immunity Panel, which evaluate 770 genes involved in the recruitment and activation of myeloid cells, was applied. Briefly, 25ng of total RNA extracted from CD45+ cells were hybridized to probes for 20 hours at 65°C. The hybridized probes were purified and counted using the nCounter Prep Station. Counts of fluorescent barcodes were obtained using the Digital Analyzer at 555 fields of view (FOV). The nCounter results were evaluated using ROSALIND® (<https://rosalind.bio/>), with a HyperScale architecture developed by ROSALIND, Inc. (San Diego, CA). Normalization, fold changes and p-values were calculated using criteria provided by Nanostring. ROSALIND® follows the nCounter® Advanced Analysis protocol of dividing counts within a lane by the geometric mean of the normalizer probes from the same lane. Housekeeping probes to be used for normalization are selected based

on the geNorm algorithm as implemented in the NormqPCR R library (Perkins et al., 2012). Abundance of various cell populations is calculated on ROSALIND using the Nanostring Cell Type Profiling Module. ROSALIND performs a filtering of Cell Type Profiling results to include data that have scores with a p-Value greater than or equal to 0.05. Fold changes and p-Values are calculated using the fast method as described in the nCounter® Advanced Analysis 2.0 User Manual. P-value adjustment was performed using the Benjamini-Hochberg method of estimating false discovery rates (FDR). Clustering of genes for the final heatmap of differentially expressed genes was performed using the PAM (Partitioning Around Medoids) method using the fpc R library, that takes into consideration the direction and type of all signals on a pathway, the position, role and type of every gene, etc. Hypergeometric distribution was used to analyze the enrichment of pathways, gene ontology, domain structure, and other ontologies. The topGO R library (Alexa et al., 2019), was exploited to determine local similarities and dependencies between GO terms in order to perform Elim pruning correction. Several database sources were referenced for enrichment analysis, including Interpro (Mitchell et al., 2019), NCBI (Geer et al., 2009), MSigDB (Subramanian et al., 2005; Liberzon et al., 2011), REACTOME (Fabregat et al., 2018), WikiPathways (Slenter et al., 2017). Enrichment was calculated relative to a set of background genes relevant for the experiment.

5.7 Statistical analysis

Data were analyzed using Prism Graphpad 9.4 software version and are shown as mean +/- SEM as reported in the figure legends. Results were analyzed using t-test, one-way or two-way ANOVA with the Sidak-Bonferroni correction when applicable. Statistical analysis was performed with Prism software or SPICE software. Statistical significance was defined as $P < 0.05$.

6. REFERENCES

- Abate-Daga D., *et al.* (2014) A novel chimeric antigen receptor against prostate stem cell antigen mediates tumor destruction in a humanized mouse model of pancreatic cancer. *Hum Gene Ther.* 25(12):1003-12
- Abramson JS., *et al.* (2020) Lisocabtagene maraleucel for patients with relapsed or refractory large B-cell lymphomas (TRANSCEND NHL 001): a multicentre seamless design study. *Lancet* 396:839-52
- Acharya N., Sabatos-Peyton C., Anderson C. (2020). Tim-3 finds its place in the cancer immunotherapy landscape. *J. Immunother. Cancer* 8(1):e000911
- Adachi K. *et al.* (2018) IL-7 and CCL19 expression in CAR-T cells improves immune cell infiltration and CAR-T cell survival in the tumor. *Nat. Biotechnol.* 36(4):346-351
- Adusumilli, P.S., Cherkassky, L., Villena-Vargas, J., Colovos, C., Servais, E., Plotkin, J., Jones, D.R., and Sadelain, M. (2014). Regional delivery of mesothelin-targeted CAR T cell therapy generates potent and long-lasting CD4-dependent tumor immunity. *Sci. Transl. Med.* 6, 261ra151.
- Ahmed N., *et al.* (2017). HER2-Specific Chimeric Antigen Receptor–Modified Virus-Specific T Cells for Progressive Glioblastoma. A Phase 1 Dose-Escalation Trial. *JAMA Oncol.*, 3(8):1094-1101
- Akella N.M., Ciraku L., Reginato M.J. (2019). Fueling the fire: emerging role of the hexosamine biosynthetic pathway in cancer. *BMC Biology*, 17:52
- Alexa A, Rahnenfuhrer J. (2019). topGO: Enrichment Analysis for Gene Ontology. *R package version 1.38.1*
- Amendola, M., Venneri, M. A., Biffi, A., Vigna, E. & Naldini, L. (2005). Coordinate dual-gene transgenesis by lentiviral vectors carrying synthetic bidirectional promoters. *Nat. Biotechnol.* 23, 108–116
- Arcangeli S., Bove C., Mezzanotte C., *et al.* (2022). CAR T cell manufacturing from naive/stem memory T lymphocytes enhances antitumor responses while curtailing cytokine release syndrome. *JCI*, 132(12):e150807
- Arnold, J. N., Saldova, R., Hamid, U. M. A. & Rudd, P. M. (2008). Evaluation of the serum N-linked glycome for the diagnosis of cancer and chronic inflammation. *Proteomics* 8, 3284–3293
- Baitsch D., Bock H.H., Engel T., *et al.* (2011). Apolipoprotein E Induces Antiinflammatory Phenotype in Macrophages. *Arterioscler. Thromb. Vasc. Biol.*, 31:1160-1168.

- Balestrieri C., Alfarano G., Milan M., Tosi V., Prosperini E., Nicoli P., *et al.* (2018). Co-optation of Tandem DNA Repeats for the Maintenance of Mesenchymal Identity. *Cell*, 173:1150-1164.e14
- Banerjee A, Lang JY, Hung MC, Sengupta K, Banerjee SK, Baksi K, Banerjee DK. (2011). Unfolded Protein Response Is Required in nu/nu Mice Microvasculature for Treating Breast Tumor with Tunicamycin. *The Journal of Biological Chemistry*; 286:29127–29138.
- Barkal A.A., *et al.* (2019). CD24 signaling through macrophage Siglec-10 is a target for cancer immunotherapy. *Nature* 572, 392-396
- Barrett, D. M., Teachey, D. T. & Grupp, S. A. (2014) Toxicity management for patients receiving novel T-cell engaging therapies. *Curr. Opin. Pediatr.* 26, 43–49
- Baumeister SH., *et al* (2019) Phase I Trial of Autologous CAR T Cells Targeting NKG2D Ligands in Patients with AML/MDS and Multiple Myeloma. *Cancer Immunol. Res.*, 7(1):100-112
- Bear, A. *et al.* (2010). Enhanced Tumor Trafficking of GD2 Chimeric Antigen Receptor T Cells by Expression of the Chemokine Receptor CCR2b. *J. Immunother.* 33,138: 780–788
- Beatson R., *et al.* (2016). The mucin MUC1 modulates the tumor immunological microenvironment through engagement of the lectin Siglec-9. *Nature Immunol.*, 17, 1273-1281
- Berger C., Flowers M.E., Warren E.H., Riddell S.R. (2006). Analysis of transgene-specific immune responses that limit the in vivo persistence of adoptively transferred HSV-TK-modified donor T cells after allogeneic hematopoietic cell transplantation. *Blood* 107(6):2294-302
- Billerbeck E, Barry WT, Mu K, *et al.* (2011). Development of human CD4+FoxP3+ regulatory T cells in human stem cell factor-, granulocyte-macrophage colony-stimulating factor-, and interleukin-3-expressing NOD-SCID IL2R γ (null) humanized mice. *Blood*; 117:3076–86.
- Bonini C. *et al.* (1997). HSV-TK gene transfer into donor lymphocytes for control of allogeneic graft-versus-leukemia. *Science* 276(5319):1719-24
- Brown C, Alizadeh D, Starr R, Weng L, Wagner J, Naranjo A, *et al.* (2016). Regression of glioblastoma after chimeric antigen receptor T-cell therapy. *N. Engl. J. Med.* 375:2561–9.
- Buck D, Noguchi T, Curtis JD, Chen Q, Gindin M, Gubin MM, *et al.* (2015). Metabolic competition in the tumor microenvironment is a driver of cancer progression. *Cell* 162:1229–41.

- Burga R.A., *et al.* (2015). Liver myeloid-derived suppressor cells expand in response to liver metastases in mice and inhibit the anti-tumor efficacy of anti-CEA CAR-T. *Cancer Immunol. Immunother.* 64(7):817-29
- Cappell KM., *et al.* (2020) Long-Term Follow-Up of Anti-CD19 Chimeric Antigen Receptor T-Cell Therapy. *J. Clin. Oncol.* 10, 38(32):3805-3815
- Carpenito, C. *et al.* (2009) Control of large, established tumor xenografts with genetically retargeted human T cells containing CD28 and CD137 domains. *Proc. Natl. Acad. Sci. U. S. A.* 106, 3360–3365
- Caruana I., *et al.* (2015). Heparanase promotes tumor infiltration and antitumor activity of CAR-redirectioned T lymphocytes. *Nat. Med.*, 21(5)
- Caruso H.G. *et al.* (2015). Tuning Sensitivity of CAR to EGFR Density Limits Recognition of Normal Tissue While Maintaining Potent Antitumor Activity. *Cancer Res.* 75(17):3505-18
- Casucci, M. *et al.* (2018) Extracellular NGFR spacers allow efficient tracking and enrichment of fully functional car-t cells co-expressing a suicide gene. *Front. Immunol.*, 9
- Chacko, B. K., Scott, D. W., Chandler, R. T. & Patel, R. P. (2011). Endothelial surface N-glycans mediate monocyte adhesion and are targets for anti-inflammatory effects of peroxisome proliferator-activated receptor γ ligands. *J. Biol. Chem.* 286, 38738–38747
- Chen C.H. *et al.* (2006). *In vivo* immune modulatory activity of hepatic stellate cells in mice. *Hepatology*, 44(5)
- Chen S., Yang J., Wei Y., Wei X. (2020). Epigenetic regulation of macrophages: from homeostasis maintenance to host defense. *Cellular and Molecular Immunol.* 17:36-49
- Chen X., Barozzi I., Termanini A., Prosperini E., Recchiuti A., Dalli J., Mietton F., Matteoli G., Hiebert S., Natoli G. (2012). Requirement for the histone deacetylase Hdac3 for the inflammatory gene expression program in macrophages. *Proc Natl Acad Sci U S A*; 109:E2865–74.
- Cheng C., Huang C., Ma T.T., Bian E.B., He Y., Zhang L., Li J. (2014). SOCS1 hypermethylation mediated by DNMT1 is associated with lipopolysaccharide-induced inflammatory cytokines in macrophages. *Toxicol. Lett.*; 225:488–97.
- Cherkassky L., Hou Z., Amador-Molina A., Adusumilli P.S. (2022). Regional CAR T cell therapy: An ignition key for systemic immunity in solid tumors. *Cancer Cell*; 40.
- Chmielewski, M. & Abken, H. CAR T Cells Releasing IL-18 Convert to T- Bethigh FoxO1low Effectors that Exhibit Augmented Activity against Advanced Solid Tumors. *Cell Rep.* 21, 3205–3219 (2017).

- Chmielewski, M., Hombach A., Heuser C., Adams G.P., Abken H. (2004). Cell Activation by Antibody-Like Immunoreceptors: increase in Affinity of the Single-Chain Fragment Domain above Threshold Does Not Increase T Cell Activation against Antigen-Positive Target Cells but Decreases Selectivity. *J. Immunol.* 173:7647-53
- Cho Y.A. *et al.* (2011). Relationship between the expressions of PD-L1 and tumor-infiltrating lymphocytes in oral squamous cell carcinoma. *Oral Oncol.* 47(12):1148-53
- Contessa JN, Bhojani MS, Freeze HH, Ross BD, Rehemtulla A, Lawrence TS. (2010). Molecular Imaging of N-linked Glycosylation Suggests Glycan Biosynthesis Is a Novel Target for Cancer Therapy. *Clinical Cancer Res.*; 16:3205–3214.
- Correia A.L. *et al.* (2021). Hepatic stellate cells suppress NK cell-sustained breast cancer dormancy. *Nature*, 594:566-571
- Daley D., Mani V.R., Mohan N., Akkad N., *et al.* (2017). Dectin-1 Activation on Macrophages by Galectin-9 Promotes Pancreatic Carcinoma and Peritumoral Immune-Tolerance. *Nat. Med.*, 23(5):556-567
- Dennis J.W. (1986). Effects of swainsonine and polyinosinic: polycytidylic acid on murine tumor cell growth and metastasis. *Cancer Res.*, 46:5131 -5136
- Dennis, J.W., Laferte, S., Waghorne, C., Breitman, M. L. & Kerbel, R. S. (1987). Beta 1-6 branching of Asn-linked oligosaccharides is directly associated with metastasis. *Science (80)*. 236, 582 LP – 585.
- Dennis J.W., Koch K., Yousefi S., VanderElst I. (1990). Growth inhibition of human melanoma tumor xenograft in athymic nude mice by swainsonine. *Cancer Res.*, 50:1867-1872
- Dennis, J.W., Nabi, I. R. & Demetriou, M. (2009). Organization, Cell Surface and disease. *Cell* 139, 1229–1241
- Dhillon B., Aleithan F., Abdul-Sater Z. and Abdul-Sater A.A. (2019). The Evolving Role of TRAFs in Mediating Inflammatory Responses. *Front. Immunol.* 10:104.
- Dillard P, Köksal H, Inderberg E-M, *et al.* (2018). A spheroid killing assay by CAR T cells. *J. Vis. Exp.* e58785.
- Dirkx, A. E. M. *et al.* (2003). Tumor angiogenesis modulates leukocyte-vessel wall interactions in Vivo by reducing endothelial adhesion molecule expression. *Cancer Res.* 63, 2322–2329
- Di Stasi A., *et al.* (2009). T lymphocytes coexpressing CCR4 and a chimeric antigen receptor targeting CD30 have improved homing and antitumor activity in a Hodgkin tumor model. *Blood* 113(25):6392-402

- Di stasi A., *et al.* (2011). Inducible apoptosis as a safety switch for adoptive cell therapy. *N. Engl. J. Med.* 365(18):1673-83
- Dobin A., Gingeras T.R. (2015). Mapping RNA- seq Reads with STAR. *Current Protocols in Bioinformatics. Current Protocols in Bioinformatics*
- Dong H., *et al.* (2002). Tumor-associated B7-H1 promotes T-cell apoptosis: a potential mechanism of immune evasion. *Nat. Med.* 8(8):793-800
- Doran SL., *et al.* (2019) T-cell receptor gene therapy for human papillomavirus-associated epithelial cancers: A first-in-human, phase I/II study. *J. Clin. Oncol.* 37, 2759–2768
- Dougan M., Dranoff G., Dougan S.K. (2019). GM-CSF, IL-3, and IL-5 Family of Cytokines: Regulators of Inflammation. *Immunity*, 50.
- Drent E, Poels R, Ruiters R, *et al.* (2019). Combined CD28 and 4-1BB costimulation potentiates Affinity-tuned chimeric antigen Receptor- engineered T cells. *Clin Cancer Res.*, 25:4014–25.
- Dudley, M. E. *et al.* (2013) Randomized selection design trial evaluating CD8+ - enriched versus unselected tumor-infiltrating lymphocytes for adoptive cell therapy for patients with melanoma. *J. Clin. Oncol.* 31, 2152–2159
- Fabregat, A. *et al.* (2018). The Reactome Pathway Knowledgebase. *Nucleic Acids Research* 46, D649-D655
- Fedorov V.D., Themeli M., Sadelain M. (2013). PD-1- and CTLA-4-based inhibitory chimeric antigen receptors (iCARs) divert off-target immunotherapy responses. *Sci. Transl. Med.* 5(215):215ra172
- Feng D., Sangster-Guity N., Stone R., Korzeniewska J., Mancl M.E., Fitzgerald-Bocarsly P., Barnes B.J. (2010). Differential requirement of histone acetylase and deacetylase activities for IRF5-mediated proinflammatory cytokine expression. *J. Immunol.*; 185:6003–12.
- Feng K., *et al.* (2018). Phase I study of chimeric antigen receptor modified T cells in treating HER2-positive advanced biliary tract cancers and pancreatic cancers. *Protein Cell.*, 9(10):838-47
- Feucht J., *et al.* (2019). Calibration of CAR activation potential directs alternative T cell fates and therapeutic potency. *Nat. Med.* 25:82-88
- Finney, H. M., Akbar, A. N. & Lawson, A. D. G. Activation of Resting Human Primary T Cells with Chimeric Receptors: Costimulation from CD28, Inducible Costimulator, CD134, and CD137 in Series with Signals from the TCR ζ Chain. *J. Immunol.* 172, 104–113 (2004).

- Forrester M.A., Wassal H.J., Hall L.S., Cao H., Wilson H.M., *et al.* (2018). Similarities and differences in surface receptor expression by THP-1 T monocytes and differentiated macrophages polarized using seven different conditioning regimens. *Cellular Immunol.* 332, 58-76
- Franken L., Schiwon M., Kurts C. (2016). Macrophages: sentinels and regulators of the immune system. *Cellular Microbiol.*, 18(4):475-487
- Freemerman AJ, Johnson AR, Sacks GN, Milner JJ, Kirk EL, Troester MA, *et al.* (2014). Metabolic reprogramming of macrophages. *J. Biol. Chem.*, 289:7884–96. doi: 10.1074/jbc.M113.522037
- Frey NV., *et al.* (2020) Optimizing Chimeric Antigen Receptor T-Cell Therapy for Adults With Acute Lymphoblastic Leukemia. *J. Clin. Oncol.*, 10;38(5):415-422
- Frigault *et al.*, (2016) Identification of chimeric antigen receptors that mediate constitutive or inducible proliferation of T cells. *Cancer Immunol. Res.* 3(4): 356-367
- Geer, LY. *et al.* (2009). The NCBI BioSystems database. *Nucleic Acids Research* 38, D492–D496
- Ghorashian S. *et al.* (2019) Enhanced CAR T cell expansion and prolonged persistence in pediatric patients with ALL treated with a low-affinity CD19 CAR. *Nat. Med.*, 25, 1408-1414
- Giavridis T., *et al.* (2018). CAR T cell-induced cytokine release syndrome is mediated by macrophages and abated by IL-1 blockade. *Nat. Med.*, 24(6):731-738
- Gill S and Brudno JN. (2021) CAR T-Cell Therapy in Hematologic Malignancies: Clinical Role, Toxicity, and Unanswered Questions. *Asco Ed Book*
- Goss P.E., Reid C.L., Bailey D., Dennis J.W. (1997). Phase IB clinical trial of the oligosaccharide processing inhibitor swainsonine in patients with advanced malignancies. *Clin Cancer Res.*, 3(7):1077-86
- Gray M.A., Stanczak M.A., Mantuano N.R., Xiao H., *et al.* (2020). Targeted glycan degradation potentiates the anticancer immune response in vivo. *Nat. Chem. Biol.* 16:1376-1384
- Greco B., Malacarne V., De Girardi F., Scotti G.M., Manfredi F., Angelino E., Sirini C., Camisa B., Falcone L., *et al.* (2022). Disrupting N-glycan expression on tumor cells boosts chimeric antigen receptor T cell efficacy against solid malignancies. *Sci. Transl. Med.*, 14, eabg3072
- Gringhuis, S. I. *et al.* (2014). Fucose-based PAMPs prime dendritic cells for follicular T helper cell polarization via DC-SIGN-dependent IL-27 production. *Nat. Commun.* 5, 1–12.

- Grosser R., Cherkassky L., CHintala N., Adusumilli P.S. (2019). Combination Immunotherapy with CAR T Cells and Checkpoint Blockade for the Treatment of Solid Tumors. *Cancer Cell*, 36(5):471-482
- Guedan S., et al. (2014). ICOS-based chimeric antigen receptors program bipolar TH17/TH1 cells. *Blood* 124, 1070–1080
- Guedan S., et al. (2018) Enhancing CAR T cell persistence through ICOS and 4-1BB costimulation. *JCI Insight* 11;3(1): e96976
- Guedan S., et al. (2022). Time 2EVOLVE: predicting efficacy of engineered T-cells – how far is the bench from the bedside? *J Immunother of Cancer*, 10:e003487
- Guerrero-Aspizua S., et al. (2020). Humanization of Tumor Stroma by Tissue Engineering as a Tool to Improve Squamous Cell Carcinoma Xenograft. *Int. J. Mol. Sci.*, 21(6), 1951
- Gullino, P. M., Clark, S. H. & Grantham, F. H. (1964). The Interstitial Fluid of Solid Tumors. *Cancer Res.* 24, 780–797
- Gust J. et al. (2017). Endothelial Activation and Blood-Brain Barrier Disruption in Neurotoxicity after Adoptive Immunotherapy with CD19 CAR-T Cells. *Cancer Discov.*, 7(12):1404-1419
- Hakomori, S. & Kannagi, R. (1983). Glycosphingolipids as tumor-associated and differentiation markers. *J. Natl. Cancer Inst.* 231–251
- Hakomori, S. (2002). Glycosylation defining cancer malignancy: New wine in an old bottle. *Proc. Natl. Acad. Sci.* 99, 10231–10233
- Han X., Zhang X., Li H., et al. (2015). Tunicamycin enhances the antitumor activity of trastuzumab on breast cancer in vitro and in vivo. *Oncotarget*; 6(36).
- Hanahan D. and Coussens L. (2012). Accessories to the Crime: Functions of Cells Recruited to the Tumor Microenvironment. *Cancer Cell* 21(3):309-322
- Hartmann, J., Schübler-Lenz, M., Bondanza, A. & Buchholz, C. J. (2017). Clinical development of CAR T cells—challenges and opportunities in translating innovative treatment concepts. *EMBO Mol. Med.* 9, 1183–1197
- Haslauer T et al. (2021) CAR T-Cell Therapy in Hematological Malignancies. *Int. J. Mol. Sci.* 22, 8996
- Haso, W. et al. (2013) Anti-CD22-chimeric antigen receptors targeting B-cell precursor acute lymphoblastic leukemia. *Blood* 121, 1165–1171

- Hatano, K., Miyamoto, Y., Nonomura, N. & Kaneda, Y. (2011). Expression of gangliosides, GD1a, and sialyl paragloboside is regulated by NF- κ B-dependent transcriptional control of α 2,3-sialyltransferase I, II, and VI in human castration-resistant prostate cancer cells. *Int. J. Cancer* 129, 1838–1847
- Hetz C., Zhang K. and Kaufman R.J. (2020). Mechanisms, regulation and functions of the unfolded protein response. *Nat Rev/Mol. Cell Biol.* 21:421-438
- Hinrichs, C. S. & Rosenberg, S. A. (2014) Exploiting the curative potential of adoptive T-cell therapy for cancer. *Immunol. Rev.* 257, 56–71
- Hornýák, L. *et al.* (2018). The Role of Indoleamine-2,3-Dioxygenase in Cancer Development, Diagnostics, and Therapy. *Front. Immunol.* 9, 151
- Hoyos V *et al.* (2010) Engineering CD19-specific T lymphocytes with interleukin-15 and a suicide gene to enhance their anti-lymphoma/leukemia effects and safety. *Leukemia* 24(6):1160-70
- Hou AJ., Chen LC., Chen YY. (2021). Navigating CAR-T cells through the solid-tumor microenvironment. *Nat Rev/Drug Discov.*, 20, 531-550
- Hu, W. *et al.* (2019). CRISPR/Cas9-mediated PD-1 disruption enhances human mesothelin-targeted CAR T cell effector functions. *Cancer Immunol. Immunother.* 68, 365–377
- Hudecek M., Lupo-Stanghellini MT., Kosasih PL., Sommermeyer D., Jensen MC., Rader C, *et al.* (2013) Receptor affinity and extracellular domain modifications affect tumor recognition by ROR1-specific chimeric antigen receptor T cells. *Clin. Cancer Res.*, 19: 3153–64
- Hudecek, M. *et al.* (2015) Antigen Receptors Is Decisive for in Vivo Antitumor Activity. *Cancer Immunol. Res.* 3, 125–135
- Jacob F., Ming G., Song H. (2020). Generation and biobanking of patient-derived glioblastoma organoids and their application in CAR T cell testing. *Nat. Protocols* 15, 4000-4033
- Jacob F, Salinas RD, Zhang DY, *et al.* (2020). A patient-derived glioblastoma organoid model and Biobank recapitulates inter- and Intra-tumoral heterogeneity. *Cell* 180:188–204.
- Jacobson C., *et al.* (2020) Primary Analysis of Zuma-5: A Phase 2 Study of Axicabtagene Ciloleucel (Axi-Cel) in Patients with Relapsed/Refractory (R/R) Indolent Non-Hodgkin Lymphoma (iNHL). *Blood* 136:40-41
- Jandus C., Boligan K.F., Chijioke O., Liu H., Dahlhaus M., Démoulin T., Schneider C., *et al.* (2014). Interactions between Siglec-7/9 receptors and ligands influence NK cell-dependent tumor immunosurveillance. *J. Clin. Invest.* 124, 1810–1820 (2014).

Jayaraman J., Mellody MP., Hou AJ., Desai RP., Fung AF., Huynh Thuy Pham A., Chen YY., Zhao W. (2020) CAR-T design: Elements and their synergistic function. *EBioMedicine* 58:102931

Jayasingam S.D. *et al.* (2020). Evaluating the Polarization of Tumor-Associated Macrophages Into M1 and M2 Phenotypes in Human Cancer Tissue: Technicalities and Challenges in Routine Clinical Practice. *Front Oncol.* 24;9:1512

Jha A.K., *et al.* (2015). Network Integration of Parallel Metabolic and Transcriptional Data Reveals Metabolic Modules that Regulate Macrophage Polarization. *Immunity*, 42: 419-430

John L.B., *et al.* (2013). Anti-PD-1 antibody therapy potently enhances the eradication of established tumors by gene-modified T cells. *Clin. Cancer Res.* 19(20):5636-46

Jonnalagadda M., Mardiros A., Urak R., Wang X., Hoffman LJ., Bernanke A., *et al.* (2015) Chimeric antigen receptors with mutated IgG4 Fc spacer avoid fc receptor binding and improve T cell persistence and antitumor efficacy. *Mol. Ther.* 23:757– 68

Kakarla S., *et al.* (2013). Antitumor effects of chimeric receptor engineered human T cells directed to tumor stroma. *Mol Ther.* 21(8):1611-20

Kalos, M. *et al.* (2012). T cells with chimeric antigen receptors have potent antitumor effects and can establish memory in patients with advanced leukemia. 3,

Kang N., Gores G., Shah V. (2011). Hepatic Stellate Cells: Partners in Crime for Liver Metastases? *Hepatology*, 54(2):707-713

Kang H., Yang B., Zhang K., Pan Q., Yuan W., Li G., Bian L. (2019). Immunoregulation of macrophages by dynamic ligand presentation via ligand–cation coordination. *Nat. Comm.*, 10:1696

Kaneko S, Mastaglio S, Bondanza A, *et al.* (2009). IL-7 and IL-15 allow the generation of suicide gene-modified alloreactive self-renewing central memory human T lymphocytes. *Blood*, 113:1006–15.

Kannagi, R., Yin, J., Miyazaki, K. & Izawa, M. (2008). Current relevance of incomplete synthesis and neo-synthesis for cancer-associated alteration of carbohydrate determinants-Hakomori's concepts revisited. *Biochim. Biophys. Acta - Gen. Subj.* 1780, 525–531

Katz S.C., Burga R.A., McCormack E., *et al.* (2015). Phase I hepatic immunotherapy for metastases study of intra-arterial chimeric antigen receptor-modified T-cell therapy for CEA+ liver metastases. *Clin. Cancer. Res.*; 21:3149–59.

Katz S.C., Hardaway J., Prince E., *et al.* (2020). HITM-SIR: phase Ib trial of intraarterial chimeric antigen receptor T-cell therapy and selective internal radiation therapy for CEA⁺ liver metastases. *Cancer Gene Ther.* ;27:341-355.

- Katz S.C., Moody A.E., Guha P., *et al.* (2020). HITM-SURE: Hepatic immunotherapy for metastases phase Ib anti-CEA CAR-T study utilizing pressure enabled drug delivery. *Jitc*; 8:e001097
- Katzenelenbogen, Y. *et al.* (2020). Coupled scRNA-Seq and intracellular protein activity reveal an immunosuppressive role of TREM2 in cancer. *Cell*
- Kawalekar, O. U. *et al.* (2016). Distinct Signaling of Coreceptors Regulates Specific Metabolism Pathways and Impacts Memory Development in CAR T Cells. *Immunity* 44, 380–390
- Keu K.V., *et al.* (2017). Reporter gene imaging of targeted T cell immunotherapy in recurrent glioma. *Sci. Transl. Med.* 9(373):eaag2196
- Kim S., Joe Y., Oh Jeong S., Zheng M., Back S.H., Park S.W., Ryter S.W., Chung H.T. (2014). Endoplasmic reticulum stress is sufficient for the induction of IL-1b production via activation of the NF- κ B and inflammasome pathways. *Innate Immunity*, (8):799-815
- Klichinsky M., *et al.* (2020). Human chimeric antigen receptor macrophages for cancer immunotherapy. *Nat. Biotechnol.* 38, 947-953
- Kloss C.C., Condomines M., Cartellieri M., Bachmann M., Sadelain M. (2013). Combinatorial antigen recognition with balanced signaling promotes selective tumor eradication by engineered T cells. *Nat. Biotechnol.* 31(1):71-5
- Koneru M, Purdon TJ, Spriggs D, *et al.* (2015). IL-12 secreting tumor- targeted chimeric antigen receptor T cells eradicate ovarian tumors in vivo. *Oncoimmunol.* 4:e994446.
- Koning N, van Eijk M, Pouwels W, Brouwer MSM, Voehringer D, Huitinga I, *et al.* (2010). Expression of the inhibitory CD200 receptor is associated with alternative macrophage activation. *J. Innate Immun.*, 2: 195–200. pmid:20375636
- Kouo T, Huang L, Pucsek AB, Cao M, Solt S, Armstrong T, *et al.* (2015). Galectin-3 shapes antitumor immune responses by suppressing CD8⁺ T cells via LAG- 3 and inhibiting expansion of Plasmacytoid dendritic cells. *Cancer Immunol. Res.* 3:412–23
- Kowolik, C. M. *et al.* (2006). CD28 costimulation provided through a CD19-specific chimeric antigen receptor enhances in vivo persistence and antitumor efficacy of adoptively transferred T cells. *Cancer Res.* 66, 10995–11004
- Kurtoglu, M. *et al.* (2007). Under normoxia, 2-deoxy-D-glucose elicits cell death in select tumor types not by inhibition of glycolysis but by interfering with N-linked glycosylation. *Mol. Cancer Ther.* 6, 3049–3058
- Kurtoglu, M., Maher, J. C. & Lampidis, T. J. (2007). Differential Toxic Mechanisms of 2-Deoxy-D-Glucose versus 2-Fluorodeoxy-D -Glucose in Hypoxic and Normoxic Tumor Cells. *Antioxid. Redox Signal.* 9, 1383–1390

- Kuzet S.E. and Gaggioli C. (2016). Fibroblast activation in cancer: when seed fertilizes soil. *Cell Tissue Res.* 365(3):607-19
- Kwark T., Wang F., Deng H., Condamine T., *et al.* (2020). Distinct Populations of Immune-Suppressive Macrophages Differentiate from Monocytic Myeloid-Derived Suppressor Cells in Cancer. *Cell Reports*, 33(13), 108571
- Lakins M.A, Ghorani E., Munir H., Martins C.P., Shields J.D. (2018). Cancer-associated fibroblasts induce antigen-specific deletion of CD8+ T Cells to protect tumour cells. *Nat. Commun.* 9:948
- Lamers C.H. *et al.* (2006). Treatment of metastatic renal cell carcinoma with autologous T-lymphocytes genetically retargeted against carbonic anhydrase IX: first clinical experience. *J. Clin. Oncol.* 24(13):e20-2
- Lau K.S., *et al.* (2007). Complex N-glycan number and degree of branching cooperate to regulate cell proliferation and differentiation. *Cell* 129, 123–134
- Lee DW., *et al.* (2014). Current concepts in the diagnosis and management of cytokine release syndrome. *Blood*, 124(2):188-95
- Lee, H.-W. *et al.* (2002). 4-1BB Promotes the Survival of CD8 + T Lymphocytes by Increasing Expression of Bcl-x L and Bfl-1. *J. Immunol.* 169, 4882–4888
- Leon E., Ranganathan R., Savoldo B. (2020) Adoptive T cell therapy: Boosting the immune system to fight cancer. *Semin Immunol.* 49: 101437
- Li, C. W. *et al.* (2016). Glycosylation and stabilization of programmed death ligand-1 suppresses T-cell activity. *Nat. Commun.* 7, 1–11
- Li C.W., *et al.* (2018). Eradication of triple negative breast cancer cells by targeting glycosylated PD-L1. *Cancer Cell* 33(2):187-201
- Li H., *et al.* (2020). Modeling tumor development and metastasis using paired organoids derived from patients with colorectal cancer liver metastases. *J. Hematol. Oncol.* 13:119
- Li W., Cao T., Luo C., Cai J., Zhou X., Xiao X., Liu S. (2020). Crosstalk between ER stress, NLRP3 inflammasome, and inflammation. *Appl. Microbiol. Biotechnol.*, 104:6129-6140
- Li X. *et al.* (2016). An air-liquid interface culture system for 3D organoid culture of diverse primary gastrointestinal tissues. *Methods Mol. Biol.* 1422, 33–40
- Li Y., Liu D., Wang Y., Su W., Liu G., Dong W. (2021). The Importance of Glycans of Viral and Host Proteins in Enveloped Virus Infection. *Front. Immunol.* 12:638573

- Li Z., Wang J., Zhang X., *et al.* (2020). Proinflammatory S100A8 Induces PD-L1 Expression in Macrophages, Mediating Tumor Immune Escape. *J. Immunol.*, 204:2589–2599
- Liao Y., Smyth G.K., Shi W. (2014). FeatureCounts: an efficient general purpose program for assigning sequence reads to genomic features. *Bioinformatics*, 30:923–30
- Liberzon, A. *et al.* (2011). Molecular signatures database (MSigDB) 3.0. *Bioinformatics* 43, 1739-1740
- Ling YH, Li T, Perez-Soler R, Haigentz M Jr. (2009). Activation of ER stress and inhibition of EGFR N-glycosylation by tunicamycin enhances susceptibility of human non-small cell lung cancer cells to erlotinib. *Cancer Chemother. Pharmacol.*; 64:539–548.
- Liu X. *et al.* (2015). Affinity-tuned ErbB2 or EGFR chimeric antigen receptor T cells exhibit an increased therapeutic index against tumors in mice. *Cancer Res*; 75:3596–607
- Liu, X. *et al.* (2016). A chimeric switch-receptor targeting PD1 augments the efficacy of second-generation CAR T cells in advanced solid tumors. *Cancer Res.* 76, 1578– 1590
- Long, A., Haso, W. & Mackall, C. L. (2015). 4-1BB Costimulation Ameliorates T Cell Exhaustion Induced by Tonic Signaling of Chimeric Antigen Receptors. *Nat. Med.* 21, 581– 590
- Luo W., Napoleon JV., Zhang F., *et al.* (2022). Repolarization of Tumor-Infiltrating Myeloid Cells for Augmentation of CAR T Cell Therapies. *Front. Immunol.* 13:816761
- Lynn, R. C. *et al.* (2015) Targeting of folate receptor β on acute myeloid leukemia blasts with chimeric antigen receptor-expressing T cells. *Blood* 125, 3466–3476
- Ma R.Y., Black A., Qian B.Z. (2022). Macrophage diversity in cancer revisited in the era of single-cell omics. *Trends Immunol.*; 43(7).
- MacKinnon A.C., *et al.* (2008). Regulation of alternative macrophage activation by galectin-3, *J. Immunol.* 180 (4) 2650–2658.
- Majzner R.G., *et al.* (2020). Tuning the Antigen Density Requirement for CAR T-cell Activity. *Cancer Discov.* 10(5):702-723.
- Maloney, D. G. *et al.* (1997) IDEC-C2B8 (rituximab) anti-CD20 monoclonal antibody therapy in patients with relapsed low-grade non-Hodgkin's lymphoma. *Blood* 90, 2188–2195.
- Mantovani A., *et al.* (2017). Tumour-associated macrophages as treatment targets in oncology. *Nat Rev Clin Oncol.* 14(7):399-416.

- Manzari B., *et al.* (2007). Induction of macrophage glutamine: fructose-6-phosphate amidotransferase expression by hypoxia and by picolinic acid, *Int. J. Immunopathol. Pharmacol.* 20 (1): 47–58.
- Markley, J. C. & Sadelain, M. (2010). IL-7 and IL-21 are superior to IL-2 and IL-15 in promoting human T cell-mediated rejection of systemic lymphoma in immunodeficient mice. *Blood* 115, 3508–3519.
- Martinez F.O., Gordon S., Locati M., Mantovani A. (2006). Transcriptional profiling of the human monocyte-to-macrophage differentiation and polarization: new molecules and patterns of gene expression. *J. Immunol.*, 177(10):7303-11.
- Martinez M. and Moon E.K. (2019). CAR T Cells for Solid Tumors: New Strategies for Finding, Infiltrating, and Surviving in the Tumor Microenvironment. *Front. Immunol.* 10:128.
- Maschek, G. *et al.* (2004). 2-Deoxy-D-glucose increases the efficacy of adriamycin and paclitaxel in human osteosarcoma and non-small cell lung cancers in vivo. *Cancer Res.* 64, 31–34.
- Mastaglio S., *et al.* (2017). NY-ESO-1 TCR single edited stem and central memory T cells to treat multiple myeloma without graft-versus-host disease. *Blood*, 130(5):606-618.
- Mastermann K., *et al.* (2019). The tyrosine kinase inhibitor dasatinib acts as a pharmacologic on/off switch for CAR T cells. *Sci. Transl. Med.* 11(499):eaau5907.
- Maude, S. L. *et al.* (2018). Tisagenlecleucel in children and young adults with B-cell lymphoblastic leukemia. *N. Engl. J. Med.* 378, 439–448.
- Mazzone M., Menga A., Castegna A. (2018). Metabolism and TAM functions-it takes two to tango, *FEBS J.* 285 (4) 700–716.
- McWhorter F.Y., Wang T., Nguyen P., Chung T., Liu W.F. (2013). Modulation of macrophage phenotype by cell shape. *PNAS*, 110(43):17253-17258.
- Méndez-Huergo, S. P., Blidner, A. G. & Rabinovich, G. A. (2017). Galectins: emerging regulatory checkpoints linking tumor immunity and angiogenesis. *Curr. Opin. Immunol.* 45, 8–15.
- Milone, M. C. *et al.* (2009). Chimeric receptors containing CD137 signal transduction domains mediate enhanced survival of T cells and increased antileukemic efficacy in vivo. *Mol. Ther.* 17, 1453–1464.
- Mitchell, A. *et al.* (2019). InterPro in 2019: improving coverage, classification and access to protein sequence annotations. *Nucleic Acids Research* 47, D351–D360.
- Morgan RA., *et al.* (2006) Cancer regression in patients after transfer of genetically engineered lymphocytes. *Science* 126–129. 10.1126.

- Morgan R.A. *et al.* (2010). Case report of a serious adverse event following the administration of T cells transduced with a chimeric antigen receptor recognizing ERBB2. *Mol. Ther.* 18(4):843-51.
- Motz, G. T. *et al.* (2014). Tumor endothelium FasL establishes a selective immune barrier promoting tolerance in tumors. *Nat. Med.* 20, 607–615.
- Munk K., Pritzer E., Kretzschmar E., Gutte B., Garten W., Klenk H.D. (1992). Carbohydrate masking of an antigenic epitope of influenza virus haemagglutinin independent of oligosaccharide size. *Glycobiol.*, 2(3):233-240.
- Munshi NC., *et al.* (2021) Idecabtagene Vicleucel in Relapsed and Refractory Multiple Myeloma. *N. Engl. J. Med.*, 384:705-716.
- Nap M., Mollgard K., Burtin P., Fleuren G. (1988). Immunohistochemistry of carcino-embryonic antigen in the embryo, fetus and adult. *Tumour Biol.*, 9(2-3):145-53.
- Narayan V., *et al.* (2022). PSMA-targeting TGF β -insensitive armored CAR T cells in metastatic castration-resistant prostate cancer: a phase 1 trial. *Nat. Med* 28: 724-734.
- Nastoupil LJ. *et al.* (2020). Standard-of-Care Axicabtagene Ciloleucel for Relapsed or Refractory Large B-Cell Lymphoma: Results From the US Lymphoma CAR T Consortium. *J. Clin. Oncol.* 38(27):3119-3128.
- Neal, J.T. *et al.* (2018). Organoid modeling of the tumor immune microenvironment. *Cell* 175, 1972–1988.
- Neelapu, S. S. *et al.* (2017). Axicabtagene ciloleucel CAR T-cell therapy in refractory large B-Cell lymphoma. *N. Engl. J. Med.* 377, 2531–2544.
- Ninomiya S., *et al.* (2015). Tumor indoleamine 2,3-dioxygenase (IDO) inhibits CD19-CAR T cells and is downregulated by lymphodepleting drugs. *Blood*, 125(25):3905-3916.
- Norelli M., Camisa B., Barbiera G., *et al.* (2018). Monocyte-derived IL-1 and IL-6 are differentially required for cytokine-release syndrome and neurotoxicity due to CAR T cells. *Nat. Med*, (24):739-748.
- Oomizu S, Arikawa T, Niki T, Kadowaki T, Ueno M, Nishi N, *et al.* (2012). Galectin-9 suppresses Th17 cell development in an IL-2-dependent but Tim-3-independent manner. *Clin. Immunol.* 143:51–8.
- O'Rourke, D. M. *et al.* (2017). A single dose of peripherally infused EGFRvIII-directed CAR T cells mediates antigen loss and induces adaptive resistance in patients with recurrent glioblastoma. *Sci. Trans. Med.* 9.
- Palmieri E.M., *et al.* (2017). Pharmacologic or genetic targeting of glutamine synthetase skews macrophages toward an M1-like phenotype and inhibits tumor metastasis, *Cell Rep.* 20 (7) 1654–1666.

- Park D.D., *et al.* (2020). Resident and elicited macrophages differ in expression of their glycomes and lectins. *bioRxiv*.
- Park, J. R. *et al.* (2007). Adoptive transfer of chimeric antigen receptor re-directed cytolytic T lymphocyte clones in patients with neuroblastoma. *Mol. Ther.* 15, 825–833.
- Park S., Shevlin E., Vedvyas Y., Zaman M., Park S., Hsu YMS, *et al.* (2017) Micromolar affinity CAR T cells to ICAM-1 achieves rapid tumor elimination while avoiding systemic toxicity. *Sci. Rep.* 7:1–15.
- Parkhurst, M. R. *et al.* (2011). T cells targeting carcinoembryonic antigen can mediate regression of metastatic colorectal cancer but induce severe transient colitis. *Mol. Ther.* 19, 620–626.
- Partridge E.A., *et al.* (2004). Regulation of cytokine receptors by Golgi N-glycan processing and endocytosis. *Science*, 306, 120–124.
- Pasquini M.C., Hu Z-H., Curran K., *et al.* (2021). Real-world evidence of tisagenlecleucel for pediatric acute lymphoblastic leukemia and non-Hodgkin lymphoma. *Blood*; 5(4):1136.
- Patel U., *et al.* (2022). CAR T cell therapy in solid tumors: A review of current clinical trials. *eJHaem*, 3(1): 24-31.
- Pereira MS, Alves I, Vicente M, Campar A, Silva MC, Padrão NA, Pinto V, Fernandes Â, Dias AM and Pinho SS. (2018). Glycans as Key Checkpoints of T Cell Activity and Function. *Front. Immunol.* 9:2754.
- Perkins, JR. *et al.* (2012). ReadqPCR and NormqPCR: R packages for the reading, quality checking and normalisation of RT-qPCR quantification cycle (Cq) data. *BMC Genomics* 13, 286+.
- Pinho S.S., *et al.* (2009). The role of N-acetylglucosaminyltransferase III and V in the post-transcriptional modifications of E-cadherin. *Hum. Mol. Genet.* 18, 2599–2608.
- Pinho, S. S. *et al.* (2012). Loss and recovery of Mgat3 and GnT-III mediated E-cadherin N-glycosylation is a mechanism involved in Epithelial-Mesenchymal-Epithelial transitions. *PLoS One* 7, 1–9.
- Pochee E., *et al.* (2013). Expression of integrins $\alpha3\beta1$ and $\alpha5\beta1$ and GlcNAc $\beta1,6$ glycan branching influences metastatic melanoma cell migration on fibronectin. *Eur. J. Cell Biol.* 92, 355–362.
- Posey, A. D. *et al.* (2016). Engineered CAR T Cells Targeting the Cancer-Associated Tn-Glycoform of the Membrane Mucin MUC1 Control Adenocarcinoma. *Immunity* 44, 1444–1454.

- Priceman S.J., *et al.* (2018). Regional Delivery of Chimeric Antigen Receptor-Engineered T Cells Effectively Targets HER2 + Breast Cancer Metastasis to the Brain. *Clin Cancer Res.* 24(1):95-105.
- Pulè, M. A. *et al.* (2005). A chimeric T cell antigen receptor that augments cytokine release and supports clonal expansion of primary human T cells. *Mol. Ther.* 12, 933–941.
- Qi C., *et al.* (2022). Claudin18.2-specific CAR T cells in gastrointestinal cancers: phase 1 trial interim results. *Nat. Med.*, 28: 1189-1198.
- Qin, J. Z., Xin, H. & Nickoloff, B. J. (2010). 2-Deoxyglucose sensitizes melanoma cells to TRAIL-induced apoptosis which is reduced by mannose. *Biochem. Biophys. Res. Commun.* 401, 293–299.
- Qin Y., *et al.* (2012). Alteration of protein glycosylation in human hepatic stellate cells activated with transforming growth factor- β 1. *J. Proteomics*, 75:4114-4123.
- Quintarelli C. *et al.* (2018) Choice of costimulatory domains and of cytokines determines CAR T-cell activity in neuroblastoma. *Oncoimmunol.* 15; 7(6):e1433518.
- Raez, L. E. *et al.* (2005). Combining glycolytic inhibitors with chemotherapy: Phase I trial of 2-deoxyglucose and docetaxel in patients with solid tumors. *J. Clin. Oncol.* 23, 3190.
- Raez, L. E. *et al.* (2013). A phase i dose-escalation trial of 2-deoxy-d-glucose alone or combined with docetaxel in patients with advanced solid tumors. *Cancer Chemother. Pharmacol.* 71, 523–530.
- Ralser, M. *et al.* (2008). A catabolic block does not sufficiently explain how 2-deoxy-D-glucose inhibits cell growth. *Pnas* 105, 17807–17811.
- Ramos *et al.* (2008) *In Vivo* Fate and Activity of Second- versus Third-Generation CD19-Specific CAR-T Cells in B Cell Non-Hodgkin's Lymphomas. *Mol. Ther.* 5; 26(12): 2727-2737.
- Ramos CA., *et al.* (2020) Anti-CD30 CAR-T Cell Therapy in Relapsed and Refractory Hodgkin Lymphoma. *J. Clin. Oncol.* 10;38(32):3794-3804.
- Raudvere U., Kolberg L., Kuzmin I., Arak T., Adler P., Peterson H., *et al.* (2019). g:Profiler: a web server for functional enrichment analysis and conversions of gene lists (2019 update). *Nucleic Acids Research*, 47:W191–8
- Reinfeld B.I., Madden M.Z., Wolf M.M., Chytil A., Bader J.E., Patterson A.R., Sugiura A., Cohen A.S., Ali A., Do B.T., *et al.* (2021). Cell-programmed nutrient partitioning in the tumour microenvironment. *Nature*, 593

- Renner K, Singer K, Koehl G, Geissler E, Peter K, Siska P, *et al.* (2017). Metabolic hallmarks of tumor and immune cells in the tumor microenvironment. *Front. Immunol.* 8:248.
- Richman S.A. *et al.*, (2018). High-Affinity GD2-Specific CAR T Cells Induce Fatal Encephalitis in a Preclinical Neuroblastoma Model. *Cancer Immunol. Res.* 6(1):36-46.
- Robbins PF., *et al.* (2011) Tumor regression in patients with metastatic synovial cell sarcoma and melanoma using genetically engineered lymphocytes reactive with NY-ESO-1. *J. Clin. Oncol* 29, 917–924.
- Robinson M.D., McCarthy D.J., Smyth G.K. (2010). EdgeR: a Bioconductor package for differential expression analysis of digital gene expression data. *Bioinformatics*, 26:139–40
- Rodriguez E., Boelaars K., Brown K., Eveline Li R.J., Kruijssen L., *et al.* (2021). Sialic acids in pancreatic cancer cells drive tumour-associated macrophage differentiation via the Siglec receptors Siglec-7 and Siglec-9. *Nat. Commun.*, 12:1270
- Rodriguez-Garcia A., *et al.* (2021). CAR-T cell-mediated depletion of immunosuppressive tumor-associated macrophages promotes endogenous antitumor immunity and augments adoptive immunotherapy. *Nat Commun.* 12:877
- Rodriguez-Mantuano N., *et al.* (2019). Emerging role of glycosylation in the polarization of tumor-associated macrophages. *Pharm. Res.* 146:104285.
- Rosenberg, S. A. *et al.* (1988) Use of tumor-infiltrating lymphocytes and interleukin-2 in the immunotherapy of patients with metastatic melanoma. A preliminary report. *N. Engl. J. Med.* 319, 1676–1680.
- Rosenberg, S. A. *et al.* (2011) Durable complete responses in heavily pretreated patients with metastatic melanoma using T-cell transfer immunotherapy. *Clin. Cancer Res.* 17, 4550–4557.
- Roybal, K. T. *et al.* (2016). Precision tumor recognition by T cells with combinatorial antigen-sensing circuits. *Cell* 164, 770–779.
- Saeland E., *et al.* (2012). Differential glycosylation of MUC1 and CEACAM5 between normal mucosa and tumour tissue of colon cancer patients. *Int. J. Cancer*, 131(1):117-28.
- Sadelain M., Brentjens R., Rivière I., Park J. (2015). CD19 CAR therapy for acute lymphoblastic leukemia. *Am. Soc. Clin. Oncol. Edu. Book*, 35.
- Sackstein, R., Schatton, T. & Barthel, S. R. (2017). T-lymphocyte homing: An underappreciated yet critical hurdle for successful cancer immunotherapy. *Lab. Investig.* 97, 669–697.

- Santomasso B.D. *et al.* (2018). Clinical and Biological Correlates of Neurotoxicity Associated with CAR T-cell Therapy in Patients with B-cell Acute Lymphoblastic Leukemia. *Cancer Discov.*, 8(8):958-971.
- Sasaki K., Nishina S., Yamauchi A., Fukuda K., Hara Y., Yamamura M., *et al.* (2021). Nanoparticle-Mediated Delivery of 2-Deoxy-D-Glucose Induces Antitumor Immunity and Cytotoxicity in Liver Tumors in Mice. *Cell. Mol. Gastroenterol. Hepatol.*, 11(3):739-762
- Savoldo B., Ramos C.A., Liu E., *et al.* (2011). CD28 costimulation improves expansion and persistence of chimeric antigen receptor-modified T cells in lymphoma patients. *J. Clin. Invest.* 121(5), 1822-1826.
- Schnalzger T.E., *et al.* (2019). 3D model for CAR-mediated cytotoxicity using patient-derived colorectal cancer organoids. *EMBO J.*, 38:e100928.
- Scott, D. W., Vallejo, M. O. & Patel, R. P. (2013). Heterogenic endothelial responses to inflammation: role for differential N-glycosylation and vascular bed of origin. *J. Am. Heart Assoc.* 2, 1–18.
- Seliger B., Cabrera T., Garrido F., Ferrone S. (2002) HLA class I antigen abnormalities and immune escape by malignant cells. *Semin. Cancer Biol.* 12, 3–13
- Shang L., Hosseini M., Liu X., Kisseleva T., Brenner D.A. (2018). Human hepatic stellate cell isolation and characterization. *J. Gastroenterol.*, 53:6-17.
- Shi B., Chu J., Huang T., *et al.* (2021). The Scavenger Receptor MARCO Expressed by Tumor-Associated Macrophages Are Highly Associated with Poor Pancreatic Cancer Prognosis. *Front. Oncol.*, 11:771488.
- Shu J., *et al.* (2019). Dynamic analysis of proteomic alterations in response to N-linked glycosylation inhibition in a drug-resistant ovarian carcinoma cell line. *FEBS J.*; 286(8):1594-1605.
- Shuster SJ., *et al.* (2019). Tisagenlecleucel in Adult Relapsed or Refractory Diffuse Large B-Cell Lymphoma. *N. Engl. J. Med.*; 380:45-56.
- Siegler EL, Wang P. (2018). Preclinical models in chimeric antigen Receptor-Engineered T-cell therapy. *Hum. Gene Ther.*; 29:534–46.
- Singh, D. *et al.* (2005). Optimizing cancer radiotherapy with 2-deoxy-D-glucose: Dose escalation studies in patients with glioblastoma multiforme. *Strahlentherapie und Onkol.* 181, 507–514.
- Slenter, D. *et al.* (2017). WikiPathways: a multifaceted pathway database bridging metabolomics to other omics research. *Nucleic Acids Research* 46, D661-D667.

- Smith EL., Harrington K., Staehr M., Masakayan R., Jones J., Long TJ, *et al.* (2019) GPRC5D is a target for the immunotherapy of multiple myeloma with rationally designed CAR T cells. *Sci. Transl. Med.* 11:1–14.
- Stanczak M.A., *et al.* (2021). Targeting cancer glycosylation repolarizes tumor-associated macrophages allowing effective immune checkpoint blockade. *bioRxiv*.
- Sterner RM., *et al.* (2019). GM-CSF inhibition reduces cytokine release syndrome and neuroinflammation but enhances CAR-T cell function in xenografts. *Blood*, 133(7):697-709.
- Suarez E.R., *et al.* (2016). Chimeric antigen receptor T cells secreting anti-PD-L1 antibodies more effectively regress renal cell carcinoma in a humanized mouse model. *Oncotarget* 7:34341-34355.
- Subramanian, A. *et al.* (2005). Gene set enrichment analysis: A knowledge-based approach for interpreting genome-wide expression profiles. *PNAS* 43, 15545-15550.
- Sun L., Li C.W., Chung E.M., Yang R., Kim Y.S., *et al.* (2020). Targeting glycosylated PD-1 induces potent anti-tumor immunity. *Cancer Res.*, 80(11):2298-2310.
- Supimon K., Sangsuwannukul T., Sujitjoo J., *et al.* (2021). Anti-mucin 1 chimeric antigen receptor T cells for adoptive T cell therapy of cholangiocarcinoma. *Sci.f Reports*, 11:6276.
- Tan Y.Q., Li Y.T., Yan T.F., *et al.* (2020). Six Immune Associated Genes Construct Prognostic Model Evaluate Low-Grade Glioma. *Front. Immunol.*, 11:606164.
- Tang N., *et al.* (2020). TGF- β inhibition via CRISPR promotes the long-term efficacy of CAR T cells against solid tumors. *JCI* 5(4):e133977.
- Thistlethwaite FC., *et al.* (2017). The clinical efficacy of first-generation carcinoembryonic antigen (CEACAM5)-specific CAR T cells is limited by poor persistence and transient pre-conditioning-dependent respiratory toxicity. *Cancer Immunol. Immunother.*, 66(11): 1425-1436.
- Thomas, E. D., Lochte, H. L., Lu, W. C. & Ferrebee, J. W. (1957) Intravenous Infusion of Bone Marrow in Patients Receiving Radiation and Chemotherapy. *N. Engl. J. Med.* 257, 491–496.
- Torikai H, Reik A, Liu P-Q, *et al.* (2012). A foundation for universal T-cell based immunotherapy: T cells engineered to express a CD19- specific chimeric-antigen-receptor and eliminate expression of endogenous TCR. *Blood* 119:5697–705.
- Toscano, M. A. *et al.* (2007). Differential glycosylation of TH1, TH2 and TH-17 effector cells selectively regulates susceptibility to cell death. *Nat. Immunol.* 8, 825–834.

- Tu W., *et al.* (2021). TCF4 enhances hepatic metastasis of colorectal cancer by regulating tumor-associated macrophage via CCL2/CCR2 signaling. *Cell Death and Disease*, 12;882.
- Tumino N., *et al.* (2021). Polymorphonuclear myeloid-derived suppressor cells impair the anti-tumor efficacy of GD2.CAR T-cells in patients with neuroblastoma. *J Hematol Oncol.* 14: 191.
- Turley, S. J., Cremasco, V. & Astarita, J. L. (2015). Immunological hallmarks of stromal cells in the tumour microenvironment. *Nat. Rev. Immunol.* 15, 669–682.
- Van der Stegen SJC., Hamieh M., Sadelain M. (2015) The pharmacology of second-generation chimeric antigen receptors. *Nat. Rev. Drug. Discov.* 14(7): 499-509.
- Van Vliet, S. J. *et al.* (2013). MGL signaling augments TLR2-mediated responses for enhanced IL-10 and TNF- α secretion. *J. Leukoc. Biol.* 94, 315–323.
- Varki A and Cummings RD, E. J. *Essentials of glycobiology.*
- Viola A., Munari F., Sanchez-Rodriguez R., Scolaro T., Castegna A. (2019). The Metabolic Signature of Macrophage Responses. *Front. Immunol.*, 10:1462.
- Vlachogiannis G., *et al.* (2018). Patient-derived organoids model treatment response of metastatic gastrointestinal cancers. *Science* 359, 920–926.
- Wang L., *et al.* (2021). New-Onset Severe Cytopenia After CAR-T Cell Therapy: Analysis of 76 Patients With Relapsed or Refractory Acute Lymphoblastic Leukemia. *Front Oncol.*, 11:702644.
- Wang M., Munoz J., Goy A., *et al.* (2020). KTE-X19 CAR T-cell therapy in relapsed or refractory mantle-cell lymphoma. *N. Eng. J. Med.*, 382:1331-1342.
- Wang N., Liang H., Zen K. (2014). Molecular mechanisms that influence the macrophage M1–M2 polarization balance. *Front. Immunol.* 5:614.
- Weijtens, M. E., Willemsen, R. A., Valerio, D., Stam, K. & Bolhuis, R. L. (1996) Single chain Ig/gamma gene-redirceted human T lymphocytes produce cytokines, specifically lyse tumor cells, and recycle lytic capacity. *J. Immunol.* 157, 836–43.
- Weiskopf K., *et al.* (2013). Engineered SIRP α variants as immunotherapeutic adjuvants to anticancer antibodies. *Science* 341(6141):88-91.
- Weiskopf K., and Weissman I.L. (2015). Macrophages are critical effectors of antibody therapies for cancer. *MAbs* 7(2):303-10.
- Willemsen, R. A., Ronteltap, C., Chames, P., Debets, R. & Bolhuis, R. L. H. (2005) T Cell Retargeting with MHC Class I-Restricted Antibodies: The CD28 Costimulatory Domain Enhances Antigen-Specific Cytotoxicity and Cytokine Production. *J. Immunol.*

174, 7853–7858.

Woodsworth DJ., Dunsing V., Coombs D. (2015) Design Parameters for Granzyme-Mediated Cytotoxic Lymphocyte Target-Cell Killing and Specificity. *Biophys. J.*, 109:477–88.

Wu J., Wang Y., Jiang Z. (2021). TNFSF9 Is a Prognostic Biomarker and Correlated with Immune Infiltrates in Pancreatic Cancer. *J. Gastrointest. Cancer* 52(1):150-159.

Wu J., *et al.* (2018). Tunicamycin specifically aggravates ER stress and overcomes chemoresistance in multidrug-resistant gastric cancer cells by inhibiting N-glycosylation. *J. Exp. Clin. Cancer Res*; 37:27

Wu M.H., *et al.* (2017). Glycosylation-dependent galectin-1/neuropilin-1 interactions promote liver fibrosis through activation of TGF- β - and PDGF-like signals in hepatic stellate cells. *Sci. Reports*, 7:11006.

Xi, H. *et al.* (2011). 2-Deoxy-d-glucose activates autophagy via endoplasmic reticulum stress rather than ATP depletion. *Cancer Chemother. Pharmacol.* 67, 899–910.

Xie C., Liu C., Wu B., Lin Y., *et al.* (2016). Effects of IRF1 and IFN- β interaction on the M1 polarization of macrophages and its antitumor function. *Int. J. Mol. Med.*, 38(1):148-60.

Xu Y, Yu H, Qin H, Kang J, Yu C, Zhong J, Su J, Li H, Sun L. (2012). Inhibition of autophagy enhances cisplatin cytotoxicity through endoplasmic reticulum stress in human cervical cancer cells. *Cancer Letters*; 314:232–243.

Yamaguchi Y., Gibson J., Ou K., *et al.* (2022). PD-L1 blockade restores CAR T cell activity through IFN- γ -regulation of CD163+ M2 macrophages. *Jitc*; 10:e004400.

Yamamoto T.N., *et al.* (2019). T cells genetically engineered to overcome death signaling enhance adoptive cancer immunotherapy. *JCI*, 129(4):1551-1565.

Yang K.R., Mooney S.M., Zarif J.C., Coffey D.S., Taichman R.S., Pienta K.J. (2014). Niche inheritance: a cooperative pathway to enhance cancer cell fitness through ecosystem engineering. *J. Cell Biochem.*; 115:1478–85.

Yang J, Yan J, Liu B. (2018). Targeting VEGF/VEGFR to modulate antitumor immunity. *Front Immunol.* 9:978.

Yang X., Feng W., Wang R., Yang F., *et al.* (2018). Repolarizing heterogeneous leukemia-associated macrophages with more M1 characteristics eliminates their pro-leukemic effects. *Oncoimmunol.*, 7(4).

Yu J. *et al.* (2021). Liver metastasis restrains immunotherapy efficacy via macrophage-mediated T cell elimination. *Nat. Med.* 27, 152-164.

- Yu L., Li Z., Mei H., *et al.* (2020). Patient-derived organoids of bladder cancer recapitulate antigen expression profiles and serve as a personal evaluation model for CAR-T cells *in vitro*. *Clin. Transl. Immunol.* 10:e1248.
- Yu M.C. *et al.* (2004). Inhibition of T-Cell Responses by Hepatic Stellate Cells via B7-H1-Mediated T-Cell Apoptosis in Mice. *Hepatology*, 40(6).
- Yue Y., Huang W., Liang J., *et al.* (2015). L4I1 Is a Novel Regulator of M2 Macrophage Polarization That Can Inhibit T Cell Activation via L-Tryptophan and Arginine Depletion and IL-10 Production. *PLoS ONE*, 10(11): e0142979.
- Yuki K., Cheng N., Nakano M., Kuo C.J. (2020). Organoid models of tumor immunology. *Trends Immunol.* 41(8).
- Zhang X-L., *et al.* (2021). CTHRC1 promotes liver metastasis by reshaping infiltrated macrophages through physical interactions with TGF- β receptors in colorectal cancer. *Oncogene*, 40:3959-3973.
- Zhao WH., *et al.* (2018) A phase 1, open-label study of LCAR-B38M, a chimeric antigen receptor T cell therapy directed against B cell maturation antigen, in patients with relapsed or refractory multiple myeloma. *J. Hematol. Oncol*, 20;11(1):141.
- Zhao, Y. *et al.* (2008). Branched N-glycans regulate the biological functions of integrins and cadherins. *FEBS J.* 275, 1939–1948.
- Zhong, X. S., Matsushita, M., Plotkin, J., Riviere, I. & Sadelain, M. (2010). Chimeric antigen receptors combining 4-1BB and CD28 signaling domains augment PI 3 kinase/AKT/Bcl-X L activation and CD8 T cell-mediated tumor eradication. *Mol. Ther.* 18, 413–420.
- Zhou R., Yazdanifar M., Das Roy L., Whilding L.M., Gavrill A., Maher J., Mukherjee P. (2019). CAR T Cells Targeting the Tumor MUC1 Glycoprotein Reduce Triple-Negative Breast Cancer Growth. *Front. Immunol.*, 10:1149.
- Zhou Y., Zhou B., Pache L., Chang M., Khodabakhshi A.H., Tanaseichuk O., *et al.* (2019). Metascape provides a biologist-oriented resource for the analysis of systems-level datasets. *Nat Commun.*, 10:1523
- Zhu C, Anderson AC, Schubart A, Xiong H, Imitola J, Khoury SJ, *et al.* (2005). The Tim-3 ligand galectin-9 negatively regulates T helper type 1 immunity. *Nat. Immunol.* 6:1245–52.
- Zugmaier, G. *et al.* (2013). A Phase 1/2 Study Of Blinatumomab In Pediatric Patients With Relapsed/Refractory B-Cell Precursor Acute Lymphoblastic Leukemia. *Blood* 122, 70 LP – 70.

Camille Fini